Technical Report
TR-23-27
December 2023

Quantifying the contribution of abrasion versus block removal to subglacial erosion on basement rocks

Very-high resolution DSM analysis at Forsmark, east Sweden

Maarten Krabbendam
Andrew Finlayson
Romesh Palamakumbura
Adrian M Hall

SVENSK KÄRNBRÄNSLEHANTERING AB

SWEDISH NUCLEAR FUEL
AND WASTE MANAGEMENT CO

Box 3091, SE-169 03 Solna
Phone +46 8 459 84 00
skb.se

SVENSK KÄRNBRÄNSLEHANTERING

ISSN 1404-0344
SKB TR-23-27
ID 2026956
December 2023

Quantifying the contribution of abrasion versus block removal to subglacial erosion on basement rocks

Very-high resolution DSM analysis at Forsmark, east Sweden

Maarten Krabbendam[1], Andrew Finlayson[1],
Romesh Palamakumbura[1], Adrian M Hall[2]

1 British Geological Survey, Lyell Centre, Edinburgh
2 Institute of Geography, University of Edinburgh, Edinburgh

Keywords: Glacial erosion, Abrasion, Plucking, Morphometric analysis, Digital elevation model, Lidar, geomorphology.

Preface

The following report describes and compares the impact of the two glacial erosion processes of block removal and abrasion. It quantifies their respective Late Weichselian erosion depths at the Forsmark site as well as estimates the plucking:abrasion ratio. A detailed geomorphological analysis was conducted using drone-acquired high-resolution Digital Surface Models and orthophotos of five selected localities. The analysis also involved detailed bedrock and fracture mapping and quantitative morphometric analysis. Subsequently, the results of the geomorphological analysis were combined with previous erosion depth estimates from terrestrial cosmogenic nuclide (TCN) inventories.

The study was initiated by Jens-Ove Näslund (SKB) and it was jointly designed by Maarten Krabbendam (British Geological Survey), Adrian Hall (Landforms Scotland) and Jens-Ove Näslund. Maarten Krabbendam led the writing of the report. All authors contributed to the final version of the report. The results will be used, together with other scientific information, for constructing future scenarios of climate and climate-related processes in SKB's work on assessing long-term safety of nuclear waste repositories in Sweden.

The present report constitutes the last in a series of reports on bedrock denudation and glacial erosion with focus on the Forsmark site. The following reports have been previously published in this series:

TR-19-07: Past and future impact of glacial erosion in Forsmark and Uppland.

TR-19-18: Subglacial block removal: An analysis of driving and resisting forces under different glaciological scenarios.

TR-19-21: The sub-Cambrian unconformity in Västergötland, Sweden: Reference surface for Pleistocene glacial erosion of basement.

TR-19-22: Exploring alternative models for the formation of conspicuously flat basement surfaces in southern Sweden.

TR-22-08: Glacial erosion in the Öregrund archipelago – Potential for headward erosion towards Forsmark in future glaciations?

TR-22-09: Glacial ripping as a significant erosion mechanism in eastern Sweden: field evidence and modelling.

TR-23-01: Glacial erosion rates at Forsmark derived from terrestrial cosmogenic nuclides: additional results.

The present report was scientifically reviewed by Dr. Ingmar Borgström, Stockholm university.

Stockholm, February 2024

Jens-Ove Näslund

Abstract

Glacial erosion is generally thought to encompass two main erosion mechanisms: abrasion and block removal (by plucking or quarrying, glacial ripping, conchoidal fracturing and other processes). Landforms left by abrasion and block removal are distinct: abrasion results in smooth surfaces, marked with grooves, striae and polish; block removal leaves sockets, sharp edges and characteristic plucked faces. It is commonly assumed that erosion by block removal is faster and more important than abrasion, but few studies have provided direct, quantitative comparisons between abrasion and block removal.

In this study we estimate the depth of glacial erosion by abrasion and block removal by the Fennoscandian Ice Sheet during the last glaciation, the Late Weichselian, at the Forsmark site, east-central Sweden. We combine previous erosion depth estimates from terrestrial cosmogenic nuclide (TCN) inventories with a detailed geomorphological analysis of five selected sites at the Forsmark site: Stora Asphällan, Stånggrundet and three sites on the Lilla Sandgrund island. The geomorphological analysis used drone-acquired high-resolution Digital Surface Models (DSM) and orthophotos and involved detailed geomorphological, bedrock and fracture mapping and quantitative morphometric analysis.

The geomorphological mapping separated out three types of surfaces:

- abraded surfaces, with low roughness, long topographic wavelength (> 10 m), low slope surfaces, showing only evidence of abrasion;
- block-removal surfaces, with higher roughness, locally steep slopes, fresh fracture surfaces and a small (< 2 m) topographic wavelength of topographic highs. These surfaces include surfaces produced by typical lee-side and lateral plucking but also sockets and crescentic scars;
- re-abraded block-removal surfaces, with similar shape as the block-removal surfaces, except showing signs of minor abrasion, polishing and edge rounding.

Morphometric analysis of the DSM shows systematic differences in roughness and slope between abraded and block-removal (including re-abraded) surfaces. Field mapping showed both sharp and rounded edges in block removal domains. The abundance of sharp edges suggest that block removal was particularly active just prior to deglaciation. The Lilla Sandgrund sites showed an abundance of sockets and crescentic scars, whereas Stånggrundet showed an abundance of typical lee-side and lateral plucking features. The spatial extent of block removal surfaces (fresh and re-abraded) varies from c 50 % at the Lilla Sandgrund sites to c 90 % at Stånggrundet; fresh block removal surfaces vary from 6–37 % of surfaces; these were not separated for Stånggrundet.

Spatial variability of extent and depth of erosion by block removal is related to fracture networks. Stånggrundet, with abundant lee-side plucking surfaces, has a dense, well-connected fracture pattern with abundant gently dipping fractures that delineates small blocks. In contrast, the Lilla Sandgrund sites, with a high proportion of abraded-only surfaces and relatively abundant sockets and crescentic scars, has a lower fracture density, dominated by steeply inclined fractures, with fewer gently dipping fractures. At Stora Asphällan, significant in-site variation exists in fracture networks and geomorphological features between amphibolite and fine-grained felsic gneiss.

By modelling an extrapolated abraded surface over the present-day surface, the depth of erosion by late block removal can be spatially estimated. The estimated depth of block removal ranges from 0–1.3 m, and averaged 0.2–0.35 m where it did occur, i.e. excluding the abraded surfaces. Averaged over the entire area including the abraded surfaces, the average depth of late block removal amounted to 0.1–0.3 m.

These estimates can be combined with estimates of erosion depths from TCN inventories from previous work (Hall et al. 2019a, 2023). Results from samples from summit surfaces mapped as abraded surfaces range between 1.17–1.40 m; results from other surfaces, including re-abraded surfaces reach 2.18 m. Based on the assumption that abraded surfaces developed solely under abrasion and without block removal, the abrasion:plucking ratios, in terms of depth of erosion, varied from 16:1 to 3:1 across the different study sites. Estimates of erosion by abrasion from Wave Rock

summit areas, further inland, are considerably less: 0.2–0.4 m (Hall et al. 2023). The difference in estimated abrasion depth between Wave Rock and coastal outcrops at Forsmark maybe related to coarser rock grain size and/or higher local relief at Wave Rock. All these estimates are applicable to relative topographic highs: the excavation of topographic lows (trenches, joint-valleys) would need to be added to a regionally averaged erosion depth. The high abrasion:plucking ratio questions the common assumption that block removal is faster and more important than abrasion. The results of this study show that, at least at Forsmark, the opposite is the case.

The difference in areal extent of abraded-only surfaces – high in the Lilla Sandgrund sites; low at Stånggrundet – suggests that abraded-only surfaces diminish in total surface area as subglacial erosion progresses. This process starts with the development of sockets and crescentic scars, which progressively amalgamate into composite sockets, allowing lee-side plucking to proceed, locally aided by isolated subhorizontal fractures. Overall this leads to a progressive roughening of the surface. This implies that the development of block removal surfaces at some sites does not follow up-ice migration of lee-side steps, as in other published models of plucking.

Compared to other glacial erosion studies (including both ice sheets and smaller glaciers), the results from east Sweden show a very low overall erosion depth of crystalline rock, a very low erosion coefficient and a high abrasion:plucking ratio over the Late Weichselian glaciation. This may be caused by a combination of: i) hard basement rocks, with locally fracture patterns unfavourable for block removal; ii) a flat starting surface controlled by the Cambrian unconformity, suppressing plucking; iii) a long period of thick-ice conditions that suppressed block-removal including plucking, compared to a very short period of thin-ice, ablation-zone conditions during deglaciation that favoured block removal including plucking.

Overall, the depth of erosion at Forsmark during the Late Weichselian glaciation was low. Abrasion contributed between 0.2 to 1.5 m of erosion, in line with results from other ice-sheet settings. Block removal by plucking and formation of sockets and crescentic scars contributed another 0–1.6 m of erosion. Locally, affecting perhaps 10–20 % of the area, glacial ripping added a further 2–4 m of erosion. Somewhat deeper erosion occurred in the relatively shallow trenches and valleys in the Forsmark region.

Sammanfattning

Glacial erosion anses generellt omfatta två huvudsakliga erosionsprocesser, slipning (glacial abrasion) och avlägsnande av block (genom s.k. plockning, *glacial ripping* och andra processer). Landformer bildade av slipning respektive erosion av block är förhållandevis enkla att skilja åt: slipning resulterar i jämna bergytor, ofta med räfflor och polerade ytor, medan erosion av block resulterar i isolerade hällkar (tråg) (från vilka block har avlägsnats), skarpa kanter och karakteristiska 'plockade' sidor hos hällar. Ofta antas att erosion av block är en snabbare och viktigare process än slipning, men få studier har genomfört faktiska kvantitativa jämförelser mellan de två.

I denna studie kvantifierades djupet hos glacial erosion dels från slipning, dels från erosion av block vid Forsmarksplatsen under den senaste glaciationsfasen (sen-weichsel). Resultat på erosionsdjup från tidigare genomförda studier av terrestra kosmogent producerade isotoper (TCN) kombinerades med nya resultat från detaljerade geomorfologiska analyser av fem utvalda lokaler vid Forsmarksplatsen: Stora Asphällan, Stånggrundet och tre platser på ön Lilla Sandgrundet. Den geomorfologiska analysen baserades på högupplösta digitala ytmodeller av berghällar, konstruerade genom lidarmätning och ortofotografier från drönare. Analysen inkluderade detaljerad kartering av hällarnas geomorfologi, geologi, sprickighet och kvantitativ morfometrisk analys.

Den geomorfologiska karteringen identifierade tre typer av ytor:

- Slipade (abraderade) ytor: jämna ytor med långa topografiska våglängder (> 10 m), flack lutning och enbart med spår av slipning;
- Ytor med avlägsnade block: grövre (mindre jämna) ytor, lokalt brant lutning, färska sprickytor och en kort (< 2 m) topografisk våglängd. Dessa ytor inkluderar ytor bildade genom typisk plockning på läsidor men även hällkar och skärbrott;
- Ytor med avlägsnade block men som även har spår av viss slipning (åter-abradering), polering och kantavrundning.

Den morfometriska analysen av de digitala höjdmodellerna visar på systematiska skillnader i ytjämnhet och lutning mellan ytor som är slipade respektive utsatts för blockerosion (inklusive de som är åter-abraderade). Fältkarteringen visade på både skarpa och rundade kanter på områden med blockerosion. Den stora mängden skarpa kanter indikerar dock att blockerosionen var särskilt aktiv just innan deglaciationen. Lokalerna på Lilla Sandgrund visade på en riklig förekomst av hällkar och skärbrott, medan Stånggrundet hade en riklig förekomst av typisk läsidesplockning och lateral plockning. Den rumsliga fördelningen av ytor med blockerosion (utan och med åter-abradering) varierade från 50 % vid Lilla Sandgrund till runt 90 % vid Stånggrundet. Fördelningen av ytor med enbart sen blockerosion (dvs utan åter-abradering) varierade mellan 6 och 37 % (dessa separerades inte ut för lokalen Stånggrundet).

Den rumsliga variabiliteten hos omfattningen och djupet hos blockerosionen konstaterades vara relaterad till spricknätverket. Stånggrundet, som har en riklig förekomst av läsidesplockning, har ett tätt, väl sammanhängande sprickmönster med många flacka sprickor som avgränsar små block. I kontrast till det har lokalerna vid Lilla Sandgrund, vilka har en hög andel (enbart) slipade ytor och rikligt med skärbrott, en lägre sprickfrekvens dominerad av brant stående sprickor med färre flackt lutande sprickor. Vid Stora Asphällan förekommer en stor variation i spricknätverk och geomorfologiska former mellan partierna med amfibolit respektive finkornig felsisk gnejs.

Genom extrapolering av slipade ytor ovanför närliggande, idag lägre, ytor som skapats genom senare blockerosion (och som saknar slipning) kan djupet hos blockerosionen uppskattas rumsligt. Det uppskattade djupet hos blockerosionen är mellan 0–1,3 m, med ett medel på 0,2–0,35 m. Om man inkluderar hela området, dvs även de slipade ytorna utan blockerosion, så var medeldjupet hos den sena blockerosionen 0,1–0,3 m.

Dessa uppskattningar kan kombineras med information om erosionsdjup från terrestra kosmogena nuklider erhållen från tidigare studier (Hall et al. 2019a, 2023). Resultaten från TCN-prover tagna från toppytor karterade som slipade ytor visar på en erosion mellan 1,17–1,40 m. Prover från andra ytor,

inklusive åter-abraderade blockerosionsytor, visar en erosion på upp till 2,18 m. Under antagandet att de slipade ytorna bildats enbart genom slipning, utan avlägsnande av block, så varierade proportionen slipning:plockning, i termer av erosionsdjup, från 16:1 till 3:1 för de undersökta lokalerna. Uppskattningarna av erosion genom slipning från toppytorna vid Wave Rock, vilka ligger längre inåt land, är betydligt lägre: 0,2–0,4 m (Hall et al. 2023). Skillnaderna i uppskattat slipningsdjup mellan Wave Rock och de strandnära lokalerna kan vara relaterade till grövre kristallstorlek hos bergarten och/eller högre lokal relief vid Wave Rock. Alla dessa erosionsuppskattningar gäller för relativa topografiska höjder: erosionen av topografiska lågpunkter skulle behöva läggas till för att erhålla ett regionalt medeldjup hos erosionen.

Skillnaden i rumslig utbredning hos de enbart slipade ytorna – hög vid lokalerna vid Lilla Sandgrund och låg vid Stånggrundet – indikerar att den totala ytan som bildats enbart genom slipning minskar alltefter som den glaciala erosionen fortgår. Denna process börjar med bildandet av hällkar och skärbrott, vilka med tiden förenas i sammanlänkande hällkar, vilket främjar fortsatt läsidesplockning, lokalt gynnad av subhorisontella sprickor. Detta leder generellt till att ytan blir progressivt grövre. Detta innebär att bildandet av blockerosionsytor vid vissa platser inte medför en förflyttning av läsidesstegen mot isens flödesriktning (uppströms), som beskrivits i andra publicerade modeller av plockningsprocessen.

Jämfört med andra studier av glacial erosion (vid både inlandsisar och mindre glaciärer), uppvisar resultaten från östra Sverige ett mycket lågt generellt erosionsdjup av den kristallina berggrunden, en mycket låg erosionskoefficient, och ett högt förhållande mellan slipning:plockning under sen Weichsel. Detta kan vara orsakat av i) motståndskraftig kristallin berggrund, med lokala sprickfördelningar ogynnsamma för blockerosion, ii) en flack ursprungsyta styrd av den subkambriska inkonformiteten, vilket undertrycker plockning, och iii) en lång period av förhållanden med tjockt överliggande is, vilken undertrycker blockerosion inklusive plockning, jämfört med en mycket kort tid med tunn is under ablationszonen vid deglaciationen, gynnsamt för blockerosion och plockning.

Generellt sett så var djupet hos den glaciala erosionen i Forsmark låg under sen-weichsel. Slipning bidrog med mellan 0,2 och 1,5 m, vilket är i linje med resultat från andra lokaler med inlandsisförhållanden. Blockerosion, genom plockning och bildandet av hällkar och skärbrott, bidrog med ytterligare 0–1,6 m erosion. Lokalt bidrog glacial uppsprickning med en ytterligare erosion om 2–4 m (kanske inom 10–20 % av området). Något djupare erosion skedde i de relativt grunda klippdalarna och dalsänkorna i Forsmarksområdet.

Contents

1 Introduction 11

2 Setting 13
2.1 Ice sheet setting – Pleistocene evolution 13
2.2 Bedrock setting 15
2.3 Geomorphological setting 15

3 Erosion depths from TCN inventories near Forsmark – summary 17

4 Methods, datasets 21
4.1 DSM data preparation and analysis 21
4.2 Geomorphological and bedrock mapping 21
4.3 Fracture analysis 22
4.4 Estimation of block removal depth using Extrapolated Abrasion Surfaces 23

5 Results – Geomorphological mapping and site descriptions 25
5.1 Bedrock general characterisation 25
5.2 Fracture analysis – general observations 27
5.3 Geomorphological observations – general 30
5.4 Lilla Sandgrund NE – site description 35
5.4.1 Bedrock and fracture network characterisation 35
5.4.2 Geomorphological description 35
5.5 Lilla Sandgrund West – site description 38
5.5.1 Bedrock and fracture network characterisation 38
5.5.2 Geomorphological description 38
5.6 Lilla Sandgrund SW – site description 42
5.6.1 Bedrock and fracture network characterisation 42
5.6.2 Geomorphological description 42
5.7 Stora Asphällan – site description 46
5.7.1 Bedrock and fracture network characterisation 46
5.7.2 Geomorphological description 49
5.8 Stånggrundet – site description 51
5.8.1 Bedrock and fracture network characterisation 51
5.8.2 Geomorphological description 54
5.9 Abrasion-only surface – Närke, central Sweden 54
5.10 Edge rounding measurements 55

6 Results – Morphometric geomorphology 57
6.1 Morphometrics – separation of abraded from block removal surfaces 57
6.2 Surface area proportion of abrasion vs block removal 61
6.3 Depth of erosion by block removal volume: modelling 62
6.4 Comparison of block removal and TCN erosion depths 64

7 Discussion 67
7.1 Uncertainties 67
7.1.1 Assumption of abraded surfaces 67
7.1.2 Re-abrasion and block removal during Late Weichselian glaciation? 68
7.1.3 Other uncertainties 69
7.2 Variations in erosion depth by block removal and abrasion at the Forsmark site 69
7.2.1 Variations in abrasion rate 69
7.2.2 Variations in block removal depths: importance of fracture network type 70
7.2.3 The odd one out – amphibolite at Stora Asphällan 70
7.3 Large-scale limitations of the method 71
7.4 Comparison with other glaciated areas 71
7.4.1 Abrasion:plucking ratios and erosion coefficient estimates 71

7.5 Block removal mechanisms 73
7.6 Evolution and development of roughness of glacial erosion surfaces 74
7.7 Controls on abrasion, block removal and glacial erosion 75
7.8 Depth of erosion at Forsmark during the Late Weichselian glaciation 77

8 Conclusions 79

References 81

Appendix 1 Outcrop photo fracture analysis – Stånggrundet and Klubbudden 87

Appendix 2 Fracture results – full 89

1 Introduction

Subglacial erosion is generally thought to encompass two main erosion mechanisms: abrasion and block removal by plucking (or: quarrying) (e.g. Benn and Evans 2010, Alley et al. 2019) or other mechanisms such as conchoidal fracturing (Okko 1950, Prest 1983, Glasser and Bennet 2004, Krabbendam et al. 2017). Additional subglacial erosion mechanisms include glacial meltwater erosion (e.g. Kor et al. 1991, Eyles 2006) and glacial ripping (Hall et al. 2020, Krabbendam et al. 2022a, 2022b), which typically have more localised distribution.

The landforms left by abrasion and block removal are distinct: abrasion results in smooth surfaces, marked with grooves, striae and polish, whereas block removal such as plucking leaves sockets, sharp edges and characteristic steep plucked faces (e.g. Rastas and Seppälä 1981, Benn and Evans 2010). As it is generally accepted that plucking requires cavities on the lee-side (or lateral sides) of rock obstacles, slower and thicker ice are thought to suppress plucking and favour abrasion, whereas fast and thin ice, as well as water pressure fluctuations are thought to favour plucking (e.g. Evans 1996, Zoet et al. 2013, Alley et al. 2019). However, it is increasingly recognised that bedrock properties play an important role: densely fractured rock is more susceptible to plucking, whilst 'softer' rocks are more susceptible to abrasion (Dühnforth et al. 2010, Krabbendam and Glasser 2011, Hooyer et al. 2012, Lane et al. 2015). Thus, the relative efficacy of abrasion and block removal in a particular site is a function of both imposed (hydro)glaciological conditions and intrinsic bedrock controls, such as rock hardness and the nature of the pre-existing fracture network.

It is commonly assumed that erosion by plucking is faster and more important than abrasion (Jahns 1943, Boulton 1979, Drewry 1986, Sugden et al. 1992, Riihimaki et al. 2005, Iverson 2012, Alley et al. 2019). Boulton (1979) argued that abrasion is limited by the availability of abrasing tools (i.e. large clasts embedded in basal ice), and because these clasts must be provided by plucking, plucking must be dominant over abrasion. However, this line of reasoning assumes there is no other source of subglacial or supraglacial debris and that the bed is of constant lithology. Such assumptions that may not be valid in nature and whilst Boulton's (1979) approach appears logic at first sight, in practice it may not be a good 'rule'.

There are few studies that provide a quantitative comparison between the two mechanisms. Riihimaki et al. (2005) estimated an abrasion:plucking ratio of 1:2 from based on grain-size distribution (bed load versus suspended load) in the proglacial river issuing from the Bench Glacier, Alaska. Loso et al. (2004) estimated an abrasion:plucking ratio of c 1:4 using a similar suspended / bedload distribution, but from accumulated glaciolacustrine deposits, also in Alaska. In contrast, Herman et al. (2015) noted that erosion rates below the Franz Josef Glacier (New Zealand) increased non-linearly with ice flow velocities and assumed on that basis that abrasion was dominant over plucking. In that particular setting, this is not unexpected as the up-ice lithologies are high-grade metamorphic rocks, whilst down-ice lithologies are low-grade metamorphic, so likely softer than the tools produced subglacially (and supraglacially) in the accumulation zone. All these studies used different proglacial sediment products as a proxy for subglacial erosion. In small mountain glaciers, with very proximal deposits where fluvial transport and hence grain-size diminution are limited, this may well be a valid approach, but for larger ice sheets such methods are not appropriate, because long transport routes of the subglacial sediment would result in continuous grain size diminution after glacial erosion. Large-scale ice-sheet erosion models (e.g. Hildes et al. 2004, Ugelvig and Egholm 2018) must make assumptions as to relative efficacy of plucking and abrasion, but these assumptions are not well controlled by direct observational constraints and are hampered by poor constraints of the role and real-life distribution of fractures (see discussion in Iverson 2012).

Terrestrial cosmogenic nuclide (TCN) inventories can also be used to estimate bedrock erosion rates – or erosion depths over one or more phases of glaciation. Commonly, samples are taken from summits of tops of roche moutonnées or whalebacks (e.g. Stroeven et al. 2002a, Wirsig et al. 2017), which may only be eroded by abrasion and so that the results do not constrain erosion by plucking. Some studies have taken samples from both abraded tops and plucked faces ('stepped samples'; e.g. Briner et al. 1998, Graham et al. 2023, Hall et al. 2023), which can be used to constrain both abrasion and plucking rates. However, TCN inventories are point measurements which may not be representative of a wider

area. Hence, it is potentially problematic to extrapolate the erosion depths or rates from the individual sample (point) sites to wider areas (e.g. Rand and Goehring 2019). Since block removal is commonly spatially highly variable, this means that small datasets with TCN inventories from a few point samples are only of limited value to estimate wider average plucking rates. In other words, even if it is known that plucking has removed 1 m of rock from a particular site, we need to know how much of the wider area was subjected to by block removal. Thus, estimates of bedrock erosion depths based on TCN inventories are ideally augmented with glacial landform analysis to reliably extrapolate point results to a wider area. This approach was recently taken by Graham et al. (2023) concerning a short-lived (< 300 yr) advance-retreat cycle of the Greenland Ice Sheet in the Jakobshavn area. They arrived at an abrasion:plucking ratio of c 1:1. In this study we apply similar methods, with a more involved glacial landform analysis using high resolution Digital Surface Models (DSM) and apply the method to an entire glaciation.

In this study we set out to quantify the depth of glacial erosion by the Fennoscandian Ice Sheet during the Late Weichselian (i.e. the last glaciation, during MIS 2) by abrasion and block removal, in the area around the site of the spent nuclear fuel repository now under construction at Forsmark, situated in east-central Sweden. This adds to the already detailed analysis of past glacial erosion in the Forsmark area (e.g. Hall et al. 2019a, 2022, 2023, Krabbendam et al. 2022a).

In the Forsmark area, a number of samples have previously been analysed for terrestrial cosmogenic nuclide (TCN) inventories (Hall et al. 2019a, Heyman et al. 2019, Hall et al. 2023 – summarised in Chapter 3). All samples show nuclide inheritance, and TCN exposure modelling suggests that the depth of erosion over the last 100 000 years (including both the Early and Late Weichselian glaciations) was 1.6–3.5 m (interquartile range), whilst the depth of erosion over the last 35 000 years (Late Weichselian glaciation only) ranges from 0.2–2.2 m (Hall et al. 2019a, Heyman et al. 2019, Hall et al. 2023). Most TCN samples were taken from abraded summits of whalebacks or roches moutonnées. Hall et al. (2023) also analysed step samples to constrain the timing of block removal.

In this report we perform detailed geomorphological analysis of several well-exposed rock surfaces on coastal outcrops at Forsmark. The mapped sites include or are adjacent to the TCN sample sites. Geomorphological glacial landform analysis is performed on high-resolution UAV (Unmanned Aerial Vehicle)-obtained LiDAR DSMs and orthophotos, complemented by detailed field mapping. Areal extent of block removal can be directly quantified from the digital maps, whilst volume of block removal is estimated by subtracting the present surface from a modelled extrapolated abrasion surface (details in Section 4).

We thus use detailed geomorphological, bedrock and fracture mapping using drone-acquired high-resolution DSMs and orthophotos. Combining the results with those of previous erosion estimates from TCN inventories (Hall et al. 2019a, 2023) we attempt answer the following questions:

1. What is the relative proportion of block removal and abrasion in the vicinity of the proposed spent nuclear fuel repository at Forsmark?
2. Combined with previous TCN erosion modelling, what is the likely absolute contribution of block removal and abrasion to the erosion depth during the Late Weichselian glaciation (since ca 35 000 years) in the Forsmark area?
3. Are there spatial variations in the relative contribution of abrasion, plucking and other block removal mechanisms such as crescentic scar formation, and if so, what are the controlling factors?

We will discuss (i) uncertainties and limitations of the method, including the assumption of long-term existence of abraded-only surfaces, (ii) possible explanations of local variations in abrasion and block removal depth, and (iii) differences between typical lee-side plucking features and other block removal features such as crescentic scars.

2 Setting

2.1 Ice sheet setting – Pleistocene evolution

All of Scandinavia was repeatedly covered by ice sheets during the Pleistocene (e.g. Kleman et al. 2008). During the Late Weichselian glaciation (i.e. the last (MIS 2) phase of Weichselian ice-sheet coverage, c 35–10 ka), the Fennoscandian Ice sheet (Figure 2-1) reached as far south as Denmark and northern Germany (e.g. Stroeven et al. 2016). During deglaciation, the ice margin retreated across southernmost Sweden between c 16–13 ka. A prolonged stillstand occurred during the colder Younger Dryas stadial (c 12.7–11.7 ka), with a quasi-stable ice margin located south of Stockholm. Post-Younger Dryas ice-margin retreat was rapid (200–300 m yr^{-1}; Strömberg 1994, Hedenström and Risberg 2003). At lower elevations including the study area near Forsmark, the ice margin was marine- or lacustrine terminating (Andrén et al. 2011).

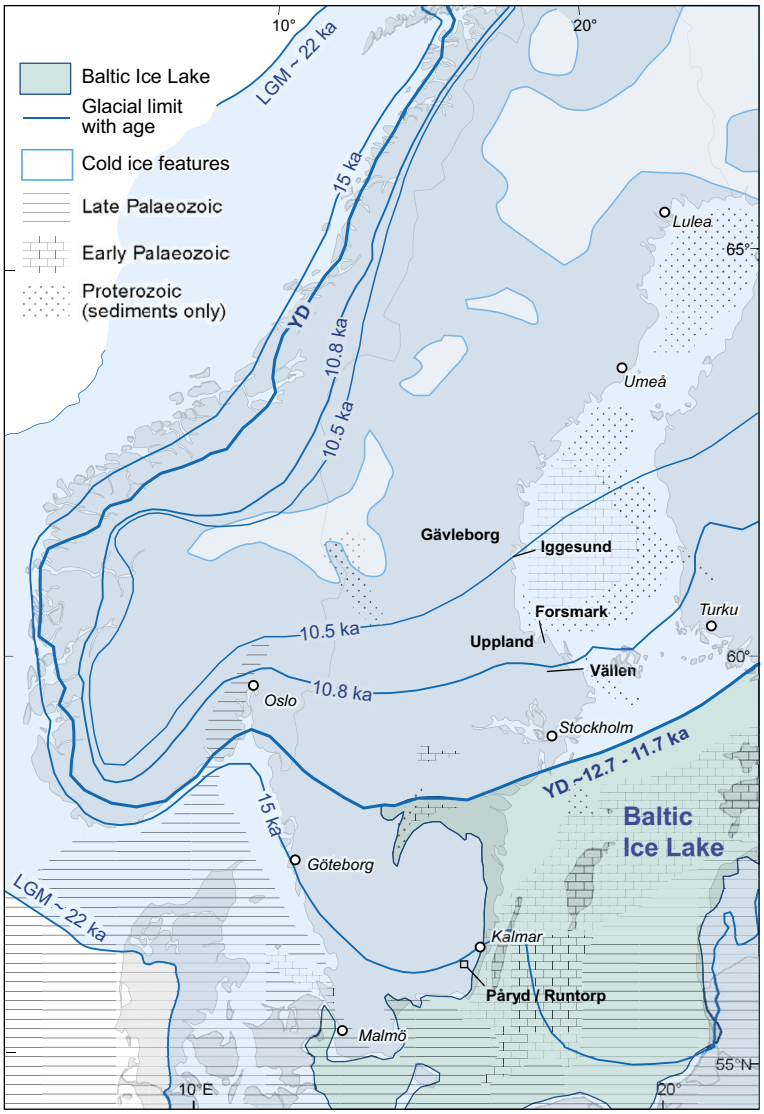

Figure 2-1. *Overview map of Fennoscandian Ice Sheet with selected margin positions, Baltic Ice Lake outline after Stroeven et al. (2016), schematic bedrock geology after Asch (2005). YD = Younger Dryas limit. Only Proterozoic ('Jotnian') and Palaeozoic sedimentary rocks are shown; Proterozoic metamorphic and igneous rocks are not shown.*

Ice flow direction in the Forsmark area (Figure 2-2A) was generally towards the south or SSE (Sohlenius et al. 2004, Hall et al. 2019a), with modelled ice flow velocities ranging from 50–400 m yr^{-1} (Patton et al. 2017). The area lies outside the areas of cold ice inferred in Scandinavia (Kleman et al. 1999), so it is likely that the Forsmark area experienced warm-based sliding throughout all or most of the period of Late Weichselian ice cover. Modelling (SKB 2020) suggest long periods of permafrost at Forsmark, so initial ice advance likely occurred over frozen ground, but warm-based sliding is possible over permafrost at depth. During final deglaciation basal meltwater fluxes were likely to be high (e.g. Greenwood et al. 2017, Shackleton et al. 2018).

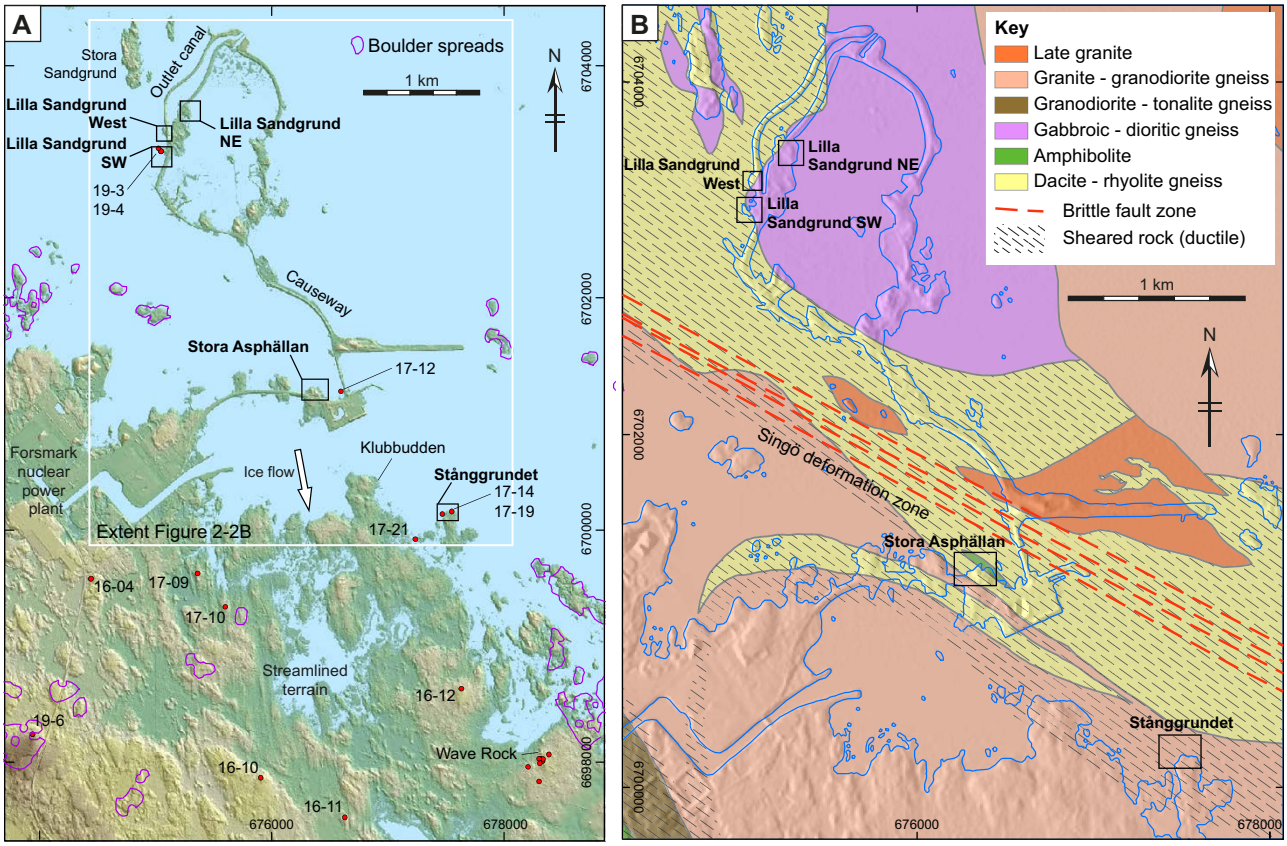

Figure 2-2. *A. Hill shade Digital Elevation Model (based on elevation data from Lantmäteriet), showing locations of five study sites. Boulder spread distribution outlined in purple, after Swedish Geological Survey (SGU) data – see also Krabbendam et al. (2022a). TCN Sample localities after Hall et al. (2019a, 2023). Note streamlined bedrock features with till tails in the SE, showing regional SSE ice flow direction. B. Simplified bedrock map, location of brittle Singö deformation zone and broad distribution of highly sheared rock after SGU data, Stephens et al. (2008) and Stephens (2010); DTM hillshade background after Lantmäteriet.*

2.2 Bedrock setting

All rocks in the study area are crystalline basement rocks, formed during the c 1.9–1.8 Ga Svecokarelian orogeny (Figure 2-2B). They are mainly igneous rocks with minor supracrustal (volcanic and sedimentary) rocks, but all metamorphosed to high-grade, during that same orogeny. The resultant rocks are high-grade, gneissose rocks of variable composition (e.g. metagranite, metagranodiorite, metadiorite, amphibolite). Ductile shearing was highly variable, so that some rock domains are strongly sheared with well-developed layering and gneissose foliation, whilst other domains are more massive and structurally near-isotropic. In the Forsmark area, such high-strain fabrics typically strike WNW–ESE or NW–SE (Figure 2-2B). All rocks cooled into the brittle regime between c 1.8 and 1.7 Ga (e.g. Hermansson et al. 2008, Söderlund et al. 2009). Brittle faulting in part followed the older ductile fabrics, so that the so-called Singö deformation zone (Figure 2-2B) is characterised by a km-wide zone of ductile shearing, with a narrower core zone of brittle faulting. Detailed studies on fractures and their mineral coatings (e.g. epidote, laumontite, calcite, adularia) have shown that fracturing occurred during different phases throughout the Proterozoic and Phanerozoic (e.g. Sandström et al. 2008, 2009). The majority fractures were thus already in existence prior to Quaternary glaciations but may have opened up further during multiple glaciation/deglaciation cycles (Carlsson 1979, Leijon 2005, Hall et al. 2019a, Krabbendam et al. 2021).

The basement rocks of eastern Sweden cooled to below c 225 °C by 1.5 Ga. Further exhumation occurred, and the area was covered by Jotnian sandstone during the Mesoproterozoic (Korja et al. 2001, Lundmark and Lamminen 2016). Subsequent burial and exhumation were followed by deposition of Cambrian sandstone and Ordovician limestone (e.g. Nielsen and Schovsbo 2011). The contact of the Cambro-Ordovician sedimentary rocks and the underlying rocks, the sub-Cambrian unconformity, is regarded as a very flat surface (Nielsen and Schovsbo 2011, Gabrielsen et al. 2015) that strongly controlled the landscape evolution of southern and eastern Sweden during the Pleistocene, as evidenced by the so-called sub-Cambrian peneplain (Lidmar-Bergström 1993, 1995, Hall et al. 2019a, 2019b). In the Forsmark area, remnants of Jotnian sandstone and Cambro-Ordovician sedimentary rocks, and hence also their respective basal unconformities, occur offshore and in small down-faulted graben. Various lines of evidence (see Lidmar-Bergström 1995, Hall et al. 2019a, 2019b) suggest that the sub-Cambrian unconformity surface would only have been a few tens of metres above the present land surface, so that erosion of basement rocks (as opposed to erosion of other younger rocks) above Forsmark only amounted to a few tens of metres. Hall et al. (2019a) further argues that in the Forsmark area, basement rocks only became exposed during the Pleistocene, largely due to ice-sheet erosion.

2.3 Geomorphological setting

The Forsmark area is an area of low relief (10–30 m), characterised by innumerous low rock hills, separated by linear valleys in various orientations (Figure 2-2A), typical of glacially eroded basement gneiss terrains. In detail, Hall et al. (2019a) recognised three terrain types:

- *Ice-roughened terrain*, characterised by extensive rock exposed on topographic highs, separated by fracture-guided valleys of variable widths and orientation. Till cover is limited to infill within the valleys and rock basins.
- *Weakly streamlined terrain,* with less exposed rock and more till cover, and elongate drumlinoid hills, commonly with till tails extending to the SSE, parallel to the regional ice flow.
- *Glacially disrupted terrain,* with overall similar characteristics of the above two terrains, but with widespread occurrence of boulder spreads and disrupted bedrock, interpreted to be caused by *glacial ripping* (Hall et al. 2020, Krabbendam et al. 2022a).

Our study sites lie in the ice-roughened terrain, just to the north (up-ice) of the onset of weakly streamlined terrain (Figure 2-2A, see also Hall et al. 2019a, Figure 4-27). Areas of glacially disrupted terrain with associated boulder spreads occur 2–3 kilometres to the NW, SW and SE (Figure 2-2A), but glacial ripping did not affect the study sites themselves (Krabbendam et al. 2022a). Nevertheless, large (> 1 m) boulders are common. Locally, boulders occur clustered in inlets that appear sheltered, possibly concentrated by post-glacial coastal processes (wave and sea ice action).

3 Erosion depths from TCN inventories near Forsmark – summary

Previous investigations have examined the impact of glacial erosion on the Precambrian basement gneiss surfaces in Uppland (Hall et al. 2019a). An important part of these assessments involved the use of Terrestrial Cosmogenic Nuclides (TCNs) from 32 surface bedrock samples along a 50 km long transect SW of Forsmark (Figure 5-2 in Hall et al. 2019a). The aim was to estimate depths and rates of glacial erosion through the last and earlier glaciations and to estimate erosion rates for possible future glaciations over the next 100 ka and 1 Ma (Hall et al. 2019a). Because most samples were from (local) summits, with few step samples, additional TCN sampling was undertaken to further constrain erosion rates at Forsmark (Hall et al. 2023). The additional samples come from 4 sites: Lilla Sandgrund, Gunnarsbo, Mohägnaden and Wave Rock. These included 5 paired sets of step samples from sites where block removal had formed small leeside and flank cliffs to small roches moutonnées. Details of all sample sites and sample preparation and analysis are provided in Hall et al. (2019a, 2023).

The calculation of cosmogenic nuclide production through time is affected by standard cosmogenic nuclide analysis parameters such as sample elevation, thickness, density, topographic shielding, and subaerial non-glacial erosion. Additional input data includes the point in time for start of the simulation, ice cover history, and post-glacial submergence under water due to changes in relative sea-level. Glacial erosion was simulated based on the depth and time dependent production of ^{10}Be and ^{26}Al for a range of scenarios. These include different TCN production rate estimates, different start times for first exposure to TCNs, and two contrasting erosion modes. For (1) *continuous glacial erosion rate* mode, glacial erosion is assumed to occur continuously during periods with ice cover (*rate)*, and the total amount of erosion scales with the duration of ice cover. For (2) incremental *glacial erosion steps* mode, glacial erosion is assumed to occur stepwise only, with cumulative erosion to a constant depth at the end of each ice cover period (*glaciation*), and the total depth of erosion scales with the number of ice cover periods (Hall et al. 2019a). We focus here on results for continuous glacial erosion rates over the last ice cover period (35.4–10.8 ka), e.g. the Late Weichselian, at coastal outcrops at Forsmark and at Wave Rock (Figure 3-1).

The TCN samples at coastal outcrops come from upstanding summit surfaces surrounded by sockets and fracture surfaces from which blocks and plates have been removed (Figure 2-4 in Hall et al. 2023). Summit samples for coastal outcrops within the yielded the following estimated erosion depths in the last ice cover period (Hall et al. 2023):

- Lilla Sandgrund SW (FORS-19-03A) 131 ± 44 cm and (FORS-19-04) 157 ± 54 cm; both from smooth abraded surfaces, within the mapped study areas in this report.
- Stånggrundet:
  - FORS-17-19: 140 ± 47 cm from a smooth abraded summit surface, within the mapped area in this study, and
  - FORS-17-14: 208 ± 73 cm from a moderately rough summit surface, that likely experienced both block removal and abrasion (see Section 5.8). The sample site lies within the area covered by DSM survey, but outside the mapped area.
- Stora Asphällan (FORS-17-12) 117 ± 41 cm; from a low-lying surface with smooth abraded top (Figure 2-4 in Hall et al. (2023). The sample site lies outside the mapped study area in this report.
- Apelviken (FORS-17-21) 215 ± 79 cm, from a low abraded surface, but the geomorphology of this surface is unclear and is not well documented. The site does not form part of the study sites in this report.

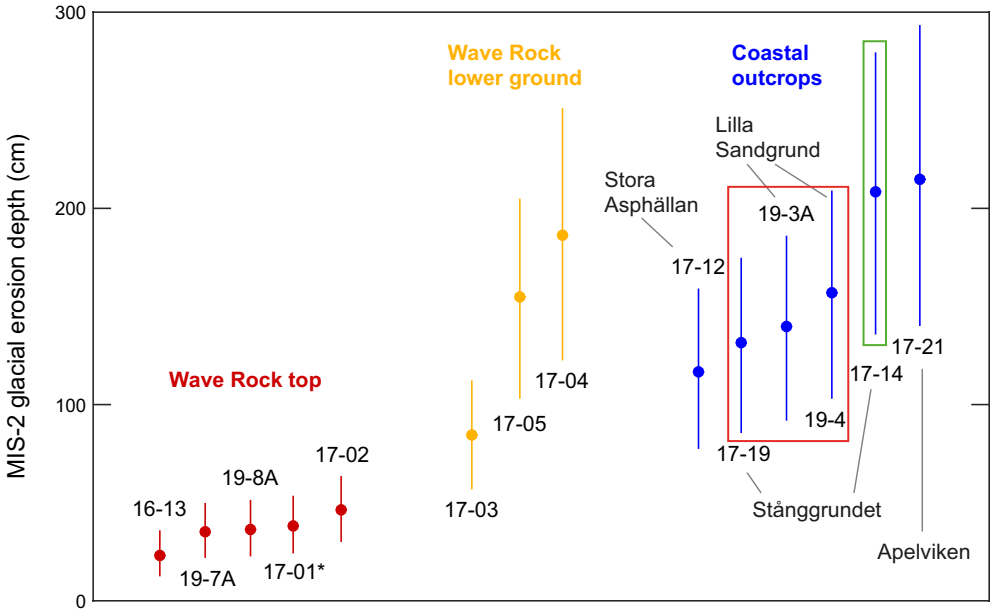

Figure 3-1. *Overview of glacial erosion depths for the last ice cover period (35.4–10.8 ka) for coastal outcrops and Wave Rock – Figure 3-1 from Hall et al. (2023). The glacial erosion depths are based on the combined ^{10}Be and ^{26}Al data for surface samples (* for sample 17-01 only ^{10}Be) and the continuous glacial erosion rate scenario. Data for the Figure is available in Table S4 in Appendix 1 of Hall et al. 2023. Sample sites that fall within areas mapped as abraded-only surfaces in the geomorphological mapping (see Section 5) shown in red box; sample 17-14 (green box) is likely from a re-abraded surface (See section 6.4).*

Results from the informally named Wave Rock, 2 km south of Stånggrundet, are also summarised here, to provide wider context. Wave Rock is a low rock hill at 8–10 m a.s.l. developed in coarse, porphyritic metatonalite (Figure 3-2A). The rock is massive in its structure, with 4–10 m spacing of vertical fractures and > 1 m spacing of subhorizontal fractures. The summit surface is smooth and carries crescentic marks and glacially polished phenocrysts (Figure 3-2A, B). TCN samples FORS-16-13, 17-01, and 17-02 (reported in Hall et al. 2019a), and 19-02, 19-07A and 19-08A (reported in Hall et al. 2023), come from the summit surface of Wave Rock. These samples have very high TCN inventories consistent with very low erosion, and yielded estimated erosion depths in the last ice cover period in the range of 23–46 cm. Hall et al. (2023) interpreted the summit area of Wave Rock to be eroded dominantly by glacial abrasion, on the basis of: (i) dominated presence of abrasional microforms, and absence of block removal features and (ii) the estimated summit erosion depths (23–46 cm) are significantly less than the spacing (> 1 m) of subhorizontal fractures.

The flanks of the hill show 0.5–2 m high rock steps with sockets where rock blocks have been removed (Figure 3-2C, D). Paired step sample 19-07A and B is from The Wave, a rock step with a well-rounded and crescentic marked edge (Figure 3-2C). Paired step sample 19-08 is from another step with a slightly rounded edge on the east flank of the hill (Figure 3-2D). The estimated erosion depths of both top samples (19-07A and 19-08 B) through the Late Weichselian glaciation are 36–35 ± 14 cm.

Lower elevation sites peripheral to Wave Rock show a patchwork of upstanding abraded surfaces and fracture surfaces and sockets from which plates and blocks have been removed by glacial erosion; the more closely fractured peripheral sites have been eroded by combined abrasion and block removal, including lee-side plucking (Figure 3-2D). Sample sites around the periphery of Wave Rock at 7 m a.s.l (FORS-17-03; 17-04 and 17-05) show lower spacing of vertical fractures (1 m or less); sample site (FORS-17-05) also shows spalling of 5–10 cm thick sheets from the top surface of a low whaleback. TCN inventories of these samples are lower, consistent with greater erosion: estimated erosion depths during the Late Weichselian glaciation are 84–186 cm. Hall et al. (2023) interpreted the erosion depths of these peripheral sites to be eroded by a combination of erosion and block removal, on the basis of presence of block removal features and depths of erosion greater than Wave Rock summit.

Comparison of TCN step sample results with summit sample results shows that in most locations the modelled deeper erosion from the lower, step samples compare well with the actual step sample depth below the summit samples, suggesting that the bedrock steps were created during the last glaciation. The exception is the Mohägnaden sample (FORS-19-06A; B) where the TCN concentrations of the summit and step samples overlap, and thus had similar overall erosion rates during the last glaciation. This suggest that block removal during the last glaciation cannot explain the results, and the best explanation is that the steps were created prior to the last glaciation, i.e. during a previous glaciation.

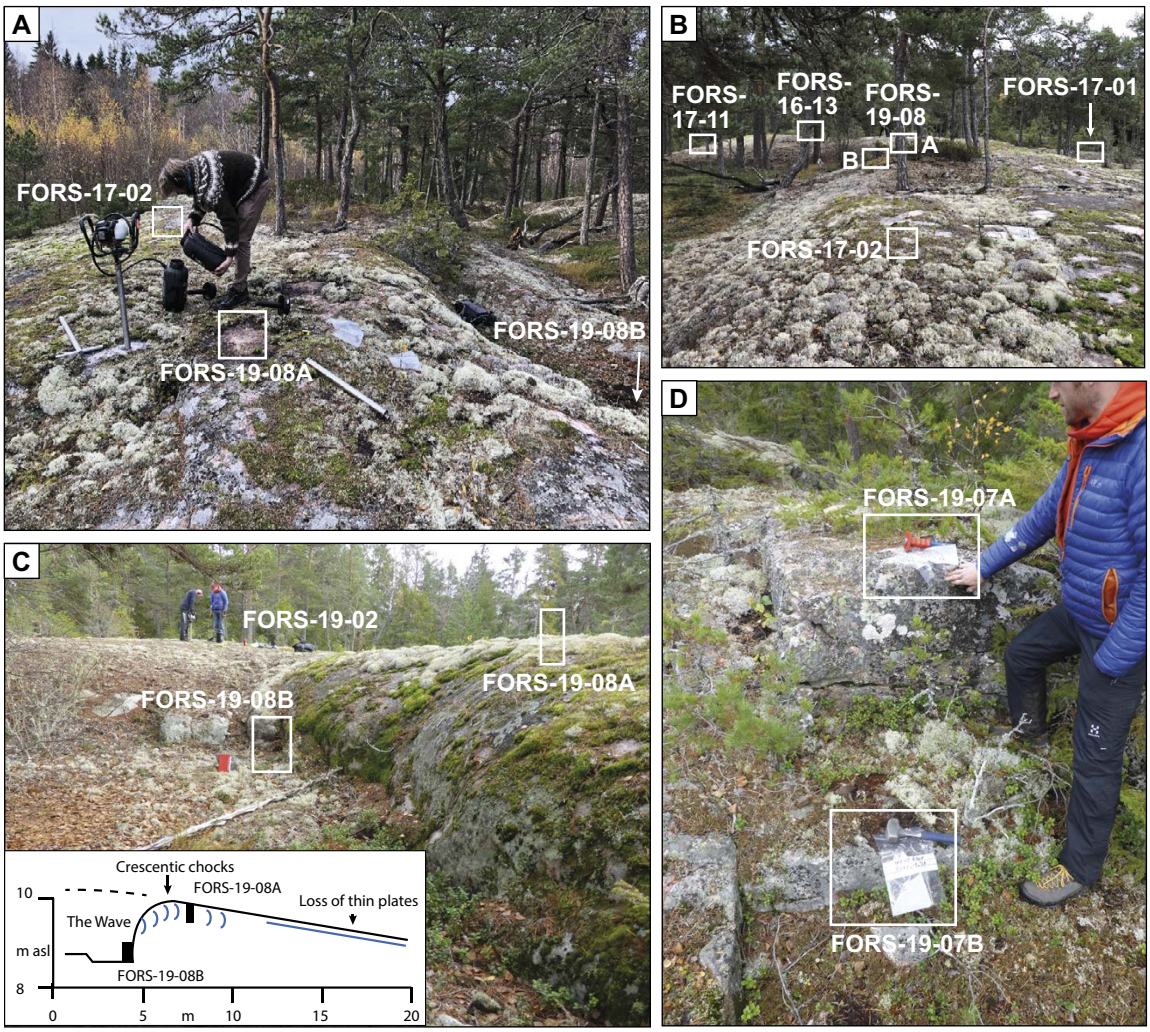

Figure 3-2. *Figure 3-2 from Hall et al. (2023). Summit surface samples from Wave Rock. A. View to W along The Wave ridge. B. View to E along The Wave ridge showing TCN sample site locations. C. Detailed view to E of The Wave step (FORS-19-07) with a sketch showing the distribution of micro-erosion forms. D. Detailed view of the second step sample site (FORS-19-08) on the eastern side of the outcrop.*

4 Methods, datasets

4.1 DSM data preparation and analysis

High-resolution LiDAR and photogrammetry were obtained by UAV (Unmanned Aerial Vehicle) drone, flown at a height of 10–25 m, in April 2020 by Amkvo AB over five selected, well-exposed rock surfaces in the vicinity of the Forsmark nuclear plant.

Digital Surface Models (DSMs) and the aerial orthophotos were used to assist with geomorphological mapping and quantitative geomorphological analyses. DSMs were used in preference to DTM (Digital Terrane Models), to avoid any artifacts resulting from the vegetation removal algorithms. Vegetated areas, although visible on the maps, were excluded from any of the quantitative morphometric analyses.

Due to variable flight altitude of the UAV drone, small variations occurred in the resolution of the raw DSMs (H 4-1). Therefore all DSMs were resampled to a horizontal resolution of 5 cm prior to any further processing or investigation. Hillshade and slope derivatives were generated from the DSMs using standard ArcGIS tools. Standard deviation of slope was used as an indicator of surface roughness (e.g. Smith 2014) and was generated using the focal statistic tool for both 5-cell (25 cm) and 10-cell (50 cm) windows. When describing roughness in the text, we mention a scale ('cm-scale roughness'): this concerns the vertical scale of roughness, i.e. the amplitude of roughness, unless explicitly mentioned otherwise.

Table 4-1. Table with original (raw) cell size of DSM with resampled cell size, for all 5 study sites.

	Lilla Sandgrund NE	Lilla Sandgrund West	Lilla Sandgrund SW	Stora Asphällan	Stånggrundet
Original cell size (m)	0.0130	0.0140	0.0170	0.0195	0.0195
Resampled cell size (m)	0.05	0.05	0.05	0.05	0.05

4.2 Geomorphological and bedrock mapping

For geomorphological mapping, the orthophotos and DSMs were used as a base map and, using ruggedized PC Tablets, detailed geomorphological maps were made in the field. Bedrock mapping was performed in the field to augment previous bedrock mapping (e.g. Stephens et al. 2008), focussing on bedrock characteristics relevant for subglacial erosion.

For the geomorphological mapping, microforms were mapped and described, edges where mapped and differentiated (where practical) in sharp and rounded edges. Surfaces were classified broadly in three categories: (Summary in Table 4-2).

- **Abraded Surfaces:** surfaces that only show evidence of abrasion. They may contain pockets of block removal, but these were separated out if visible on the DSM (in practice > 20 cm wide and > 10 cm deep).
- **Block Removal Surfaces:** surfaces that show evidence of block removal, marked by sharp edges and sharp corners; surfaces may be steeply dipping. The exposed surfaces are all some form of fracture surface: these fracture surfaces may (i) follow pre-existing joints (recognisable by joint coatings and/or continuity with joints in adjacent bedrock) or (ii) comprise new fractures, commonly conchoidal. Block Removal Surfaces includes typical plucked (quarried) faces, but also a variety of crescentic scars and sockets. In some study sites these subcategories were mapped separately; in other areas this was not practical.
- **Re-abraded surfaces:** as above but where the edges and corners are rounded, and fracture faces smoothed by subsequent abrasion.

In addition, S-forms, interpreted as formed by subglacial meltwater erosion, where also mapped. Areas covered in vegetation or boulders were also mapped – to be later excluded from the DSM analysis.

Striae were measured with a compass or – if large – digitised directly from the air photos. In the latter case, the veracity of features interpreted as striae (as opposed to for instance bedrock foliation or banding) was checked in the field.

Table 4-2. Types of different erosional surfaces, as used in the geomorphological mapping and analysis, with summary of characteristics.

Abraded surfaces	Surfaces that show only abrasion forms. These show an absence of block removal, are overall smooth at vertical scales > 1 cm, and typically form very-low angle surfaces with long-wavelength (> 10 m) relief.				
Block removal surfaces – combined	Any surface showing block removal. This may include classic-plucked surfaces, crescentic scars and sockets.	**Block removal surfaces ('fresh')**	Any surface showing block removal, with fresh fracture surfaces and sharp, angular edges.	**Sockets**	Isolated 'hollows' from which rock blocks have been removed.
				Plucked surfaces	Surfaces formed by classic lee-side and lateral plucking ('quarrying')
		Re-abraded surfaces	Any surface with block removal, but subsequently subjected to abrasion such as rounded edges and/or reduction of mm–cm scale roughness.		
S-forms	Surfaces interpreted to have formed by focussed meltwater erosion. These are normally curvilinear in shape.				
Boulder, vegetation	Surfaces on the DSM covered in boulders or vegetation or water – these were excluded from the quantitative DSM analysis.				
Extrapolated Abraded Surface	A modelled, conceptual surface, constructed from extrapolated the real abraded surfaces. The Extrapolated Abraded Surface lies above the present surface in areas of block removal.				

4.3 Fracture analysis

To characterise the 3D fracture networks in the shallow subsurface, different fracture analysis methods were deployed, comprising both field-based analysis and desktop digitisation of fracture traces from high resolution drone imagery and georeferenced outcrop photographs. The methods comprise:

A. 2D map view Drone image mapping (orthophotos and DSM). 2D drone mapping fracture analysis was performed directly on the orthophotos and DSM by digitising fracture traces, augmented by field observations. This mapping yields vertical and steeply inclined fractures.

B. 1D Scanline fracture analysis in the field. This method was used to gather additional observations on fracture orientation (azimuth and dip) and mineralisation. Due to the low relief of the outcrop, scanline analysis mainly yields data on vertical and steeply inclined fractures.

C. 2D aerial oblique window analysis in the field. To constrain the variability of horizontal and gently inclined fractures, a 2D aerial window method was employed on inclined outcrop surfaces. The inclined sample window was projected onto a vertical 2D window (section view), from which the density and vertical spacing of subhorizontal and gently inclined fractures can be calculated.

D. 2D digital photo analysis (section view) was used to provide additional data on the horizontal fracture networks – this was only performed at Stånggrundet. The full method is described in Palamakumbura et al. (2020).

Each method is aimed to characterise a different aspect of the fracture network. Distribution and connectivity of steeply inclined fractures is best captured with method A, but for gently inclined fractures with method C and D. Azimuth and dip were measured along scanlines and the 2D aerial window (B and C). Fracture analysis is always dependent on scale and resolution, so field analysis will pick out smaller and tighter fractures than the drone image analysis.

Fracture orientations derived from the DSM fracture trace mapping are shown in rose diagrams (as no dips are available); fracture orientations (azimuth and dip) from the field-based scanline and 2D aerial window analysis are presented in stereographic plots (lower hemisphere, equal area projection).

Outputs are recorded as *fracture density* (in m^{-1}) according to Singhal and Gupta (2010), which equates with P10 or P21 *fracture intensity* as defined by Sanderson and Nixon (2015). P10 is the number of fractures in a scanline, per m, whilst P21 is the total length of fractures within an area. Fracture spacing (in m) is the reciprocal of fracture density. Fracture frequency (P20) is the number of fractures per area (in m^{-2}).

The connectivity of the fracture network is based on the type of *branches* and *nodes* of the fractures (e.g. Sanderson and Nixon 2015). Nodes can be classified as an isolated tip (*I-node*), having a T or Y junction (*Y-Node*), or a crossing with another fracture (X-node). Y-nodes and X-nodes can be combined into connected nodes (*C-nodes*). Fracture segments, or branches, can then be grouped according to the character of their nodes: *I-I branches* (isolated on both ends); *C-C branches* (connected on both ends) and *I-C branches* (connected on one end; isolated at the other end). A well-connected fracture network, with a high proportion of C-C branches, will delineate individual joint-bound blocks, with the block size approximately equal to the fracture spacing. Conversely, a poorly connected fracture network, with many I-I branches, may not delineate joint-bound blocks, even if the fracture density is high.

4.4 Estimation of block removal depth using Extrapolated Abrasion Surfaces

The principle of estimating depth of erosion by block removal after abrasion is based on constructing an artificial conceptual surface – the *extrapolated abrasion surface* – and calculating the elevation difference between that surface and the real DSM surface beneath. Extrapolated abrasion surfaces can be thought of as a smooth projected surface occurring 'in the air', that joins up all mapped abraded surfaces (Figure 4-1A). The extrapolated abrasion surfaces were generated by extracting the mapped abraded surfaces from the DSMs and converting these to points, with xyz values.

The points were attributed with both elevation (z) and slope values using the 'extract multi values to points' tool in ArcGIS. The points were then filtered to remove those with slope values > 10°, reducing the likelihood of points from adjacent steeper plucked faces and edges remaining in the dataset. The extrapolated abrasion surface point values were calculated by applying the *natural neighbour tool* within ArcGIS to the elevation values on the remaining points; these points were then converted into a raster. (Very similar methods are used to construct models for Quaternary sediment thickness). The present-day surface as represented by the UAV-derived DSM raster was then subtracted from the extrapolated abrasion surface to obtain values for estimated depth of erosion by block removal below the extrapolated abrasion surface.

This method of estimating depth of block removal – in essence a geometric subtraction – relies on the assumption that the modelled, extrapolated abrasion surface represents a continuous abraded surface prior to block removal. However, it may be the case that the abraded surface was damaged by block removal during a previous glaciation (Figure 4-1A); in that case the total erosion during the last glaciation will be over-estimated. It may also be the case that some block removal occurred early during the Late Weichselian glaciation in question: in that case the relative amount of abrasion will be over-estimated. The method also relies on surfaces being extrapolated *between* areas of abraded surfaces. The overall assumption is further discussed in Section 7.1.1. In the case of roche moutonnées uncertainty occurs in extent of plucking (e.g. block 2, 3, 4) during last glaciation, unless more TCN samples are analysed further away from the plucked edge (sample at C) (see Graham et al. 2023).

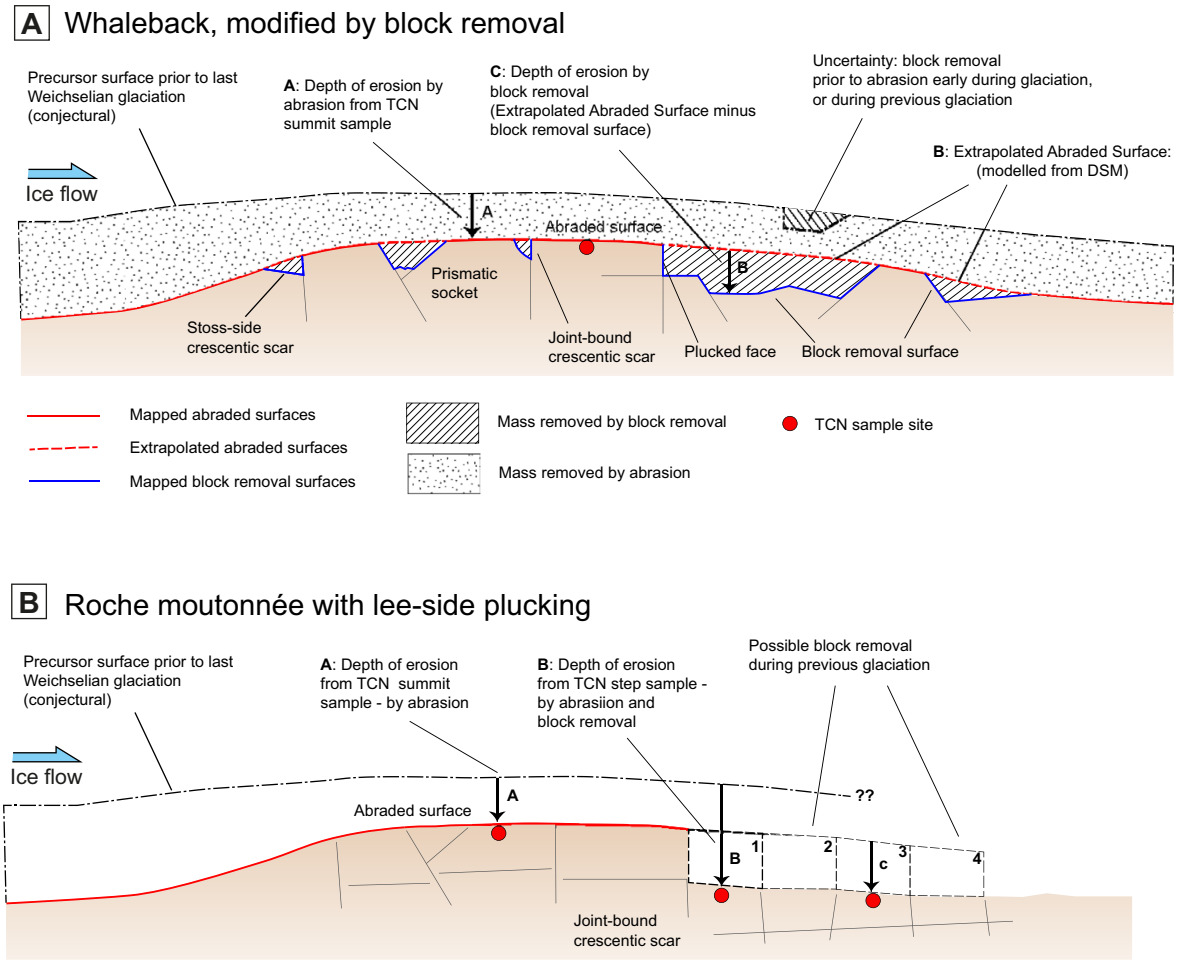

Figure 4-1. *Conceptual model of separating erosion by abrasion from erosion by block removal (by plucking and other processes). A. Whaleback, modified by block removal. Depth of abrasion is constrained by modelling of TCN inventories of abraded summit surfaces; depth of plucking is constrained by geomorphological mapping and modelling. Uncertainty occurs in that the precursor surface may have been affected by plucking in a previous glaciation. B. roche moutonnée with lee-side plucking. Depth of abrasion is constrained by modelling of TCN inventories of abraded summit surfaces at A; depth of plucking may be constrained by modelling of TCN inventories in stepped samples at B. Uncertainty occurs in extent of plucking (e.g. block 2, 3, 4) during last glaciation, unless more TCN samples are analysed further away from the plucked edge (sample at C) (see Graham et al. 2023).*

5 Results – Geomorphological mapping and site descriptions

5.1 Bedrock general characterisation

The bedrock geology has a bearing on the erodibility of the substrate as different lithologies with different fabrics and fracture characteristics respond differently to subglacial erosion. Although all rocks are basement gneisses, there are significant differences in lithology, fabric and fracture networks. Here we provide some general bedrock descriptions; descriptions for five study sites are given in the site descriptions. Although the terminology used herein is different from that Stephens et al. (2008) use, the broad classifications are consistent. The lithological observations and descriptions are also consistent but more detail relevant to subglacial erodibility is added. The following lithologies occur in the five different study areas (overview in Table 5-1):

Metadiorite. An intermediate meta-igneous rock, with approximate dioritic composition. Grainsize is coarse (1–4 mm) and the rock has a distinct speckly appearance (Figure 5-1A). The rock is 'massive': it has no penetrative banding or foliation and no strong anisotropy, although some narrow (< 5 cm) shear zones occur. This rock falls in the 'Group B – Diorite, metamorphic' in Stephens et al. (2008).

Felsic gneiss. These comprise felsic gneiss, typically of granitic to tonalitic composition, with poorly developed layering (Figure 5-1B). For a gneiss, the grainsize is quite fine (< 1–2 mm). Imposed ductile foliation can be strong or weak. These rock falls in the 'Group B – Granite, granodiorite, tonalite, metamorphic' in Stephens et al. (2008).

Felsic gneiss – banded. These comprise a strongly layered gneiss, with very distinct layers of different compositions, dominated by fine-grained (< 1–2 mm) felsic gneiss but with abundant and distinct alternating layers of intermediate gneiss and thin mafic, amphibolite layers (Figure 5-1C). Layering is typically on a 1–20 cm scale. The layering is likely a combination of original layering (by intrusive or extrusive processes) and superimposed strong ductile shearing. These rock falls in the 'Group A – Felsic to intermediate volcanic rock, metamorphic' in Stephens et al. (2008).

Amphibolite. Dark mafic rock, rich in amphibole, with highly variable grainsize (fine to coarse) and variable foliation development (Figure 5-1D). Generally occurs as thin (5–50 cm) layers within more felsic rock, but a wider (c 10 m) body occurs at Stora Asphällan.

Pegmatite – aplite veins. Various veins of granitic composition have intruded the older rocks, varying in thickness from 1 cm to c 1 m. These can vary from very coarse grained (> 10 mm, having a pegmatitic texture) to quite fine grained (< 2 mm, having an aplitic texture, e.g. Figure 5-1C). Some such veins and dykes cross-cut all the local ductile fabrics and appear to be undeformed themselves; elsewhere the veins are folded and deformed towards the local fabric. Whether this is due to different generations of dyke intrusion or heterogeneity of later imposed strain is uncertain. These rock falls in the 'Group D – Granite; pegmatite' but may include 'Group C – metagranitoids as dyke' in Stephens et al. (2008).

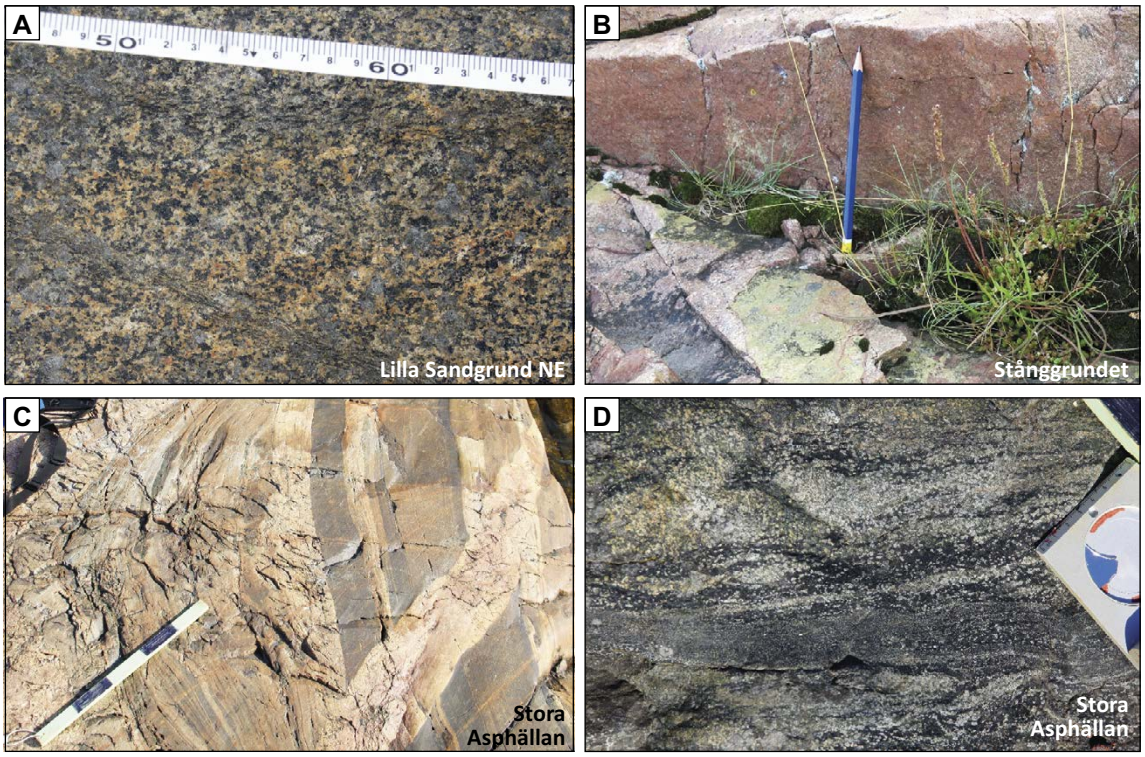

Figure 5-1. *Lithologies and fracture patterns. A. 'Massive', poorly foliated metadiorite. Lilla Sandgrund NE. B. Felsic gneiss, poorly banded, medium-fine grained. Note fracture surface with epidote and chlorite coating. Stånggrundet. C. Strongly banded felsic gneiss (possibly meta-rhyolite), with intermediate gneiss and amphibolite layers. Curving layering caused by boudinage. Cut by late aplitic granite vein. Stora Asphällan. D. Coarse and fine amphibolite, moderately well layered, poorly foliated. Stora Asphällan.*

Table 5-1. Summary table of dominant lithologies in the five study sites, compared to the grouping of Stephens et al. (2008). Note: 'layering' is a lithological layering, that may or may not constitute a mechanical discontinuity. 'Cleavage' is a ductile fabric that does constitute a mechanical discontinuity.

	Lilla Sandgrund NE	**Lilla Sandgrund West**	**Lilla Sandgrund SW**	**Stora Asphällan**	**Stånggrundet**
Lithology	Metadiorite, coarse-grained	Felsic gneiss, fine-grained	*West:* Felsic gneiss, fine-grained *East:* metadiorite, coarse	*West:* Felsic gneiss, banded, fine-grained; *East:* amphibolite: fine-to-coarse grained	Felsic gneiss, fine-grained
Layering, foliation, cleavage	No to poor foliation	Well-developed layering, NNE–SSW strike, oblique to ice flow	*West:* good layering, and cleavage, NNW–SSE strike, subparallel to ice flow *East:* No to poor foliation	*West:* moderate-good layering, poor cleavage, NW–SE strike, oblique to ice flow; *East:* No to poor foliation	moderate- to well-developed layering, WNW–ESE trending, high angles to ice flow; poor cleavage
Grouping (Stephens et al. 2008)	Group B – diorite	Group A – Felsic to intermediate volcanic rock	Group A and Group B	Group A and Group B – amphibolite	Group B – granite-granodiorite-tonalite

5.2 Fracture analysis – general observations

Fracture patterns are highly variable across the five sites. The Stånggrundet site is by far the most densely fractured, with a P21 density for steep fractures of 1.7 m^{-1} (drone image fracture mapping), roughly twice as dense as the other areas (Table 5-2). The other fracture density parameters at Stånggrundet are also twice as high as the other sites, albeit with different densities, inherent to the fracture analysis method (see Methods, Section 4.3). Stånggrundet also shows the highest connectivity, with 90 % C-C and C-I branches (Figure 5-2); Lilla Sandgrund West shows the lowest connectivity, with a high proportion of I-I and C-I branches (c 60 %). If only connected (C-C), steep fractures are considered, the fracture density at Stånggrundet is 2–5 times higher than the other areas. The Lilla Sandgrund sites have reasonably dense fracture networks in mapview (e.g. steep and subvertical fractures), but many fractures are unconnected so that the connected fracture density (P21 Density; C-C only) is very low. For subhorizontal to gently dipping fractures a similar picture emerges. Stånggrundet has numerous gently inclined fracture (2D aerial oblique window spacing: 0.6 m) whilst the Lilla Sandgrund sites have few (2D aerial window spacing: 1.2 to > 5 m) or no gently inclined fractures.

Table 5-2. Summary table of fracture parameters for all five study sites.

	Unit	Lilla Sandgrund NE	Lilla Sandgrund SW	Lilla Sandgrund West	Stora Asphällan	Stånggrundet
Drone image fracture mapping (2D – map view; steep fractures)						
Density (P21)	m^{-1}	1.15	0.82	0.70	1.10	1.73
Spacing	m	**0.87**	**1.22**	**1.43**	**0.91**	**0.58**
Frequency (P20)	m^{-2}	0.79	0.43	0.45	0.85	0.99
Density (P21) C-C only	m^{-1}	0.26	0.17	0.1	0.29	0.56
Density (P21) C-C and C-I only	m^{-1}	0.78	0.53	0.38	0.75	1.32
1D Scanline						
Intensity (P11) (mean)	*n*	3.33	4.30	3.08	4.88	6.48
Density (P10) (mean)	m^{-1}	1.22	2.05	1.10	2.51	5.43
Spacing (mean)	m	**0.82**	**0.49**	**0.91**	**0.40**	**0.18**
2D Window – oblique view (subhorizontal and gently inclined fractures < 35° only)						
Density (P21) (mean)	m^{-1}	0.20	0.00	0.15	0.85	1.65
Spacing	m	**4.99**	**n/a**	**6.89**	**1.17**	**0.61**
Frequency (P20) (mean)	*n*	0.14	0.02	0.18	0.61	0.92
Outcrop photo fracture mapping – section (2D section view – steep and gently dipping fractures)						
Density (P21)	m^{-1}					18.38
Spacing	m					**0.06**

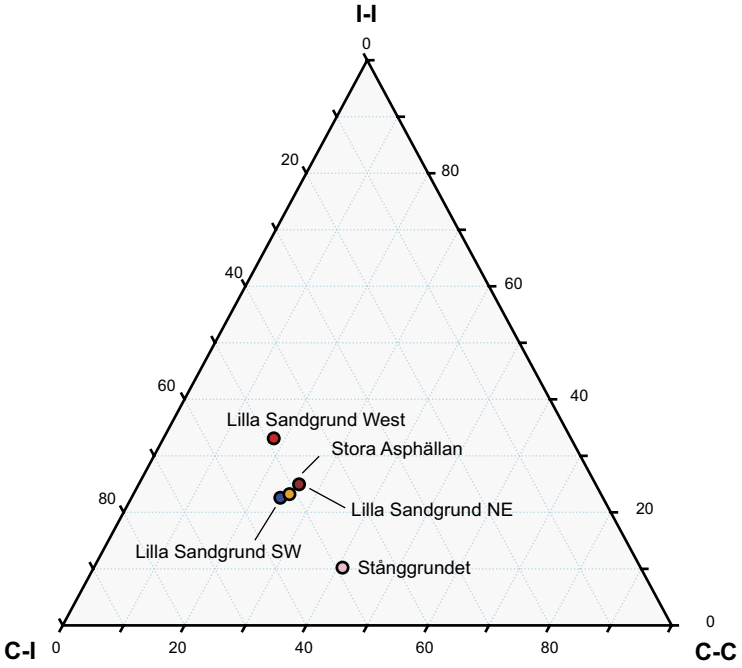

Figure 5-2. *Ternary diagram of connectivity of fracture branches. C-C are connected branches; I-I are isolated, unconnected branches, and C-I are partially connected branches.*

Fracture orientations (Figure 5-3) are dominated by broadly two subvertical sets: WNW–ESE and SW–NE. However, the relative proportion of these varies from site to site. More details are given in the individual site descriptions.

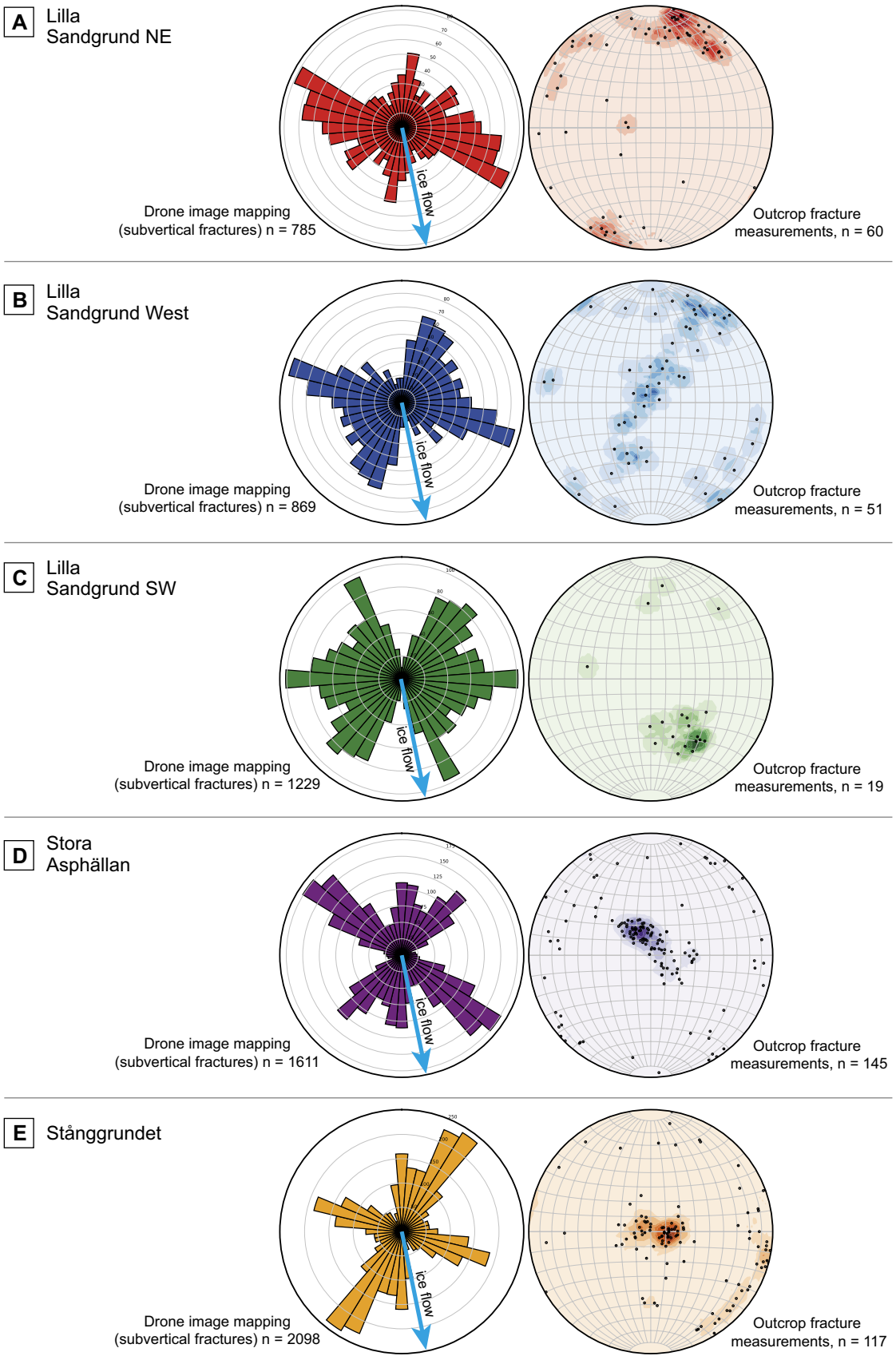

Figure 5-3. *Rose plots: digitised fractures traces from drone imagery (mainly returning subvertical and steeply inclined fractures). Stereoplot: fracture orientations from field measurement. Lower hemisphere, equal area projection.*

5.3 Geomorphological observations – general

At Forsmark, a variety of small-scale glacial erosional features occur (Figures 5-4, 5-4, 5-6). Many of these are well-known and described in the literature, such as abraded surfaces with striae, plucked (or quarried) surfaces and S-forms (Embleton and King 1975, Benn and Evans 2010, Prest 1983, Kor et al. 1991). However, some erosional features have only rarely been described whereas others have – to our knowledge – not been described in the literature before. Here we provide a general summary of the geomorphological observations with short characteristics of the different features, as used as classification for the geomorphological mapping.

Abraded surfaces occur in all localities and are characterised by a low-roughness (on the metre-decimetre scale), with low slopes (< 10°) and very low curvature, less than c 5° m^{-1} (Figure 5-4A). These low curvature surfaces mean that whalebacks with abrasion-dominated surfaces have a large half-wavelength, typically 10–50 m (e.g. Figure 5-4A); in contrast, the re-abraded surfaces have half wavelength of 1–2 m. Striae are abundant and are commonly long and locally up to 10 mm deep. In layered lithologies, abrasion affected different rocks differently (Figure 5-4B): thin layers of fine-grained amphibolite typically show deeper abrasion. On the mm scale the abraded surfaces are rougher than the polished surfaces of re-abraded surfaces, defined below, possibly due to longer exposure to subglacial weathering. Abraded surfaces may show crescentic fractures ('friction cracks' – see below) or have a '*chipped*' appearance (Figure 5-4C). Pegmatite dykes appear to be particularly susceptible to such chipping. Sockets may occur within the abraded surfaces.

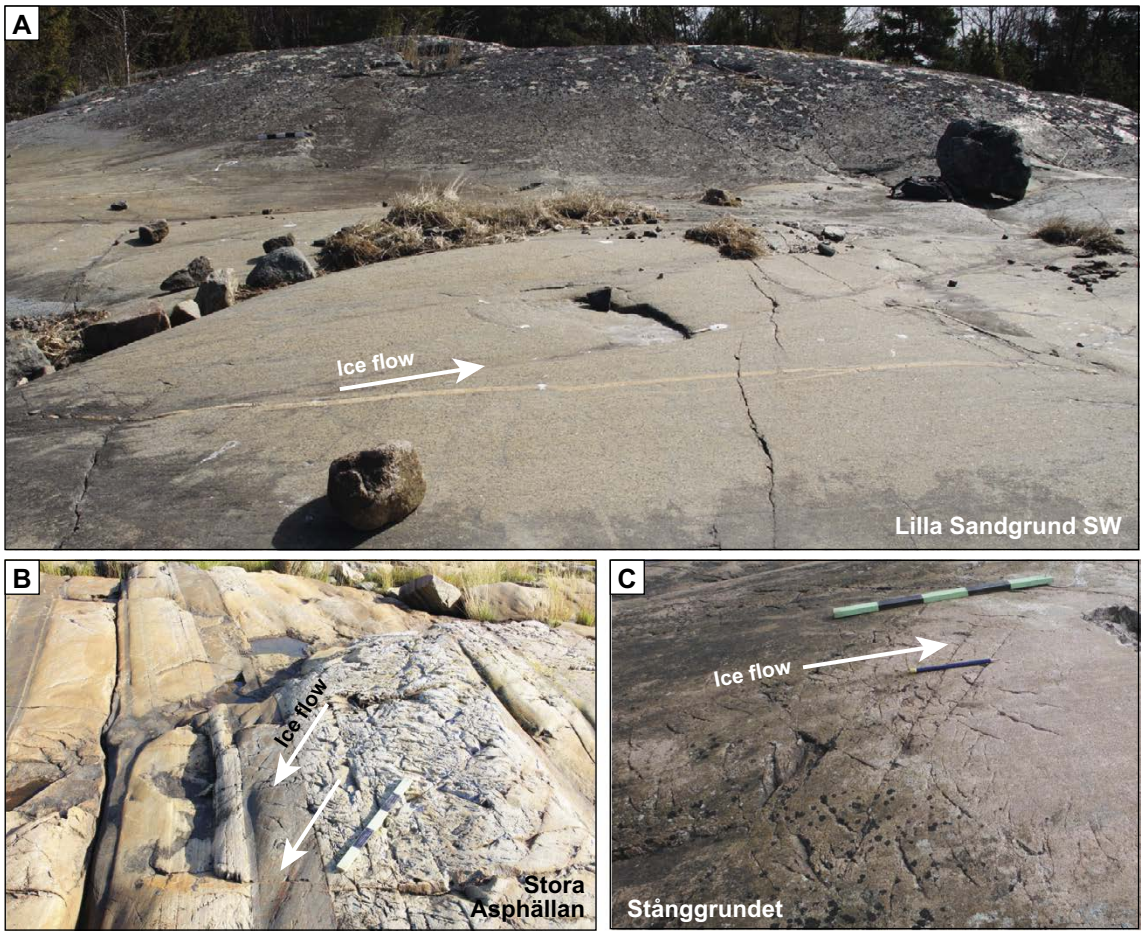

Figure 5-4. *Outcrop photos of abraded surfaces. A. Overview of Lilla Sandgrund SW: very low-curvature abraded surface, with minor chipping. Large erratic likely in situ; smaller boulders likely transported by post-glacial coastal processes. Note absence of subhorizontal fractures in whaleback in the background. Note 'spalling' of thin plates in the foreground. B. Abrasion surface on layered rock; striae and ice flow anti-clockwise from layering. Different rock types show different rates of abrasion; felsic rock shows extensive chipping. Stora Asphällan. C. Crescentic fractures ('friction cracks') on abraded top surface, slightly dipping up-ice. Stånggrundet.*

Block removal surfaces
These are any surface that has experienced *any* form of block removal, be it classic lee-side plucking or crescentic scarring or socket formation (Figure 5-5). Block removal surfaces are by definition fracture surfaces (a rock fragment has broken off the rock mass); such fracture surfaces can be newly formed, or follow pre-existing joints or fractures. Many newly formed fractures are conchoidal, others form the base of sockets, in which case that base has a ragged appearance (Figure 5-6F). If a fracture surface follows a pre-existing fracture, that surface is normally planar and shows continuity with a pre-existing fracture within the adjacent rock mass. In some cases, in particular at Stånggrundet, the distinction between the different block removal features proved transitional and/or ambiguous, preventing systematic mapping. In that case, all surfaces were mapped as "block removal surfaces (undivided)", to distinguish them from the abraded surfaces. The term will also be used when combining different block removal surfaces (Table 4-2).

Re-abraded surfaces
Re-abraded surfaces form initially by some form of block removal, but sharp edges have been rounded, and fracture surfaces have become smooth (Figure 5-5B). Although edges are rounded, the curvature of these surfaces is always greater (> to >> 45° m^{-1}) than that of purely abraded surfaces. The half-wavelength is inherited from the block removal surfaces, and is generally in the order of 0.5–2 m. In many places, composite sockets or lee-side regions of a roches moutonnées showed evidence of both fresh block removal and re-abraded surfaces. This suggests progressive excavation of such a socket. Commonly re-abraded surfaces are very smooth at the mm-scale, with a distinct polished feel, smoother than the abraded surfaces.

Plucked (quarried) surfaces show sharp edges above steep steps, normally down-ice or lateral-facing. The steep to subvertical plucked faces are typically (but not always) following pre-existing fractures (Figure 5-5A, B, C). Depending on the fracture orientation, lee-side, lateral or oblique plucking may dominate (Figure 5-5C). Plucked edges may be sharp and fresh, or show variable edge-rounding (Figure 5-5B).

Crescentic fractures
Crescentic fractures (e.g. Harris 1943, Okko 1950, Slocum 1978, Wintges 1985) are steeply dipping fractures, with a distinct curve, concave down-ice, not related to pre-existing fractures. At Forsmark, they are typically 5–20 cm long, but only appear to penetrate the rock surface by 2–5 cm (Figure 5-4C). They are common on abraded top and stoss sides and some surfaces contain so many crescentic fractures they overlap. The consistent curvature suggests a strong component of oblique contact stress, with a horizontal stress component parallel to ice flow.

Crescentic fractures in themselves do not remove rock, but they weaken the top surface of the rock. Where a patch of dense crescentic fracturing occur, individual fractures may link, and small *chips* (1–5 cm^3) may be removed from the rock surface (Figure 5-4C); when many of these chips amalgamate, they may evolve into a small *socket*. When crescentic fractures occur close to a steep pre-existing fracture, larger fragments may be removed: this situation is transitional to a *joint-bound crescentic scar* or *sockets* (see below and Figure 5-6A). Some lithologies appear to be more prone to crescentic fracturing (felsic rocks and pegmatite), presumably a function of their lower fracture toughness. *Chattermarks* are a specific set of crescentic fractures that appear in a row, parallel to ice flow (Benn and Evans 2010): these have not been observed at Forsmark.

Edge flaking
Edge flaking (or: edge chipping) has, to our knowledge, not been recognised as a macroscopic glacial erosional feature, but is well known to engineers and material scientists (Hangl et al. 1997) and flint knapping analysis (e.g. Speth 1972), and is particularly important for the design of dental materials (e.g. Quinn et al. 2000). Whalley and Krinsley (1974) and Sharp and Gomez (1986) observed edge flaking or very similar resultant textures at the grain scale in tills. Edge flaking consist of a curved, conchoidal fracture that does not follow pre-existing fractures. They occur close to a free edge (formed by a previous block removal event): in essence a flake is chipped off the edge (Figure 5-5D), modifying a previously formed plucked edge. Locally, crescentic fractures occur close to a previously plucked edge and appear to control or instigate edge flaking (Figure 5-5E).

Figure 5-5. *Outcrop photos of plucked surfaces and edges. White arrows = ice flow direction. Ab = abraded surface. A. Series of plucked edges, in densely fractured rock. Most plucked edges follow pre-existing fractures; the 'flats' follow pre-existing gently dipping fractures. Klubbudden. B. Lee-side and lateral plucking. Some plucked edges are fresh (PF); others are edge-rounded (rPF). Stånggrundet. C. Lateral plucking, controlled by N–S trending vertical fractures and subhorizontal fractures, slightly oblique to SSE-directed ice flow. Stånggrundet. D. Edge-flaking (EF) on edge formed by plucking (PF) that followed pre-existing fractures (Fr). Stora Asphällan. E. Combined plucking along fracture (Fr), edge-flaking (EF) and crescentic fracturing (CF). Note that density of crescentic fractures increases towards the free edge. Stånggrundet.*

Joint-bound crescentic scars

These are hollows or scars bound on the down-ice side by a pre-existing, planar, typically subvertical fracture surface and on the up-ice side by a new curved, conchoidal fracture. (Krabbendam et al. 2017). (Note that the 'classic' crescentic scars as described by Prest (1983) and Embleton and King (1975) do not note any relationship with a pre-existing fracture). The conchoidal fractures are typically shallow

dipping (20–30°) in the down-ice direction (Figure 5-6A). The edges of the scars are commonly rounded, suggesting that this type of scar developed some time prior to final deglaciation. A series of joint-bound crescentic scars may develop along the same 'master' fracture (Figure 5-6E).

'Reverse' joint-bound crescentic scars

These are similar to the joint-bound crescentic scars, except the pre-existing fracture is dipping down-ice, and the new fracture faces up-ice (Figure 5-6B). Normally the pre-existing fracture shows a gentle to moderate dip (20–60°) down-ice. The up-ice facing edge is typically curved or crescentic and does not follow any pre-existing fracture. The up-ice facing edge may show edge rounding due to subsequent abrasion. These features with the present relation to pre-existing fracture have, to our knowledge, not been described before.

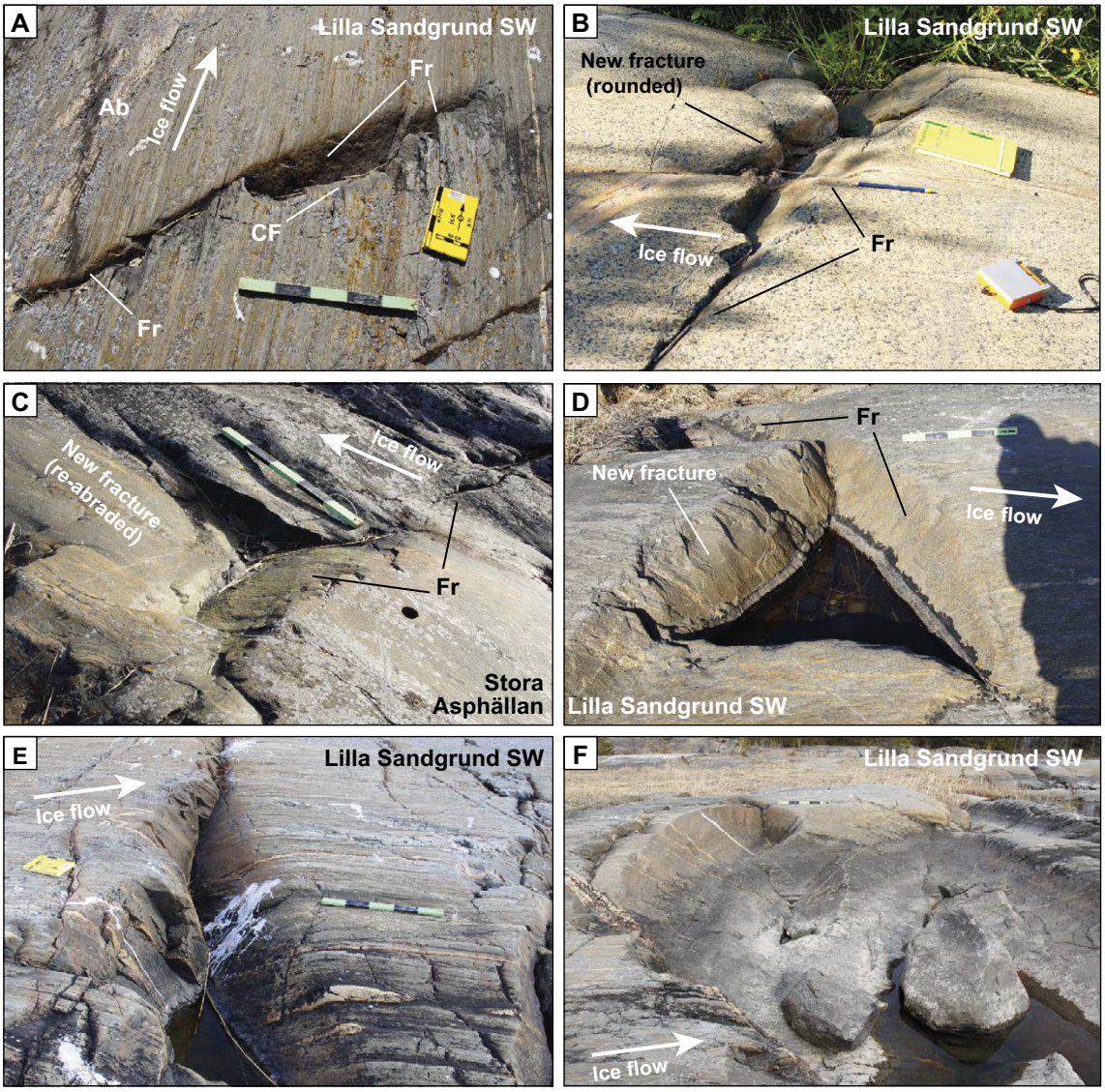

Figure 5-6. *Outcrop photos of sockets and joint-bound crescentic scars. A. Joint-bound crescentic scar, with existing fracture (Fr) on down-ice side and new conchoidal fracture (CF) in up-ice side. Lilla Sandgrund SW. B. 'Reverse joint-bound crescentic scar', with existing inclined fracture (Fr) on up-ice side and new fracture (strongly rounded) on up-ice side. C. Stoss-side joint-bound crescentic scar. Existing gently inclined fracture (Fr) on up-ice side, new fracture (re-abraded) on down-ice side. Stora Asphällan. D. Prismatic socket, triangular. Existing steeply inclined fracture (Fr) on down-ice side. Lilla Sandgrund SW. E. Composite socket, comprising a series of amalgamated joint-bound crescentic scars, with existing fracture (Fr) on down-ice side and new conchoidal fractures on up-ice side. Lilla Sandgrund SW. F. Composite socket, comprising amalgamated triangular sockets. Note ragged nature of the base of the socket, not constrained by subhorizontal fractures. Lilla Sandgrund SW.*

Stoss-side joint-bound crescentic scars

Whereas most joint-bound crescentic scars occur on the flatter top surfaces of roche moutonnées, this type of conchoidal fracturing occur on the stoss side. These scars can be noticeably bigger (10–30 cm deep) than those on flatter surfaces. Normally, they are bound by a pre-existing fracture on one side, and on the other side by new fracture facing (Figure 5-6C). New conchoidal fractures may link, resulting in a long (> 1 m) new fracture and large amount of material removed (approaching 1 m^3). The largest examples found occur on fairly steeply dipping (> 20°) stoss sides, as at Stora Asphällan. To our knowledge, these features have not been described in detail before.

Sockets

Sockets are distinct and relatively deep hollows with steep sides (Hall et al. 2019a), varying in depth from 5–50 cm, typically bound by fracture surfaces on one or more sides (Figure 5-6D). They can be closed on all sides, or open, normally on the down-ice side. Commonly they are triangular, with two or three sides controlled by fractures. Sockets are typically triangular or prismatic in shape – commonly controlled by the intersection of pre-existing joints: *prismatic sockets*. In some cases, the socket is open, more or less in the down-ice direction (in which case the situation is somewhat transitional to classic lee-side plucking) – these are termed *open sockets*. Small sockets can amalgamate into larger, composite (or nested) sockets.

Composite features

In numerous places different features have amalgamated to form composite hollows, often forming rock pools. Joint-bound crescentic scars, formed close together, can merge to form a linear set of amalgamated scars (Figure 5-6E). Prismatic sockets, possible combined with edge flaking, crescentic scarring and lee-side or lateral plucking, can merge to form amalgamated sockets (Figure 5-6F). Commonly such composite features show both rounded and sharp, angular edges suggesting a progressive development during deglaciation. The base of these composite features is typically ragged, with a variety of rough, fresh fracture surfaces, not controlled by subhorizontal fractures (Figure 5-6F).

Glacial striae

Glacial striae were measured and digitised on both abraded surfaces and re-abraded surfaces. They consistently point towards 170–160° (Figure 5-7). A smaller population points towards c 150°. At some locations the main set of glacial striae (to 170–160°) was seen to overprinted by striae with a more SE direction, suggesting a late phase of ice flow towards c 150°. This is consistent with the findings of Sohlenius et al. (2004).

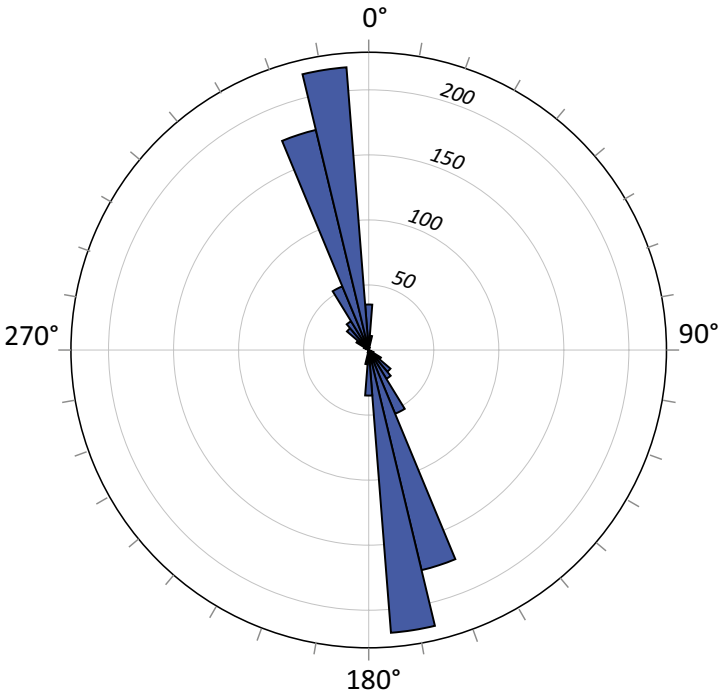

Figure 5-7. *Rose plot of measured and digitised glacial striae, n = 556.*

S-forms. The definition of S-forms is somewhat confused; Kor et al. (1991) probably provides the best summary. We take them here to mean smooth, but pronounced curvilinear features, that are likely formed by subglacial meltwater erosion. At Forsmark, S-forms are relatively rare and small: most are less than 5–20 cm deep and a few metres long at most. They are broadly aligned to ice flow. Locally they are controlled by lithology: many follow thin layers of fine-grained amphibolite, presumably as this rock type shows lower resistance to abrasion by debris-laden meltwater.

5.4 Lilla Sandgrund NE – site description

5.4.1 Bedrock and fracture network characterisation

The dominant rock at the Lilla Sandgrund NE site (Figure 5-8) is an intermediate meta-igneous rock (Figure 5-8B), with approximate dioritic composition (metadiorite). Grainsize is medium to coarse (1–4 mm) and the rock has a distinct speckly appearance. The rock is 'massive': it has no penetrative banding or foliation and no strong anisotropy, although some narrow (< 5 cm) shear zones occur. This rock falls in the 'Group B – Diorite, metamorphic' in Stephens et al. (2008). A few thin (< 10 cm) amphibolite layers occur in the area, trending NE–SW. Both the metadiorite and the amphibolite are cut by granitic dykes. These dykes have very variable grainsize, from a pegmatitic texture (grainsize 10–30 mm) to aplitic texture (grain size < 2 mm). The main dykes, locally > 1 metre thick, trend broadly E–W, at high angle to ice flow.

Lilla Sandgrund NE is dominated by a WNW–ESE trending fracture set (Figure 5-3A) which is distinct in both the drone mapping and the field data. The area is dominated by steep, subvertical fractures with > 50 % of measured fractures having dips > 70°. Horizontal fractures are rare in this area, with only a handful (n = 3) measured; none of these has great persistence. The WNW–ESE trending fractures are long fractures and show variable aperture from open to tight. Shorter and discontinuous NNE–SSW, NE–SW and E–W trending fractures are observed between the major set. The density of vertical fractures (Table 5-2) derived from the drone mapping is thus relatively high (P21 density 1.15 m^{-1}, spacing: 0.87 m), with similar figures derived from the 1D scanline analysis. The density of gently inclined fractures, derived from the 2D window analysis is very low (P21 density 0.2 m^{-1}, spacing: 5 m). The connectivity is low, with only 26 % of fractures having C-C branches (Figure 5-2; Table 5-2). Fracture density along a line parallel to SSE-directed ice flow is relatively high, but low at high angle to ice flow.

5.4.2 Geomorphological description

Numerous surfaces form a semi-continuous smooth surface at Lilla Sandgrund NE, and exhibit a SSW-trending set of striations that is particularly clear in water-washed areas. These surfaces are characterized by low slope angles (< 10–20°) and low roughness values and are interpreted as abraded surfaces (Figure 5-8C, D). These abraded surfaces are interspersed between areas where the surface is lower and rougher. These are interpreted as block removal surfaces and are commonly bounded on at least one side by fractures and steeper slopes (Figure 5-9A).

Edge flaking is also locally apparent where the up-ice abraded surface joins the plucked areas. The areas of block removal can be divided into those which only show evidence of plucking and those which have been affected by plucking followed by later abrasion. For example, a particularly well-defined east-dipping fracture surface (25° dip slope) approximately 30 square meters in area is apparent in the northern part of the site. Fracture coating is still present on the surface, which has been marked by glacial striations (Figure 5-9B). The surface is interpreted to have been initially produced by block removal along the fracture plane, followed by abrasion; these are mapped as re-abraded surfaces (Figure 5-8D).

Several S-forms were mapped across the site. These generally trend towards the south to SSE (Figure 5-8D) and follow amphibolite bands (Figure 5-9C). They are clearly defined but only comprise a small fraction of the surface area (1 %).

Overall 43 % of the surface at Lilla Sandgrund NE has been interpreted as purely abraded, with 56 % having been subjected to block removal (including both plucked and re-abraded surfaces) (Table 6-1).

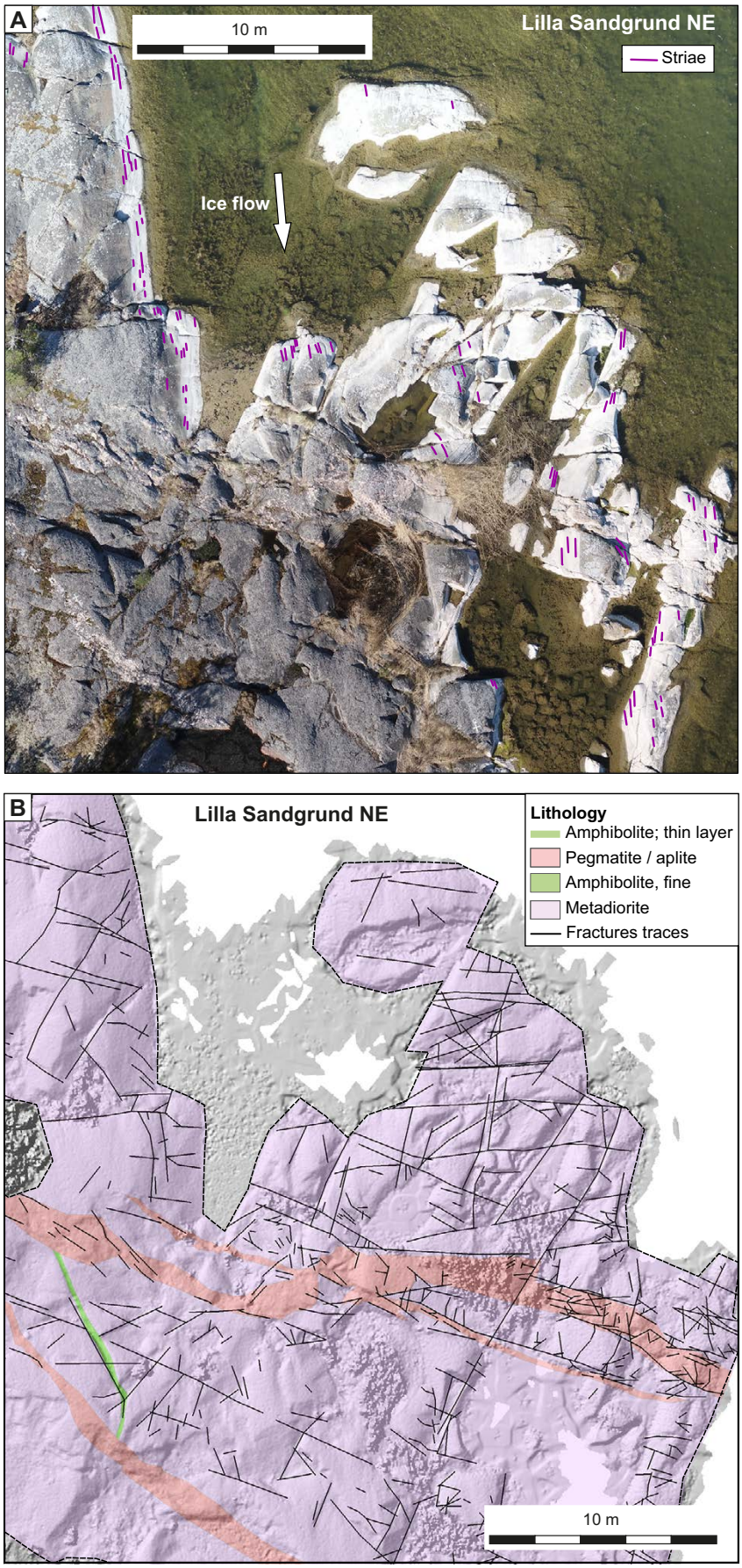

Figure 5-8. *Drone-acquired imagery and mapping for Lilla Sandgrund NE. A. Orthophoto, with striae traces. B. Lithology and fracture traces; hillshade from DSM as background.*

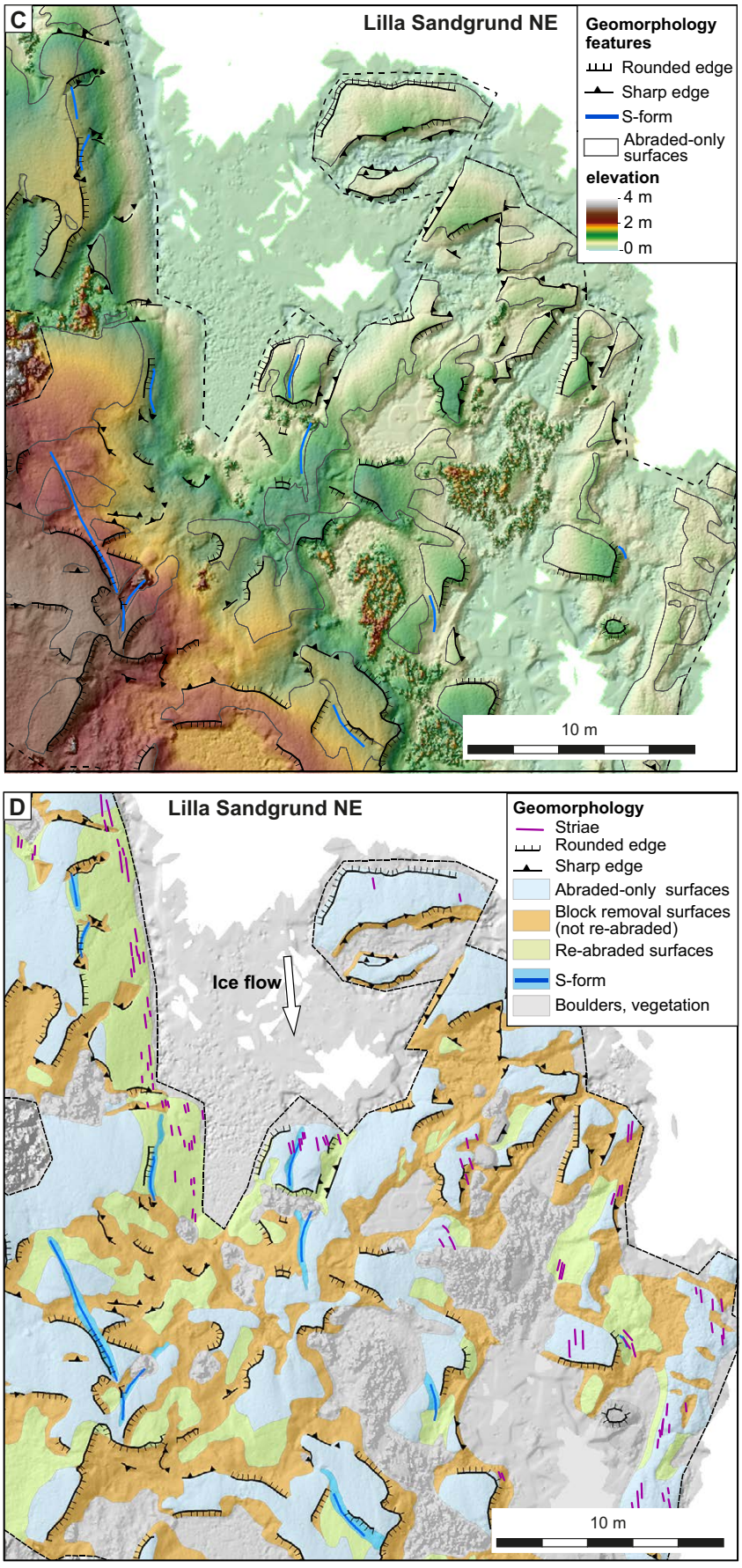

Figure 5-8 (cont). *C. Elevation with hillshade, linear geomorphological features and outlines of abraded surfaces. D. Geomorphological mapping, with hillshade.*

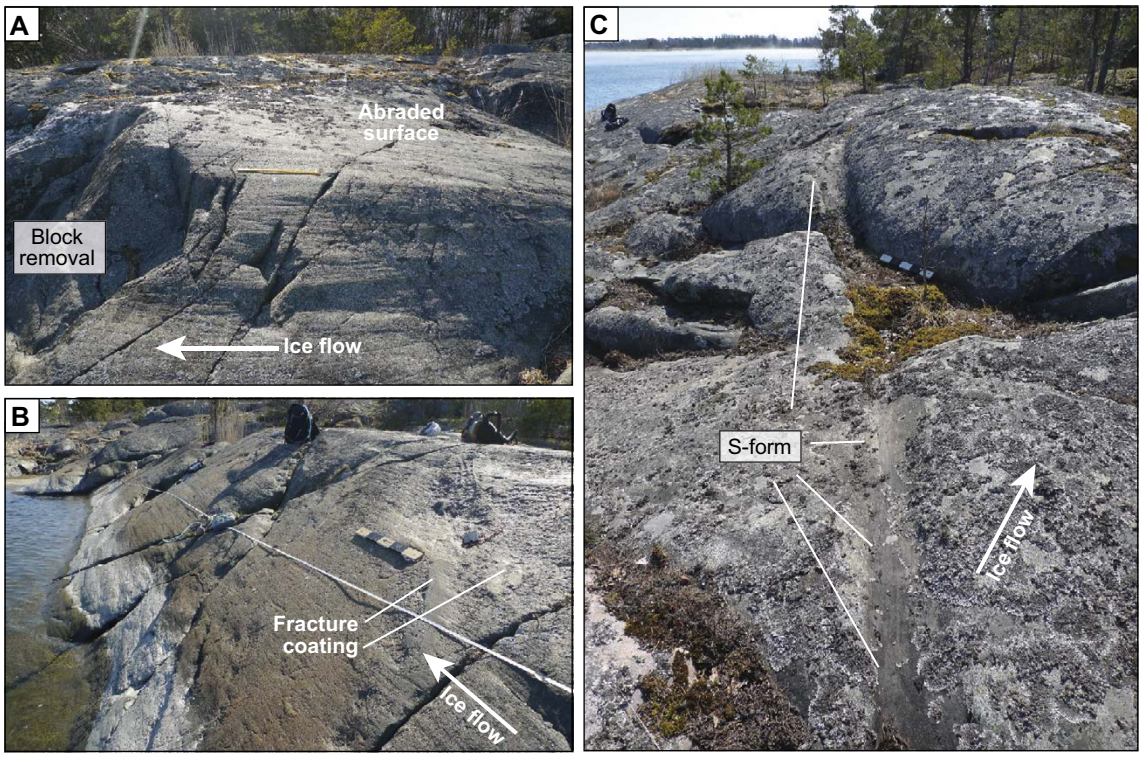

Figure 5-9. *Outcrop photos Lilla Sandgrund NE. A. Abraded surface, with block removal (lee-side plucking and lateral plucking) on the left. Ice flow right to left. B. Smooth surface with fracture coating still present. Although abraded, the overall surface was likely formed by block removal along a fracture plane. Classified as re-abraded surface. C. S-form, following a thin, fine-grained amphibolite layer. View to SE.*

5.5 Lilla Sandgrund West – site description

5.5.1 Bedrock and fracture network characterisation

The dominant rock type here is a fine-grained felsic rock, strongly sheared with well-developed layering. The layering is subvertical and trends NNE–SSW, at moderate angles to SSE-directed ice flow (Figure 5-10A, B). A network of substantial, pegmatitic granite dykes occur at angles to the main foliation, varying in width from < 0.1–5 m.

The drone image fracture mapping suggests a dominant WNW–ESE fracture set, with a subordinate NNE–SSW set (Figure 5-3). This latter set is parallel to the ductile foliation (Figure 5-10B). The fractures vary from open, tight to coated and are mineralised with a quartz and hematite. Over 50 % of the measured fractures dip over 53°. The drone mapping and the scanline returned the lowest density of fractures of all areas (P21 density 0.70 m^{-1}, spacing: 1.43 m; P10 density: 1.1 m^{-1}, spacing 0.91 m) (Table 5-2).

Only few gently inclined or subhorizontal fractures were observed within the 2D oblique window analysis, and density of these fractures is low (P21 density: 0.15 m^{-1}; spacing: 6.9 m). Fracture connectivity is low, with only 18 % of fractures comprising C-C branches (Figure 5-2; Table 5-2).

5.5.2 Geomorphological description

The site comprises a c 80 m long, N–S trending whaleback with several features characteristic of block-removal across its surface (Figure 5-10C, D). The northern stoss side of the whaleback is a low-angle, very smooth and abraded surface (Figure 5-11A), with local steps indicative of stoss-side block removal (Figure 5-11B). These small, plucked areas have been subjected to subsequent abrasion (demonstrated by presence of striations and polishing) with exception of areas close to the plucked edge where breaks in slope and rough surfaces suggests little or no subsequent abrasion.

The NW margin of the large rock moutonnée is characterized by laterally plucked surfaces with varying degrees of edge rounding (Figure 5-11D). Quantitative edge rounding measurements performed along this edge are described in Section 5.10.

On the crest of the whaleback, in the centre of the site, is a composite socket, with the present edge characteristic of stoss-side plucking with angular edges (Figure 5-11C). The floor of the feature, however, is rough and 'ragged' and large parts of this surface do not to follow pre-existing fractures but rather appear to be formed by breaking of intact bedrock.

A boulder with diameter of 1 m and two angular sides provides sits near crest of site (Figure 5-11E). This is largest boulder seen in area and may be indicate of largest size of block that have been removed in local area: the angular edges suggest limited transport.

Overall, 46 % of the surface is interpreted as abraded-only surfaces, with 54 % having been subjected to block removal (including re-abraded surfaces) (Table 6-1). Re-abraded surfaces occur in two settings: associated with freshly plucked surfaces but down-ice from freshly plucked edges; and as shallow scoops without clear lee-side edges (in SW of study site). The material lost from this surface is likely shallow.

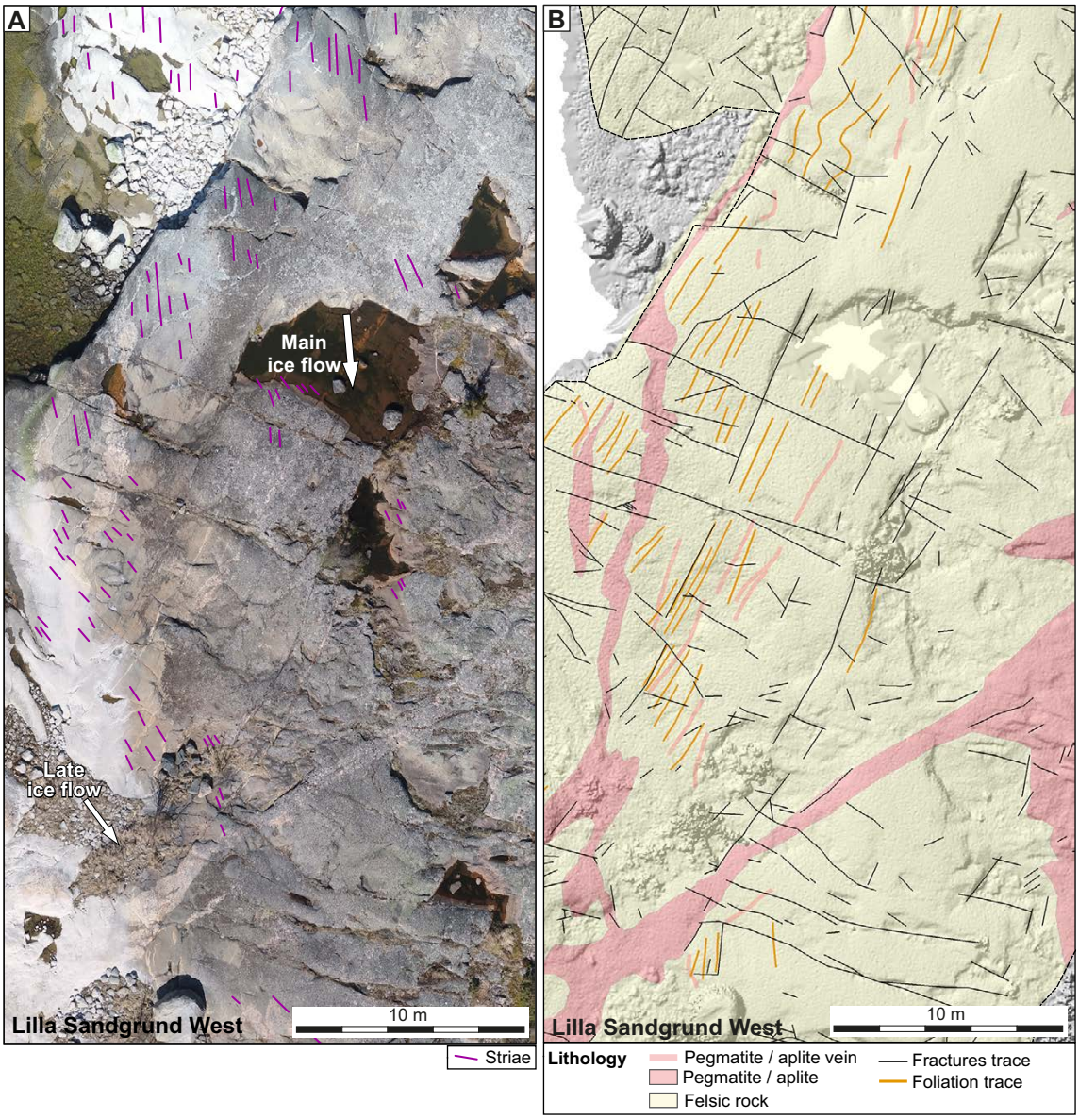

Figure 5-10. *Drone-acquired imagery and mapping for Lilla Sandgrund West. A. Orthophoto, with striae traces. B. Lithology and fracture traces; hillshade from DSM as background.*

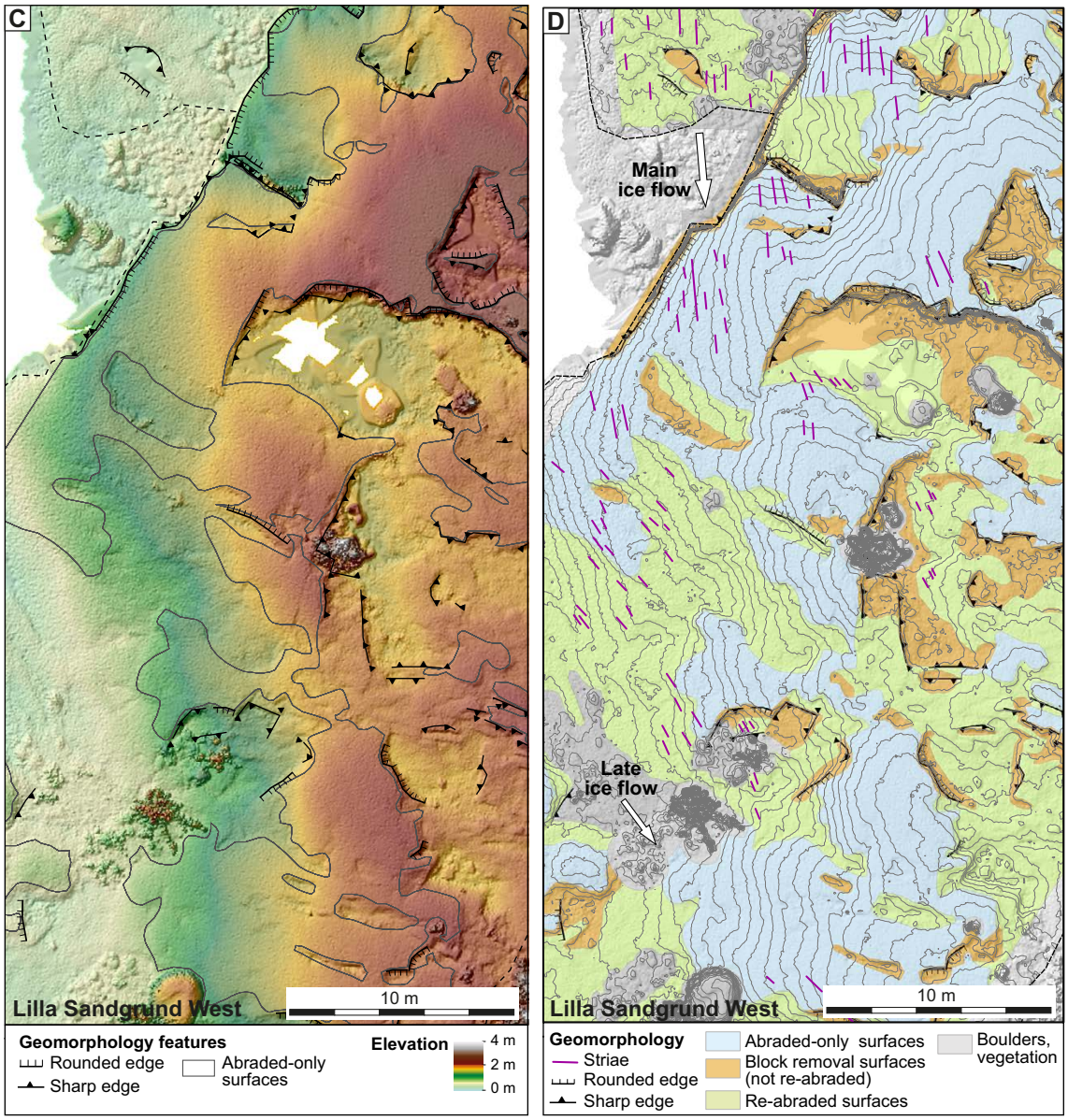

Figure 5-10 (cont). *C. Elevation with hillshade, linear geomorphological features and outlines of abraded surfaces. D. Geomorphological mapping, with hillshade.*

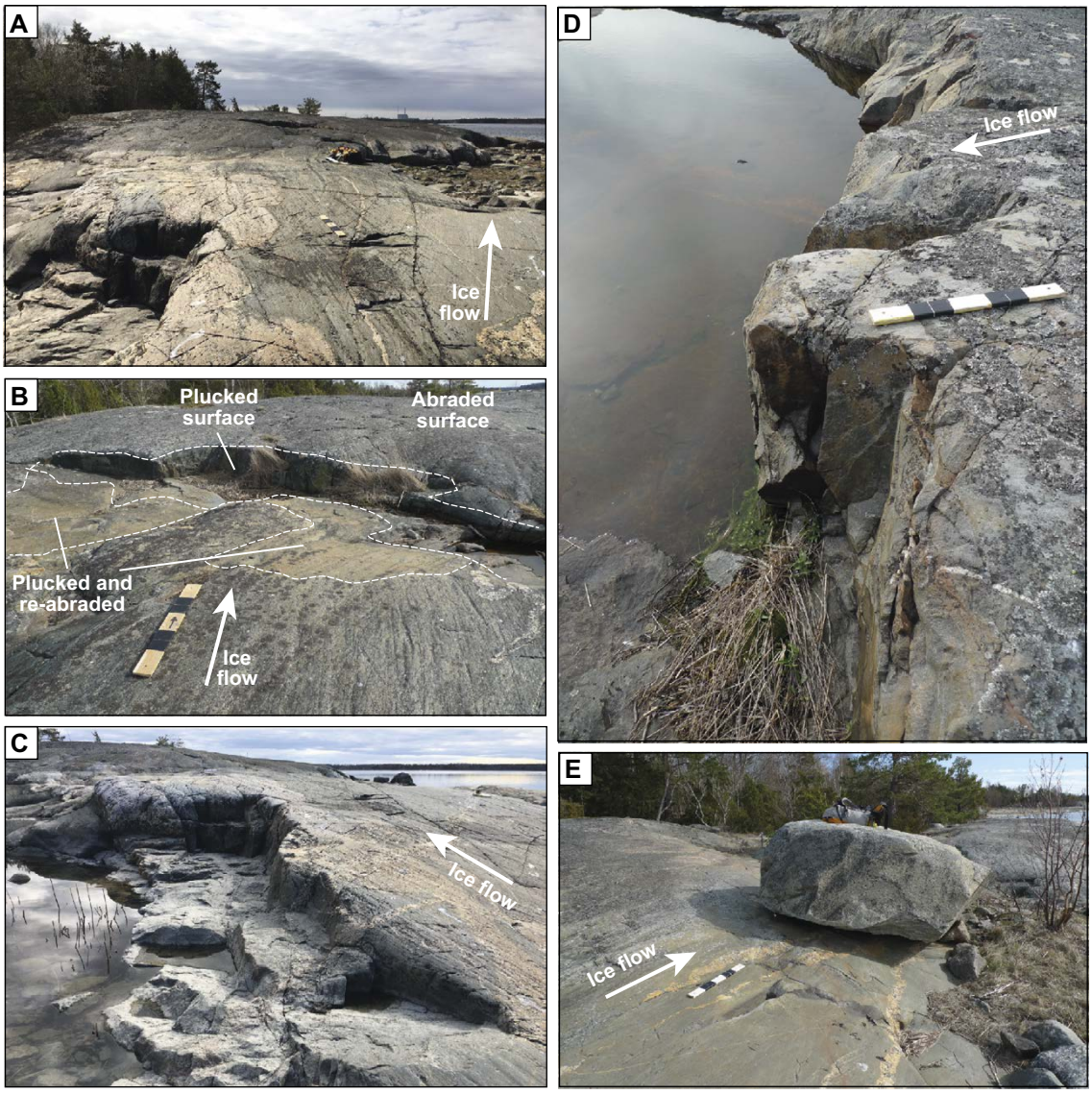

Figure 5-11. *Outcrop photos Lilla Sandgrund West. A. Down-ice overview of site, long-wavelength abraded surface with block removal to left. B. A freshly plucked edge, with plucked-and-abraded lower step (outlined), merging into abraded surface. C. Large composite open socket, with rounded and sharp edges. The floor of the open socket is ragged, formed by a series of fresh fractures, not controlled by pre-existing subhorizontal fractures D. Deep (c 1 m) step, showing lateral plucking; sharp and rounded edges. E. Large erratic on abraded surface. Rounding measurements in Section 5.10 were performed on edges in C and D.*

5.6 Lilla Sandgrund SW – site description

5.6.1 Bedrock and fracture network characterisation

The Lilla Sandgrund SW site contains two distinct lithologies (Figure 5-12A, B). In the east the rock is poorly foliated, massive intermediate metadiorite, similar to Lilla Sandgrund NE. In the west, the dominant rock type is a fine-grained felsic rock, strongly sheared with well-developed layering (banding) – similar also to Lilla Sandgrund West. This profound layering is subvertical and strikes NNW–SSE, subparallel to regional ice flow. The layering has developed (or: has reactivated) into a well-developed cleavage, forming mechanical discontinuities, that locally has been exploited by glacial erosion. Late granitic dykes, mainly with coarse pegmatitic texture, cut both the fine-grained felsic rock and the metadiorite.

Overall fracture density is low: the drone mapping returned a low density of fractures (P21: 0.82 m^{-1}, spacing 1.22 m), although the scanline survey returned a considerably higher density (P10: 2.05 m^{-1}, spacing 0.49 m) (Table 5-2). This suggests many fractures are tight, and not imaged on the orthophoto. The 2D window analysis did not pick up any subhorizontal or gently inclined fracture, so the density or spacing of gently inclined fractures cannot be quantified, except that spacing is higher than the local relief (c 3 m). Fracture connectivity is low, with only 18 % of fractures comprising C-C branches (Figure 5-2; Table 5-2). A slightly dominant steep to subvertical fracture set strikes ENE–WSW, but numerous subordinate sets strike NW–SE to SW–NE (Figure 5-3C).

5.6.2 Geomorphological description

The **western part of the area**, comprising felsic rocks, is dominated by smooth, low-curvature abraded surfaces, forming a c 30 m long whaleback. A dominant set of striae trends to SSE, whilst a late SE-trending set of striae occurs locally. There is an abundance small (< 50 cm long; < 20 cm deep) sockets, evidently controlled by the dominant ENE–WSW fracture set (Figure 5-6A; 5-12C, D; 13-A). Small sockets have amalgamated into longer (0.5–2 m) nested sockets along same fracture (Figure 5-6E). Some large, triangular sockets are controlled by the ENE–WSW and the NW–SE fracture sets, as well as the NNW–SSE trending foliation (Figure 5-4D). The overall area shows large abraded surfaces, re-abraded surfaces, and sockets with blocks still present (Figure 5-13A, B). The latter suggests that sockets grow progressively, rather than being formed in one event.

In centre, an elongate depression has developed (5 × > 25 m; c 1 m deep), which largely has been re-abraded, but has freshly plucked faces on the up-ice and the lateral sides. Lateral sides show triangular plucked edges, controlled by the two main fracture sets (Figure 5-13C). Another similar, smaller depression has a base of triangular steps, suggesting it formed by amalgamation of sockets and further removal of triangular blocks, rather than being controlled by a single basal fracture.

A substantial area, mapped as re-abraded surface, in fact comprises a complex surface showing both freshly plucked surfaces and re-abraded surfaces (Figure 5-13B). This surface has considerable roughness at a small wave-length (< 1 m), but their lowest surfaces are < 50 cm below the mapped abraded surface, suggesting shallow but relatively widespread block removal.

In the **eastern part of the area**, comprising metadiorite, outcrops are dominated by smooth abraded surfaces on their stoss sides (Figure 5-4A). Small sockets occur on the stoss and top side. The top and lee-sides of the main hill or whaleback show rougher surfaces, with a variety of freshly plucked edges, rounded plucked edges and sockets. Overall, this area can be seen as a shallow (10–30 cm) depression comprising re-abraded surfaces, which are locally further plucked, typically to a depth of 20–40 cm. Locally some ‘islands’ of abraded surfaces are still present (Figure 5-12D); these constrain the abraded surface prior to plucking and block removal.

A set of shallow (5–20 cm deep) S-forms occur on the lateral WSW side (Figure 5-12C, D; 13D).

Overall, Lilla Sandgrund SW shows 51 % of the surface area being abraded surfaces, and 48 % of the area plucked, including sockets and re-abraded surfaces (see Table 6-1).

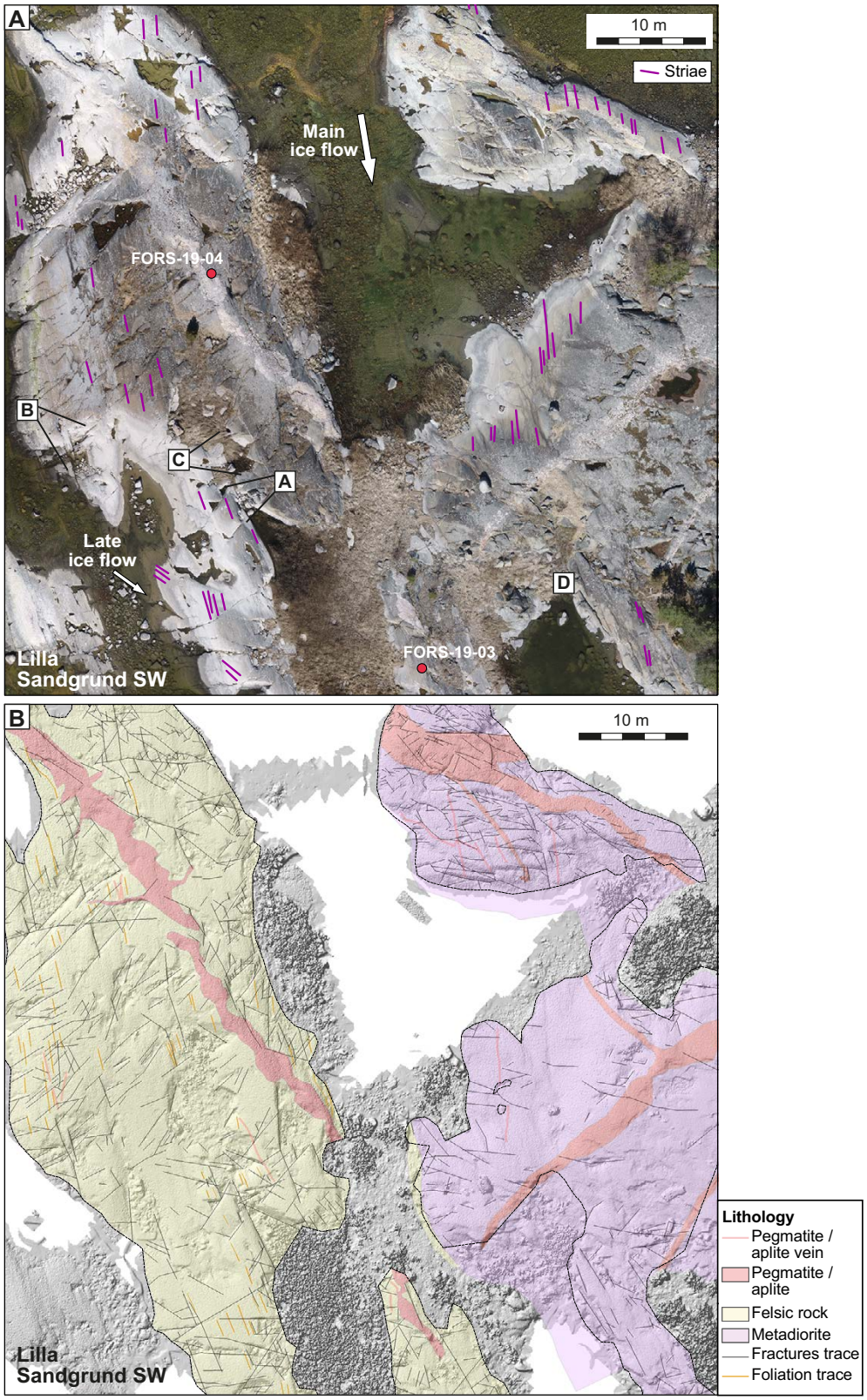

Figure 5-12. *Drone-acquired imagery and mapping for Lilla Sandgrund SW. A. Orthophoto, with striae traces. A, B, C, D: locations of field photos in Figure 5-13. B. Lithology and fracture traces; hillshade from DSM as background.*

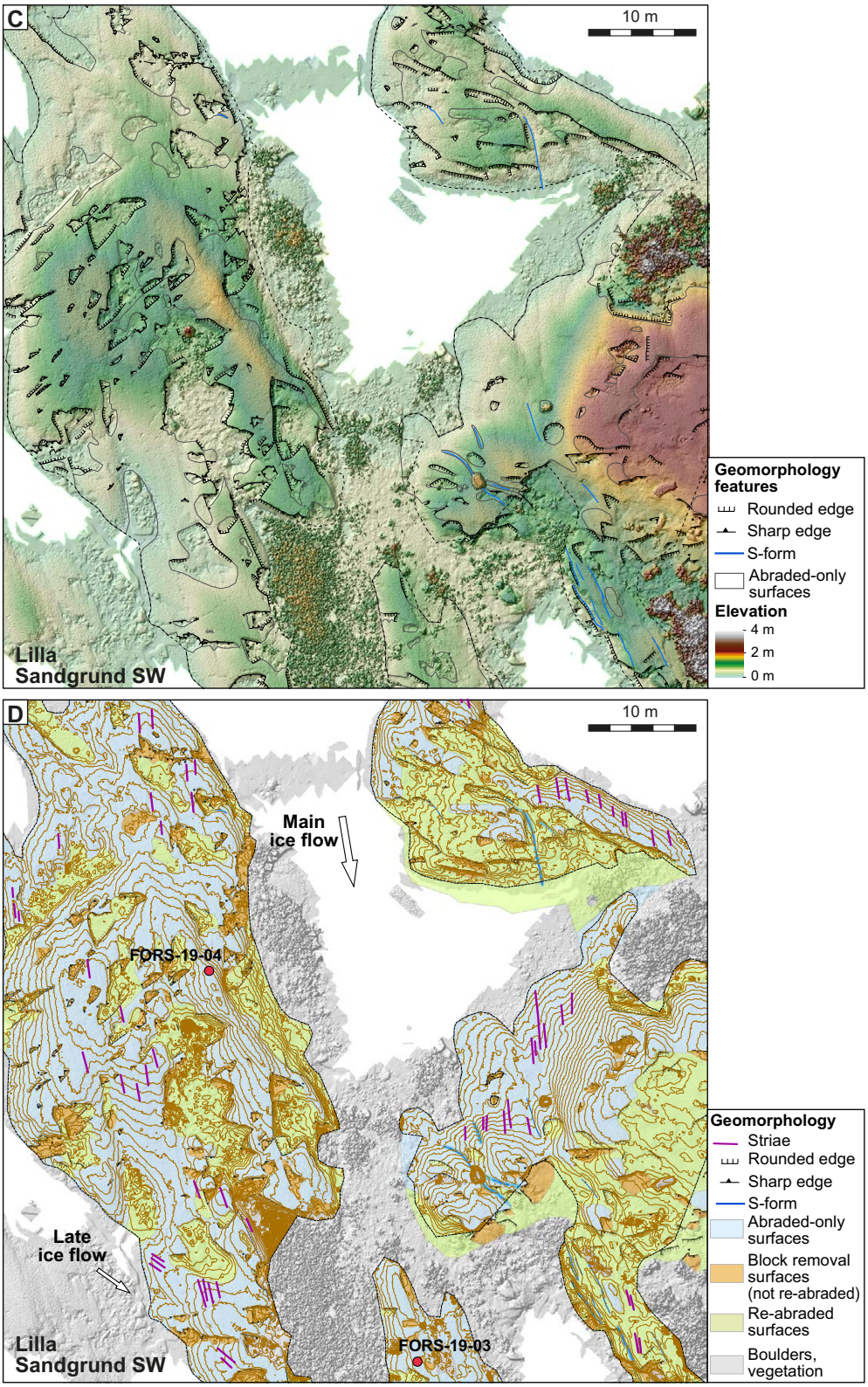

Figure 5-12 (cont). *C. Elevation with hillshade, linear geomorphological features and outlines of abraded surfaces. D. Geomorphological mapping, with hillshade.*

Figure 5-13. *Outcrop photos Lilla Sandgrund SW. Location shown on Figure 5-12A. A. Overview photo, showing abraded surfaces in the background. In foreground a freshly formed socket with some blocks still present; other sockets show rounded edges. B. Complex surface showing both freshly plucked surfaces and re-abraded surfaces. C. Central depression. Triangular facets suggest lateral plucking controlled by two fracture sets. Lee-side edges still show fracture coatings; stoss-side show pronounced edge rounding. D. S-forms.*

5.7 Stora Asphällan – site description

5.7.1 Bedrock and fracture network characterisation

The study area of Stora Asphällan (Figure 5-14) comprises two distinct lithologies, described in detail as Excursion stop 7 in Stephens et al. (2010). In the SW, it comprises mainly felsic rocks with very strong layering caused by strong, high-temperature shearing, with highly strained layers of felsic layering with different compositions as well as thin amphibolite layers, locally as strung-out boudins (Figure 5-1C; 5-15). This strong layering is subvertical and strikes NW–SE, slightly oblique to regional SSE-directed ice flow (Figure 5-4B). No profound grain-shape fabric occurs, despite the strong layering, presumably due to strong recrystallization and the absence of phyllosilicates. This unit was classified as 'Group A, felsic to intermediate volcanic rock, metamorphic', with dacitic to rhyolitic composition in Stephens et al. (2008). Immediately to the SE are the somewhat coarser granite-granodiorite rocks of Group C (Stephens et al. 2008).

In the NE the rock is a more massive amphibolite unit, with fine-medium and coarse-grained varieties (Figure 5-1D). The amphibolite is generally poorly foliated, but also contains domains that are more strongly foliated. Despite a distinct layering and locally well-developed grain-shape fabric, no cleavage or fractures developed parallel to the layering. It falls in the 'Group B: Diorite, quartz diorite and gabbro' (Stephens et al. 2008), and has been mapped as a distinct lens within the fine-grained felsic rocks of Group A.

Stora Asphällan is an area of highly variable fracture characteristics, which is strongly controlled by lithology. Overall, fracture density of steeply inclined fractures from the drone image mapping (Table 5-2) is moderate (P21 density: 1.1 m^{-1}, spacing 0.9); higher densities were obtained from the scanline (P10 density 2.51 m^{-1}, spacing 0.4 m). Fracture density of horizontal and gently inclined fractures from the 2D window mapping is fairly high (P21 density: 0.85 m^{-1}, spacing 1.17). Fracture connectivity is relatively low, with about a quarter of fractures having C-C branches (Figure 5-2; Table 5-2).

The fracture network in the amphibolite is highly anisotropic with strong N–S, NW–SE and NE–SW fracture sets (Figure 5-3D). The NW–SE and NE–SW sets comprise a series of long fractures that span the length of the outcrop (Figure 5-14B). The fractures are mostly tight with occasional open features and mineralisation is mostly quartz and epidote. The felsic rock outcrop has a fracture pattern that appears strongly controlled by the rock fabric, with a dominant NW–SE fracture set comprising long continuous fractures parallel to the ductile layering and foliation and a minor NE–SW set that comprises short interconnecting fractures. From the field data, the fracture dips across the study site are 50 % above 25° and 25 % above 72° (Figure 5-3D).

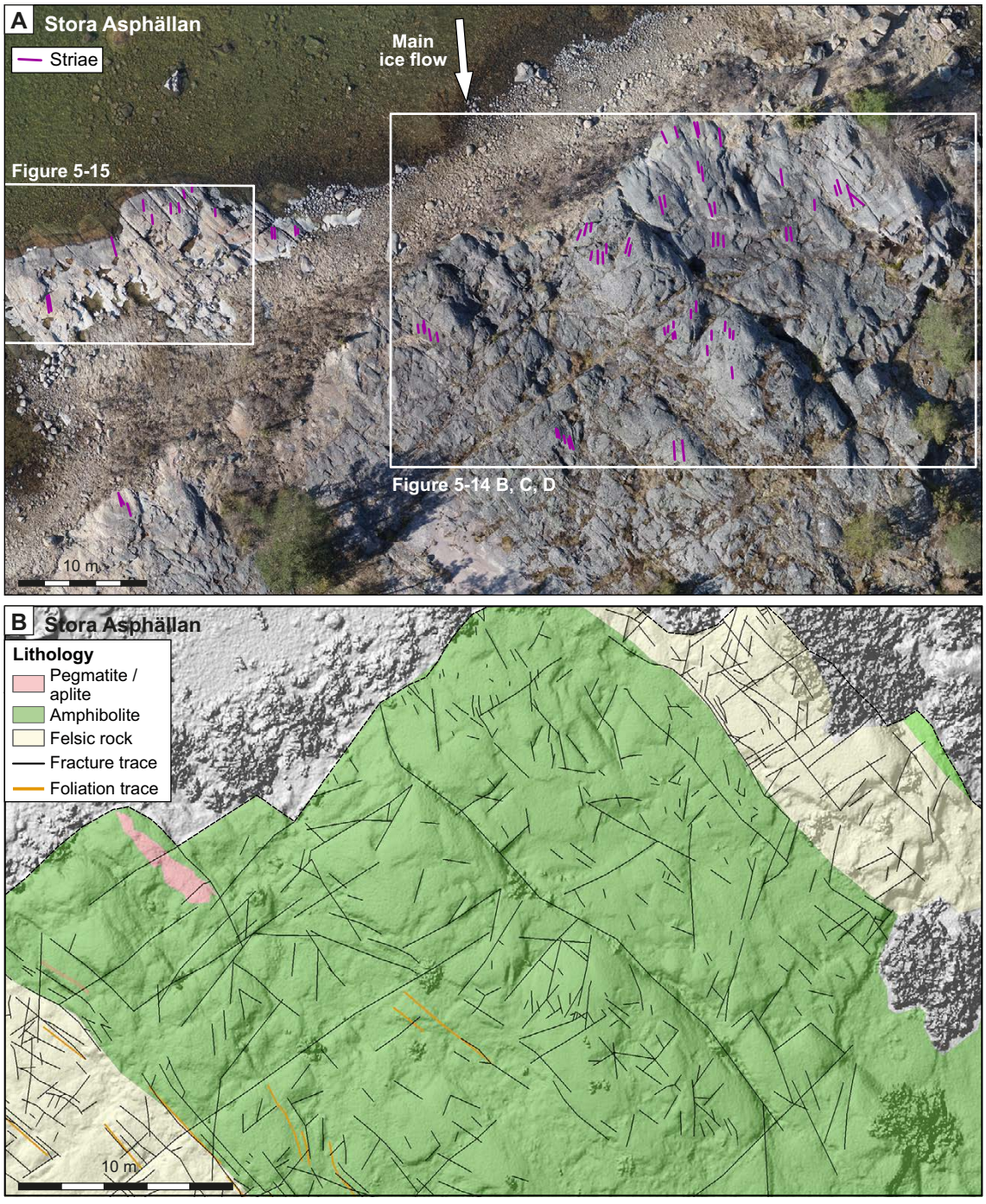

Figure 5-14. *Drone-acquired imagery and mapping for Stora Asphällan. A. Orthophoto, with striae traces. B. Lithology and fracture traces; hillshade from DSM as background. TCN sample FORS-17-12 occurs c 500 m to the east.*

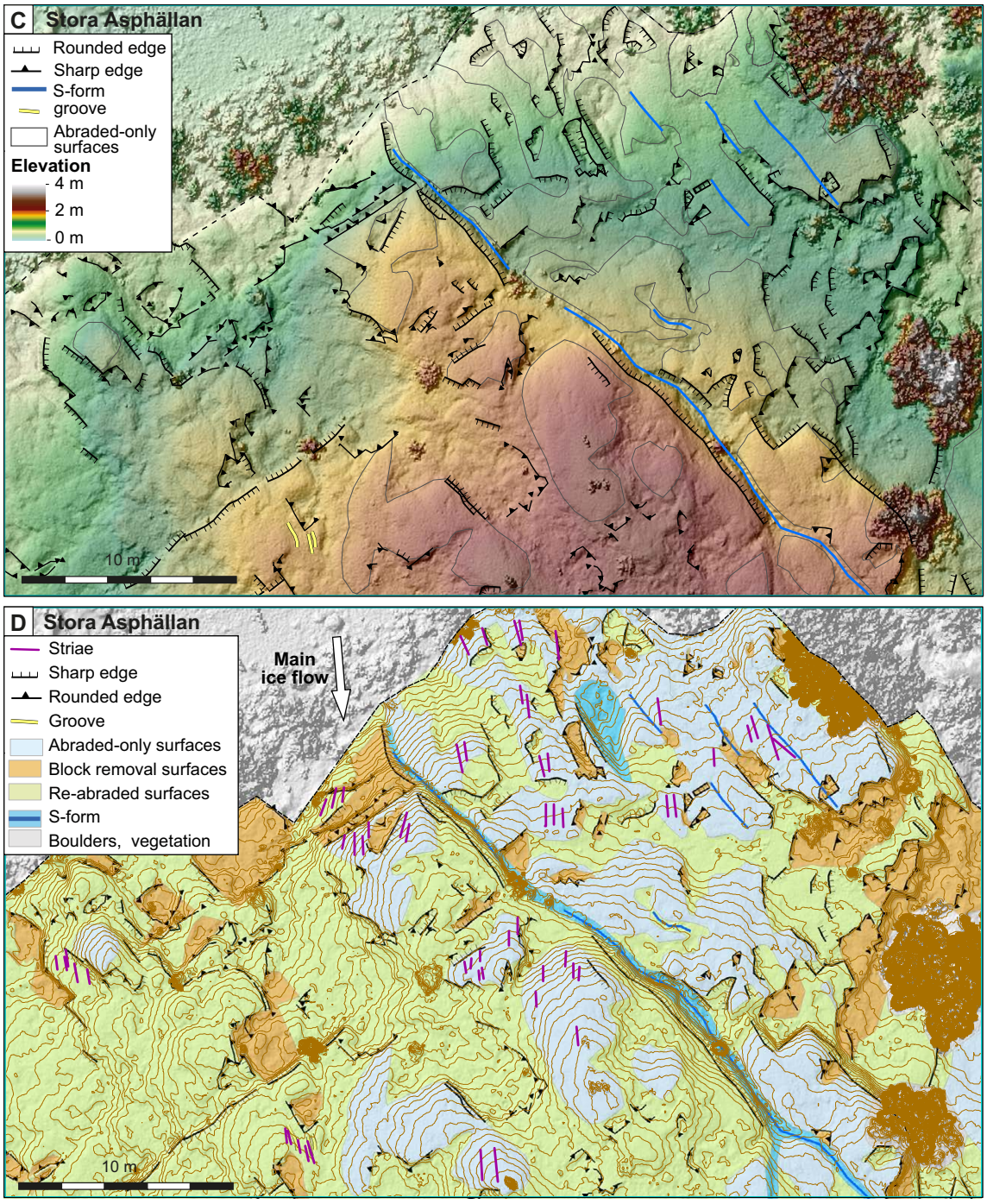

Figure 5-14 (cont). *C. Elevation with hillshade, linear geomorphological features and outlines of abraded surfaces. D. Geomorphological mapping, with hillshade.*

5.7.2 Geomorphological description

The felsic rocks in the west shows a generally flat area, with a combination of abraded surfaces, shallow plucking, and small sockets and crescentic scars (Figure 5-15). Broadly speaking, purely abraded surfaces occur on the up-ice (NNW) side (Figure 5-15D). Due to the strong lithological differences, some grooves have been abraded out: these follow the lithological bands in a SE trend, oblique to the SSE-directed ice flow (Figure 5-4B). Freshly plucked surfaces are marked by sharp edges, locally marked by additional edge flaking (Figure 5-5D). However, much of the plucked areas have been re-abraded, in particular in the down-ice direction (Figure 5-15). Both the plucked and re-abraded surfaces are shallow, and less than 30–50 cm below the abraded surface. Some abraded 'islands' still stand proud of the plucked or re-abraded surfaces. One distinct socket or scar occurs in the east, associated with a WSW–ENE trending fault. TCN sample site FORS-17-12 occurs on a flat surface, c 500 m east of the mapped site, but has a similar lithology to the felsic rocks within the mapped area. It is a very flat and smooth area, suggesting it being an abraded-only surface, but this has not been confirmed by the DSM data, as it occurs outside the area of the DSM drone survey.

The amphibolite outcrop in the east of Stora Asphällan constitutes a small hill, 3–4 m higher than flatter surrounding area (Figure 5-14C, D). Purely abraded surfaces occur throughout but occupy only a minor component of the surface. Classic lee-side plucked surfaces occur in the east, with both fresh and edge-rounded edges. On the stoss-side a group of stoss-side crescentic scars occur – among the largest seen (Figure 5-6C). A long S-form cuts the outcrop in a NW–SE trend, likely controlled by a fracture or foliation plane, and separating the highest part of the hill in the SW from some lower part in the NE (Figure 5-14C, D). However, much of the surface is classified as re-abraded, with rounded edges. Numerous sockets appear to link with S-forms, but generally have very rounded edges. Edge-rounding is more pronounced and common than in all other areas: it is possible that some block removal occurred prior to the last glaciation, and that the features here have experienced abrasion-only during the last glaciation (further discussed in Section 7.2.3). Much of the top of the hill and the western slope show a combination of shallow plucking with both fresh and rounded edges, most of this constitutes a re-abraded surface (Figure 5-14C, D).

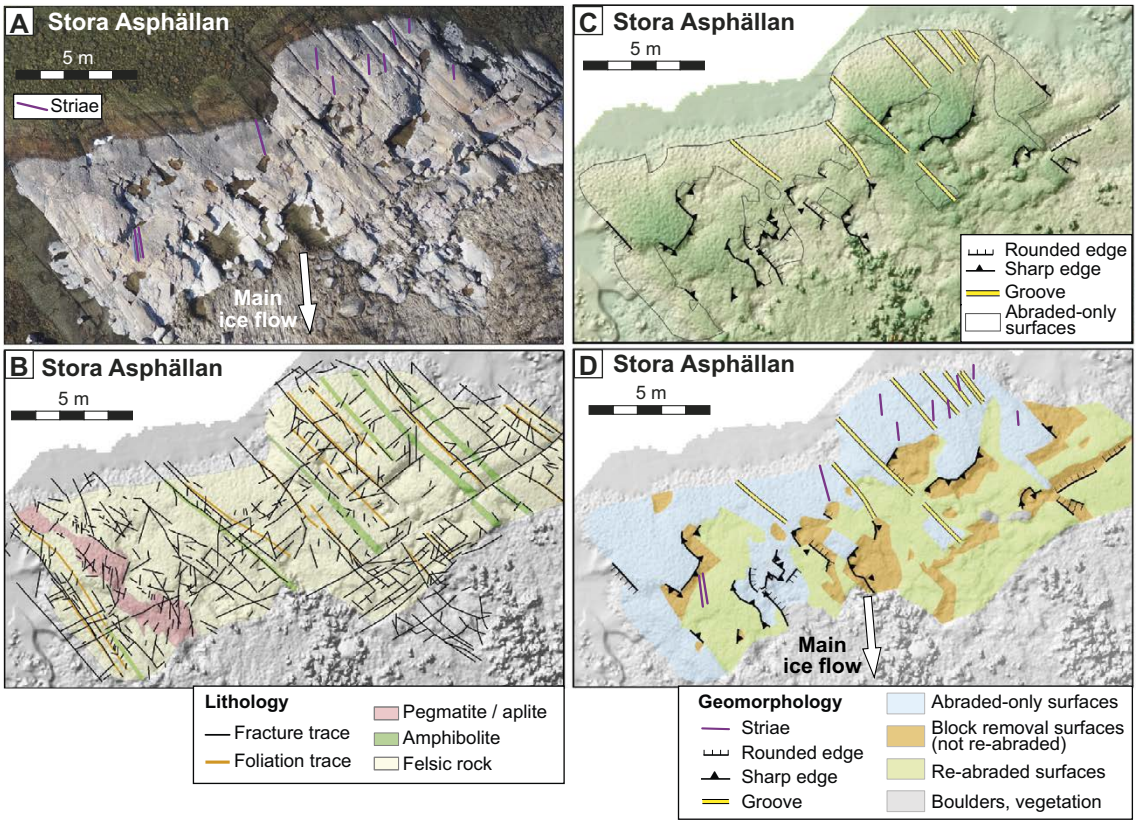

Figure 5-15. *Stora Asphällan NE sector. A. Orthophoto, with glacial striae. B. Bedrock map, with foliation traces and glacial striae. C. Elevation with hillshade, linear geomorphological features and outlines of abraded surfaces. D. Geomorphological mapping, with hillshade.*

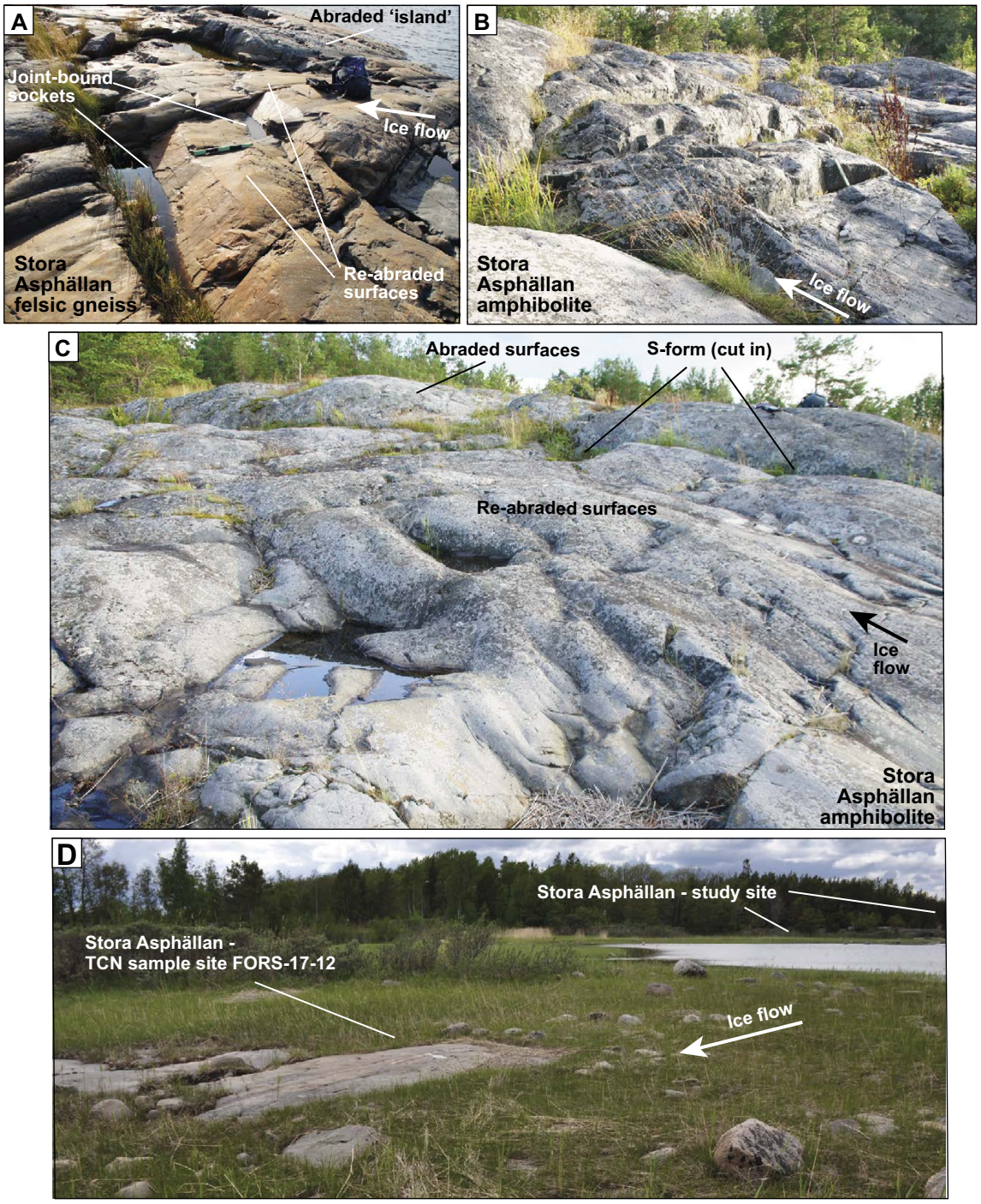

Figure 5-16. *Outcrop photos at Stora Asphällan. A. Flat surface on felsic gneiss, with abraded surfaces, re-abraded surfaces and joint-bound elongate sockets. B. Stoss-side of high amphibolite roche moutonnée, with stoss-side scars. C. Re-abraded surfaces, note small wave-length and extensive edge rounding. D. Situation of TCN sample site FORS-17-12 on felsic gneiss; Stora Asphällan site with amphibolite in the distance.*

5.8 Stånggrundet – site description

5.8.1 Bedrock and fracture network characterisation

The main lithology at the Stånggrundet site (Figure 5-17) is a siliceous felsic metamorphic rock, typically fine-grained (< 1 mm) (Figure 5-1B), with subordinate amphibolite lenses and layers, typically 10–50 cm thick. The rock falls into 'Group B aplitic granite / granodiorite' in Stephens et al. (2008) and is similar to the more fine-grained lithologies of Klubbudden, c 600 m to the ENE, described in detail as Stop 6 in Stephens (2010). Stånggrundet lies at the southern edge of the ductile shearing of the Singö Deformation Zone (Figure 2-2B; Stephens et al. 2008). The felsic rock shows a moderate- to well-developed layering of alternating thin mafic layers (< 1 mm) with felsic layers (> 10 mm).

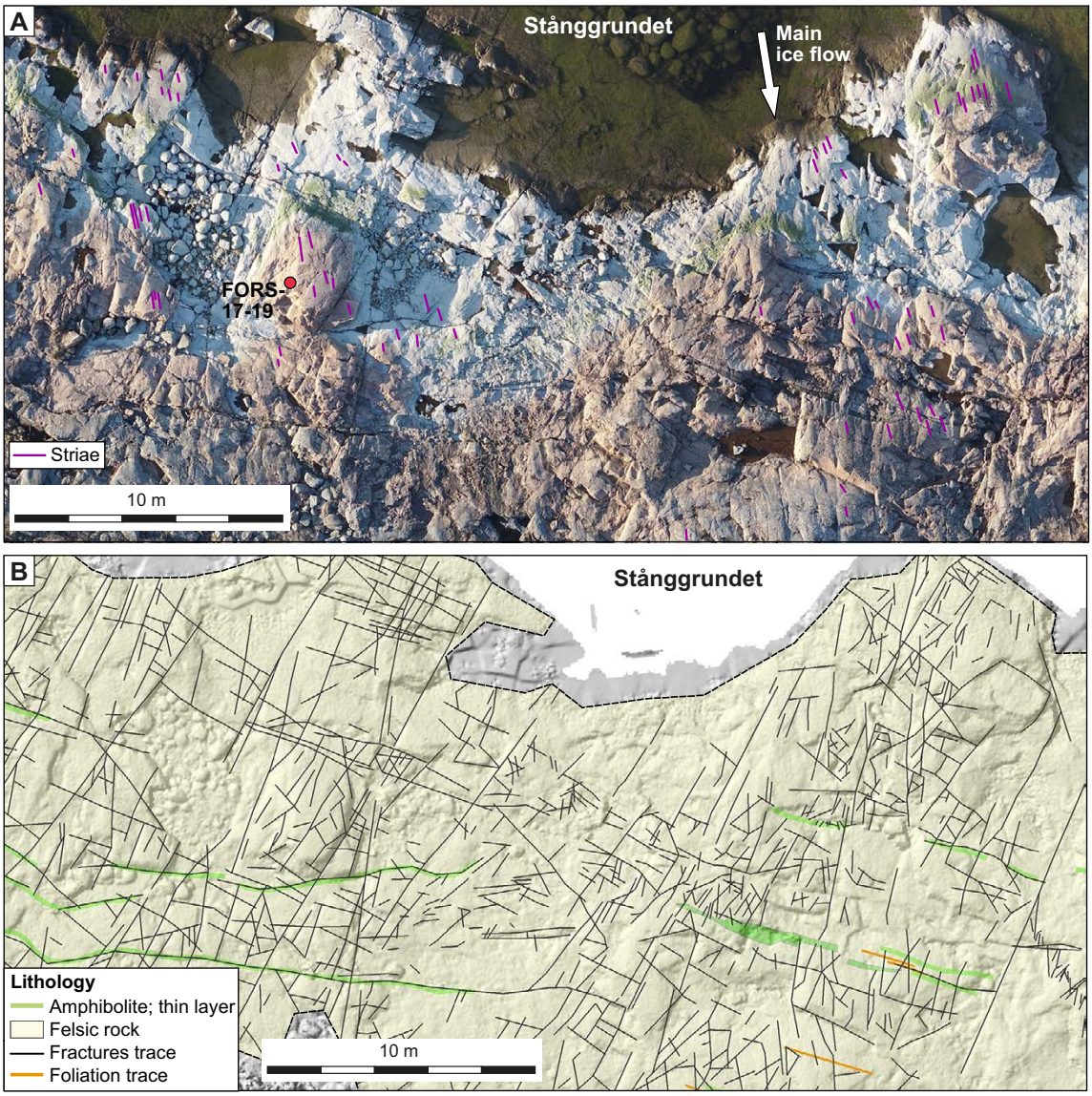

Figure 5-17. *Drone-acquired imagery and mapping for Stånggrundet. A. Orthophoto, with striae traces. B. Lithology and fracture traces; hillshade from DSM as background. Location of TCN sample site FORS-17-19 indicated; sample site FORS-17-14 lies c 70 m farther west.*

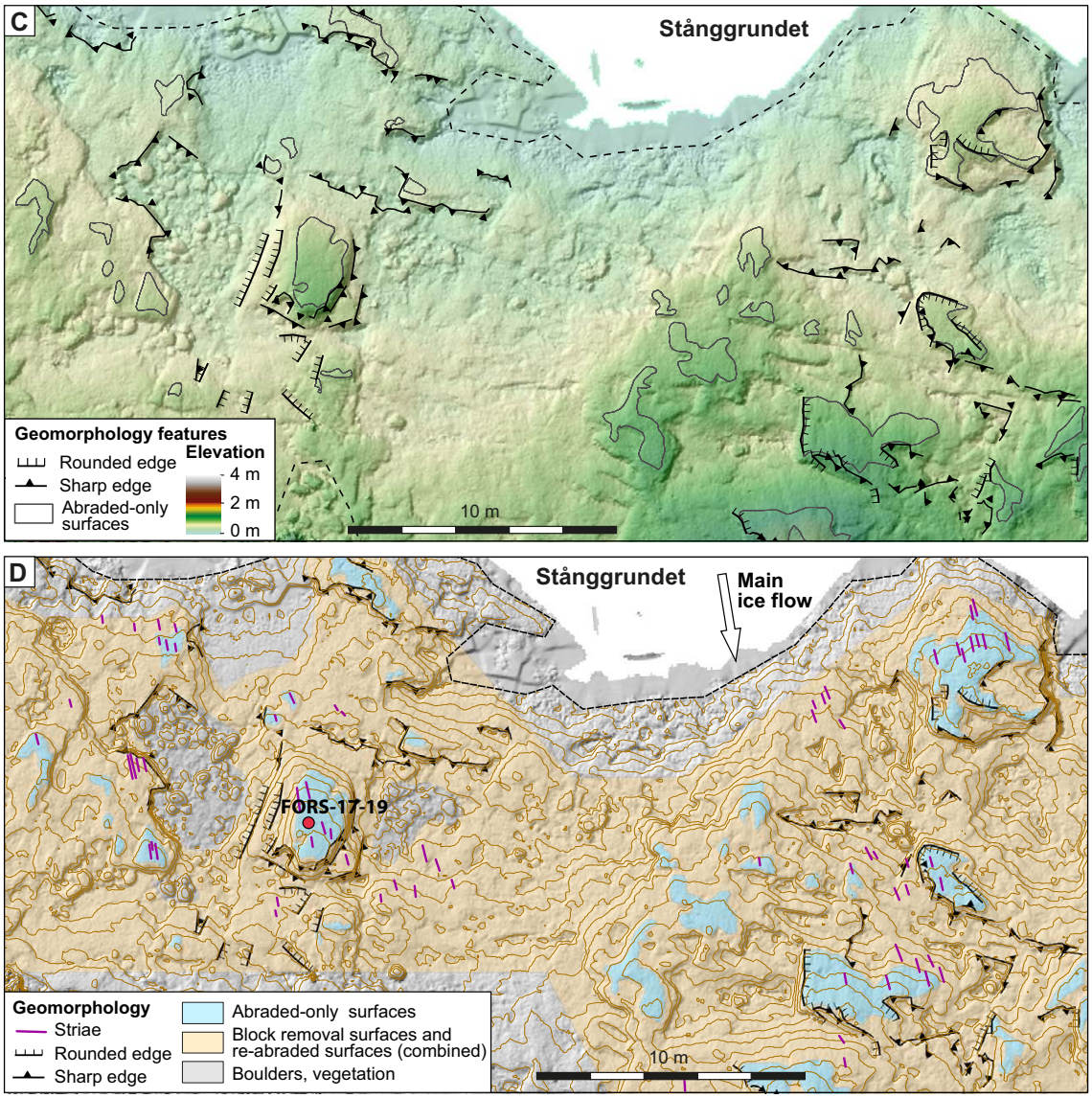

Figure 5-17 (cont). *C. Elevation with hillshade, linear geomorphological features and outlines of abraded surfaces. D. Geomorphological mapping, with hillshade. Fresh block removal surfaces and re-abraded surfaces could not be separated and are combined. Location of TCN sample site FORS-17-19 indicated.*

No strong grain shape fabric is apparent, presumably due to strong recrystallisation. The layering is not associated with penetrative foliation or mechanical discontinuities, except where coincident with the amphibolite layers, which are commonly followed by distinct and long fractures. The layering is subvertical and trends consistently WNW–ESE (Figure 5-17B), at high angles to ice flow, except in the SW side of the area, where several metre-scale folds results in irregular orientations.

Of all the areas, Stånggrundet is the most densely fractured (Table 5-2). Fracture density from the drone image mapping is the highest of all areas (P21 density: 1.73 m^{-1}, spacing 0.58 m); as is the 1D scanline density (P10 density: 5.43 m^{-1}, spacing 0.18 m). The difference again suggests many fractures are tight, and not picked up in the drone image mapping. Most fractures are tight or sealed and commonly show hematite coating, but open fractures occur closer to the surface. Density of horizontal and gently inclined fractures is much higher than at any other site (P21 density: 1.65 m^{-1}, spacing 0.61 m). These fractures generally dip gently (10–20°) to the WNW.

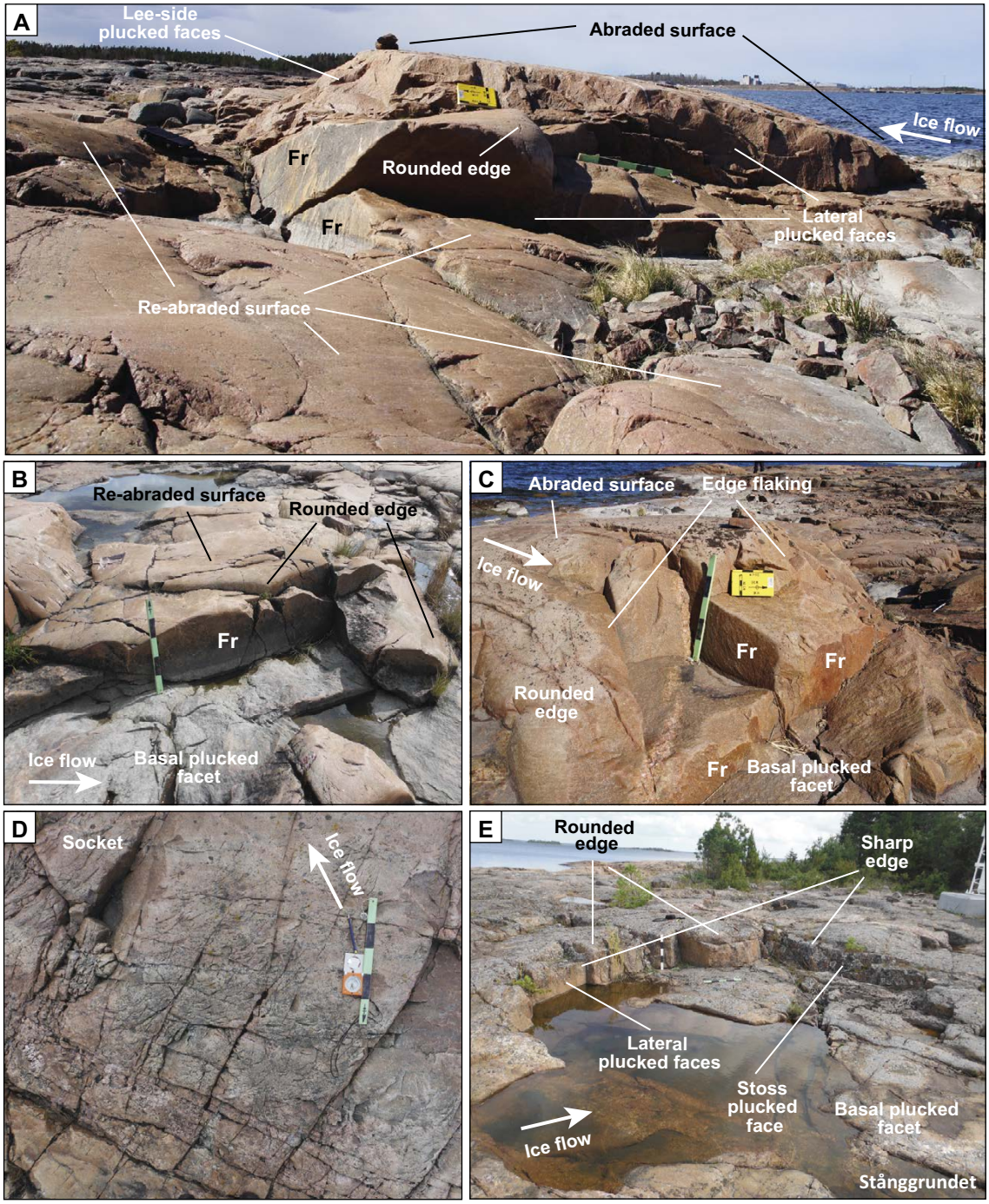

Figure 5-18. *Outcrop photos Stånggrundet. A. Upstanding roche moutonnée with abraded top, bound on lee and lateral sides by fresh plucked faces. Lower ground has abundant re-abraded surfaces. Fr = fracture surface. B. Composite feature: Freshly plucked basal facet with sharp fracture surfaces; higher level has rounded edges and re-abraded surfaces. C. Stoss-side of roche moutonnée, showing combination of fresh plucking along fractures (Fr), fresh edge flaking and rounded edges. D. Detail of abraded top of the roche moutonnée at (A): abundant crescentic fractures amalgamating into triangular socket. E. Composite socket with basal plucked facet, lateral and stoss-side plucking, and both sharp and rounded edges.*

Broadly, there is a dominant WNW–ESE and a NNE–SSW subvertical fracture set, with a subordinate N–S set, mapped in the drone imagery as well as in the field (Figure 5-3E). There is also a gently-inclined set, with a fracture spacing of 10–30 cm. Overall, the fracture network is broadly orthogonal, with joints neatly bounding blocks in the range of 10–30 cm. The outcrop photo analysis suggests an even higher fracture density (P21 density: 18.38 m^{-1}, spacing 0.06 m) (Table 5-2 and Appendix 1); these very high values maybe partly due to selection (bias) towards a very highly fractured domain.

5.8.2 Geomorphological description

Stånggrundet shows a rough surface, with very little surface area (< 3 %) occupied by abraded surfaces (Figure 5-17C, D; Table 6-1). These occur as small 'islands' of smooth abraded surfaces, surrounded by lower (0.5–1 m) ground which shows pronounced roughness (Figure 5-18A). The remaining 97 % of the area is characterised by a variety of plucked steps and surfaces, various sockets and crescentic scars. Many surfaces are re-abraded, but sharp edges are also abundant; and freshly plucked and re-abraded surfaces occur very close together (Figure 5-18B). The difference between the different block-removal features proved too ambiguous, so these features have not been mapped separately. Stepped, plucked surfaces, showing classic-lee side plucking are very common (similar to the Klubbudden site: Figure 5-5A); with plucked surfaces parallel to pre-existing (commonly mineral-coated) fracture surfaces. Lateral or oblique plucking is also common (Figure 5-5C) Plucked edges can be (i) sharp and fresh; (ii) having additional edge flaking, at lower angle than the original plucked face (Figure 5-18C); (iii) edge-rounded, showing a high degree or re-abrasion (Figure 5-5B; 5-18B).

Many of the abraded surfaces (including that containing TCN sample site FORS-17-19) show abundant crescentic fractures ('friction cracks') (Figure 5-4C; 5-18D). These crescentic fractures locally interact with pre-existing subvertical fractures to form shallow (< 10 cm) triangular sockets (Figure 5-18D). These small, shallow sockets appear to amalgamate into large ones, propagating towards the edge of the top of a roche moutonnée. Crescentic fractures also increase in abundance close to plucked edges of roches moutonnées (Figure 5-5E). Altogether it appears that these abraded surfaces experienced long and intense damage by clast-bed stresses. Re-abraded surfaces rarely show crescentic fractures, suggesting that the formation of the crescentic fractures was not a 'very late stage' phenomena at this site.

Larger (> 10 m^2) depression show irregular, ragged edges, with both sharp, fresh edges and edge-rounded ones, commonly with various radii of curvature (Figure 5-18E). This suggests that these depressions progressively enlarged over time by plucking: some early edges are rounded, and later ones are sharp. Some such depressions show sharper edges on the up-ice side, suggesting up-ice migration of the main edge as per classic lee-side plucking. However, other depressions do not show this clear progression, and may also show lateral edges that are both sharp and edge-rounded.

5.9 Abrasion-only surface – Närke, central Sweden

To assess the likelihood of abraded summit surfaces at Forsmark indeed having only experienced abrasion during the Late Weichselian glaciation we here compare these with an abraded surface exposed in a quarry near Norra Bro, south of Örebro in central Sweden. Although distant to the study areas, it is a very informative example of an abraded-only surface, with considerable relief. In this district, Cambro-Ordovician sediments are still present, unconformably overlying the basement rocks (Hall et al. 2019a). The Cambro-Ordovician unconformity occurs c 2.5 km south of this quarry, but has a very low dip, so that the present-day erosion surface of the basement rocks lies only just (10–20 m) beneath the sub-Cambrian unconformity (U2 in Hall et al. 2019a); thus only 10–20 m of basement rocks have been eroded by glacial erosion. The particular surface at the quarry (Figure 5-19) shows a predominance of abraded-only surfaces and a general absence of plucked surfaces or other block removal surfaces. Note also the lack of fractures. Nevertheless, the surface shows a relief of c 2–4 m, and can be described of being composed of nested whalebacks. The wavelength of the whalebacks varies between 5–20 m. It thus appears that, as the basement became exhumed beneath Cambro-Ordovician rocks by progressive glacial erosion, it only experienced abrasion, with little or no contribution of any form of block removal. The result is an abraded surface without sharp, plucked edges.

Figure 5-19. *Abraded surface exposed in a quarry at Norra Bro (Sweref 99: N 6565589, E 512787) just south of Örebro. The surface lies 10–20 m below the sub-Cambrian unconformity. The boulder left of centre is c 2 m high.*

5.10 Edge rounding measurements

The degree of rounding of plucked edges was measured quantitatively in field in one site (Lilla Sandgrund West; Figure 5-11) using method of Kirkbride and Bell (2010) and Cox et al. (2018). The extent of rounding is given here as an edge rounding distance representing the apparent depth of rock removed to produce the measured radius of curvature given a hypothetical starting condition of a right angle (Figure 5-20A). From 40 measurements (Figure 5-20B) the minimum extent of rounding was 0 cm (sharp edge) while the maximum was 22 cm. The median and mean were 5.8 cm and 7.1 cm respectively, with a standard deviation of 5.2 cm. While some well-rounded (large radius of curvature and extend of rounding) examples exist, the measurements are skewed towards the lower values, indicating limited edge rounding and thus suggesting a relatively short period of time for edge rounding. This in turn suggest that the majority of relatively sharp, plucked edges were formed during a relatively late stage of the last glaciation.

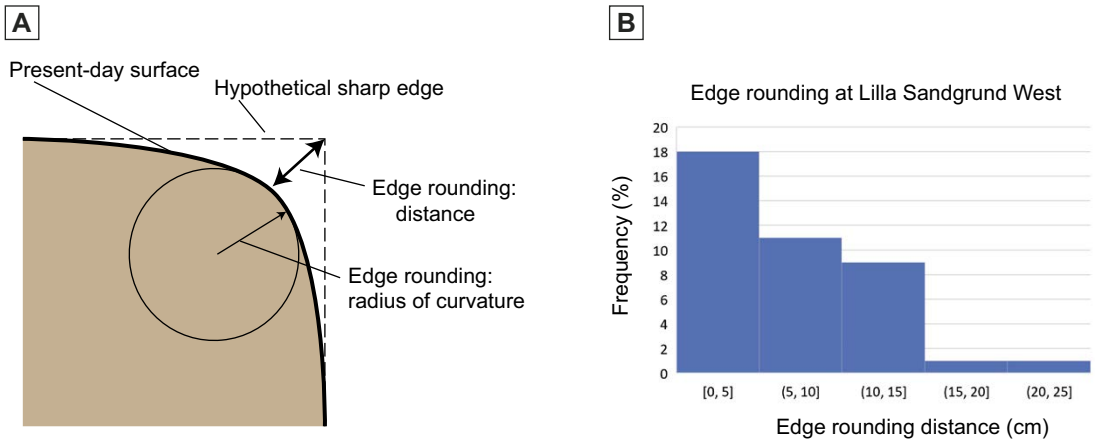

Figure 5-20. *A. Edge rounding: principle of measurements and edge rounding distance. B. Edge rounding distances measurements from Lilla Sandgrund West.*

6 Results – Morphometric geomorphology

6.1 Morphometrics – separation of abraded from block removal surfaces

All five study sites show abraded surfaces as well as plucked and other block removal surfaces. The differences in mapped surfaces are ultimately subjective – in this section we test the separation between abraded and block removal surfaces against quantitative morphometric parameters using slope maps (Figure 6-1), roughness maps (Figure 6-2), and histograms of slope and roughness (Figure 6-3). The roughness indicator used on the roughness map is the standard deviation of slope (unit in degrees) in a 50 × 50 cm window. In this section we have grouped together the plucked surfaces, sockets, and re-abraded surfaces into the combined block removal surfaces (see also Table 3-2).

Surfaces mapped as abraded surfaces in Section 5 have generally low slope and low roughness. These surfaces have slopes < 25° (Figure 6-1) and roughness < 8° (Figure 6-2). The histogram of the slope map (Figure 6-3; left-hand panels), shows a narrow range with mode of slope between 10–15° for the mapped abraded surfaces. The majority of abraded surfaces are < 20–25°, and very few steeper slopes occur. This applies to all 5 study areas. The histogram of roughness (Figure 6-3; right-hand panels) shows a narrow range (mostly < 10°) and a mode of c 5° for the abraded surfaces.

Surfaces mapped as block removal surfaces have steeper slopes and higher roughness. The histograms of slope show a wider range of slopes, with a mode between 20–25°. Slopes are up to 60°, where it should be noted that steep to vertical faces are underrepresented on the DSM as they have no surface area in map view. The histogram of roughness for the block removal surfaces shows a wide range of roughness (0–20°) and a mode of c 10°. On the roughness map, the block removal surfaces show a patchwork of rough surfaces, commonly with a roughness > 16°.

In summary, a pattern emerges wherein the mapped abraded surfaces are consistently smoother and lower slopes than mapped block removal surfaces; the field mapping of the distinction between abraded and block removal surfaces is thus consistent with the morphometrics. The block-removal surfaces show short wavelength relief, typically < 1 m, whilst the abraded surfaces do possess a relief, but with wavelength > 5–6 m.

The exception to this pattern is Stora Asphällan, where the abraded surfaces are steeper (wider range of up to 35°; mode c 15°), whilst the block removal surfaces have quite similar slopes, albeit with marginally wider spread. At this locality the separation between abraded and rock removal surfaces is less distinct, for reasons discussed in Section 7.2.3.

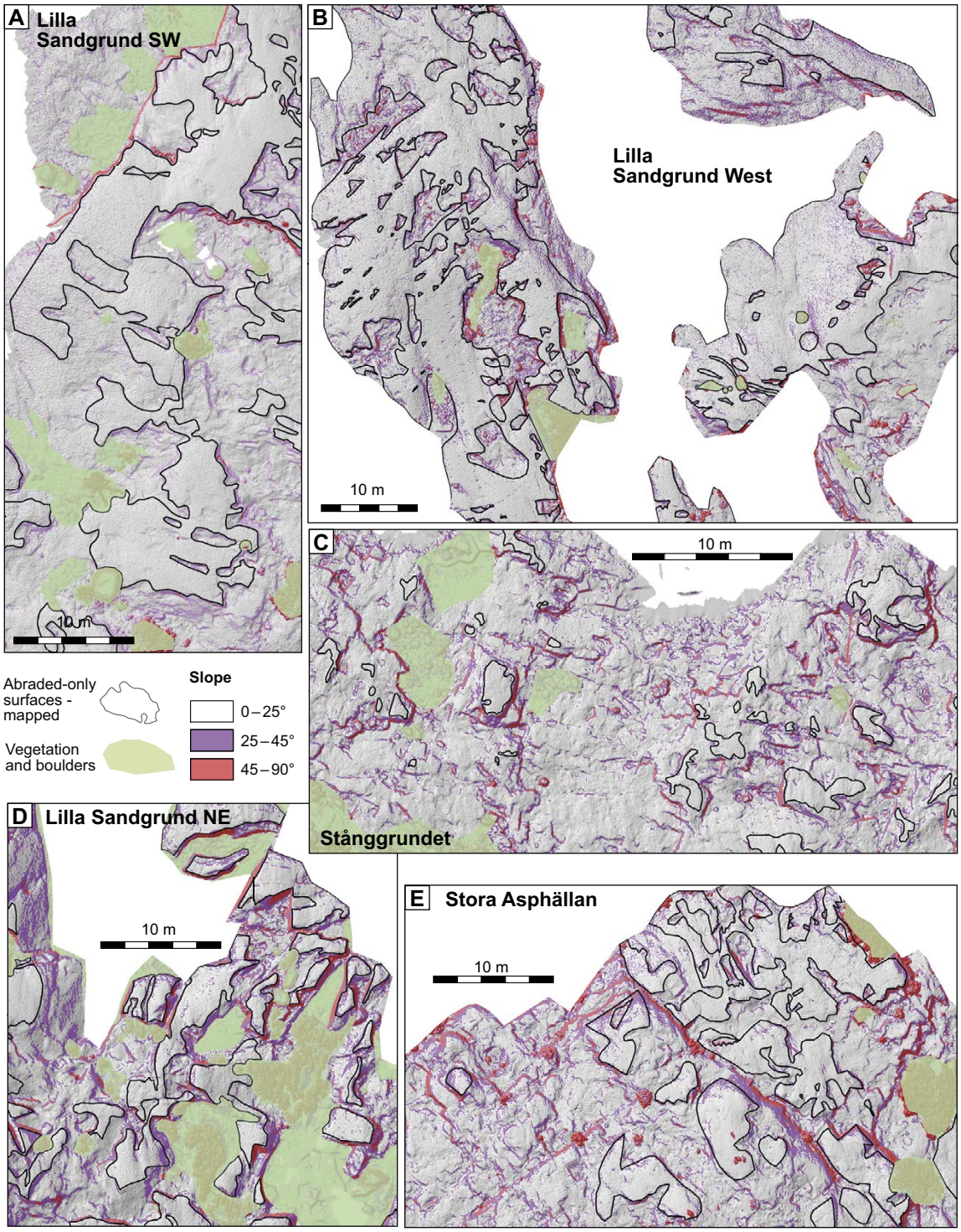

Figure 6-1. *DSM hill shade with slope, classed in three classes: 0–25°, 25–45° and > 45°. Surfaces mapped as abraded are outlined. Areas of vegetation and boulders shown with green mask.*

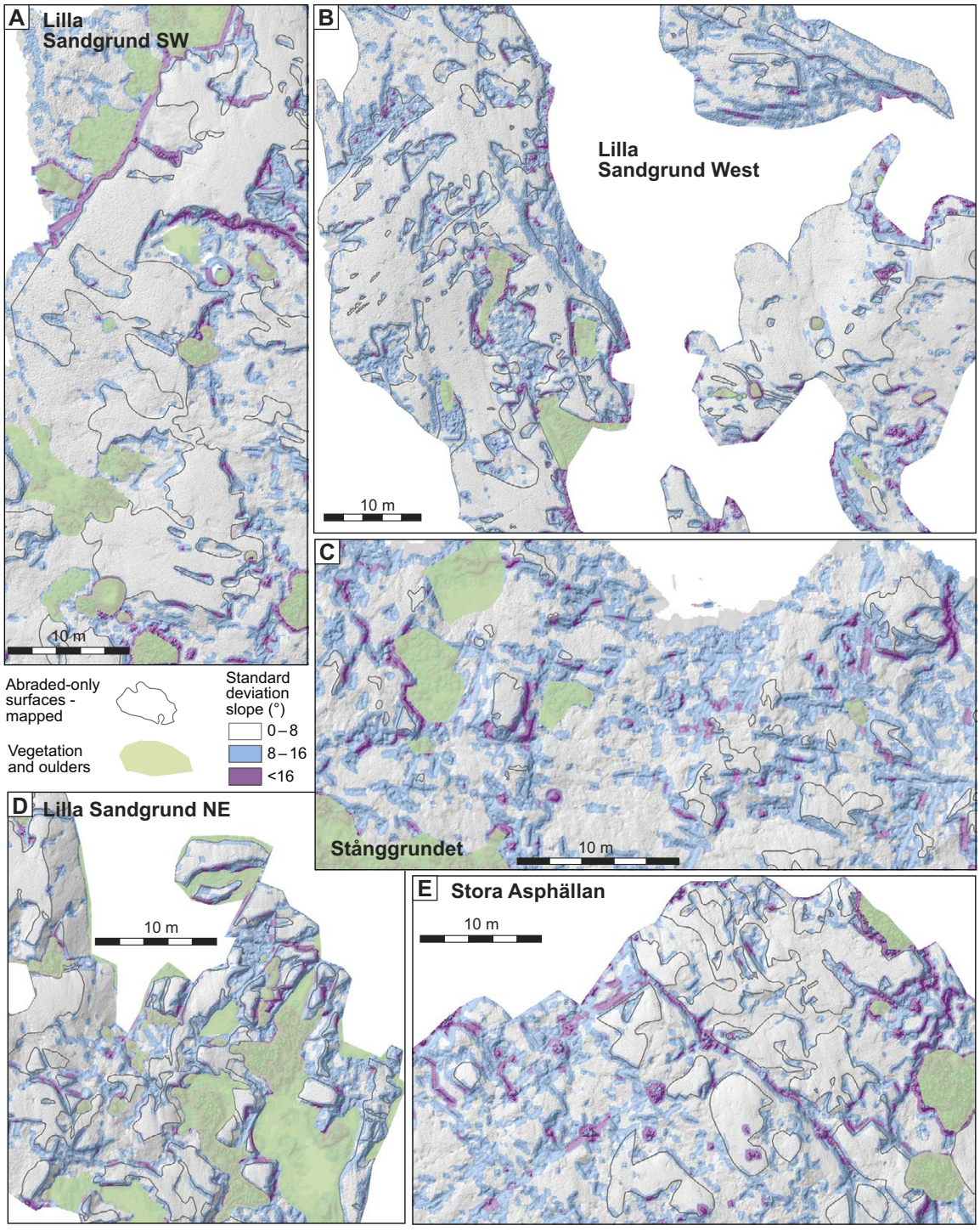

Figure 6-2. *DSM hill shade, with standard deviation of slope in a 50 x 50 cm window (a roughness indicator), shown in three classes: 0–8°, 8–16° and > 16°. Surfaces mapped as abraded are outlined. Areas of vegetation and boulders shown with green mask..*

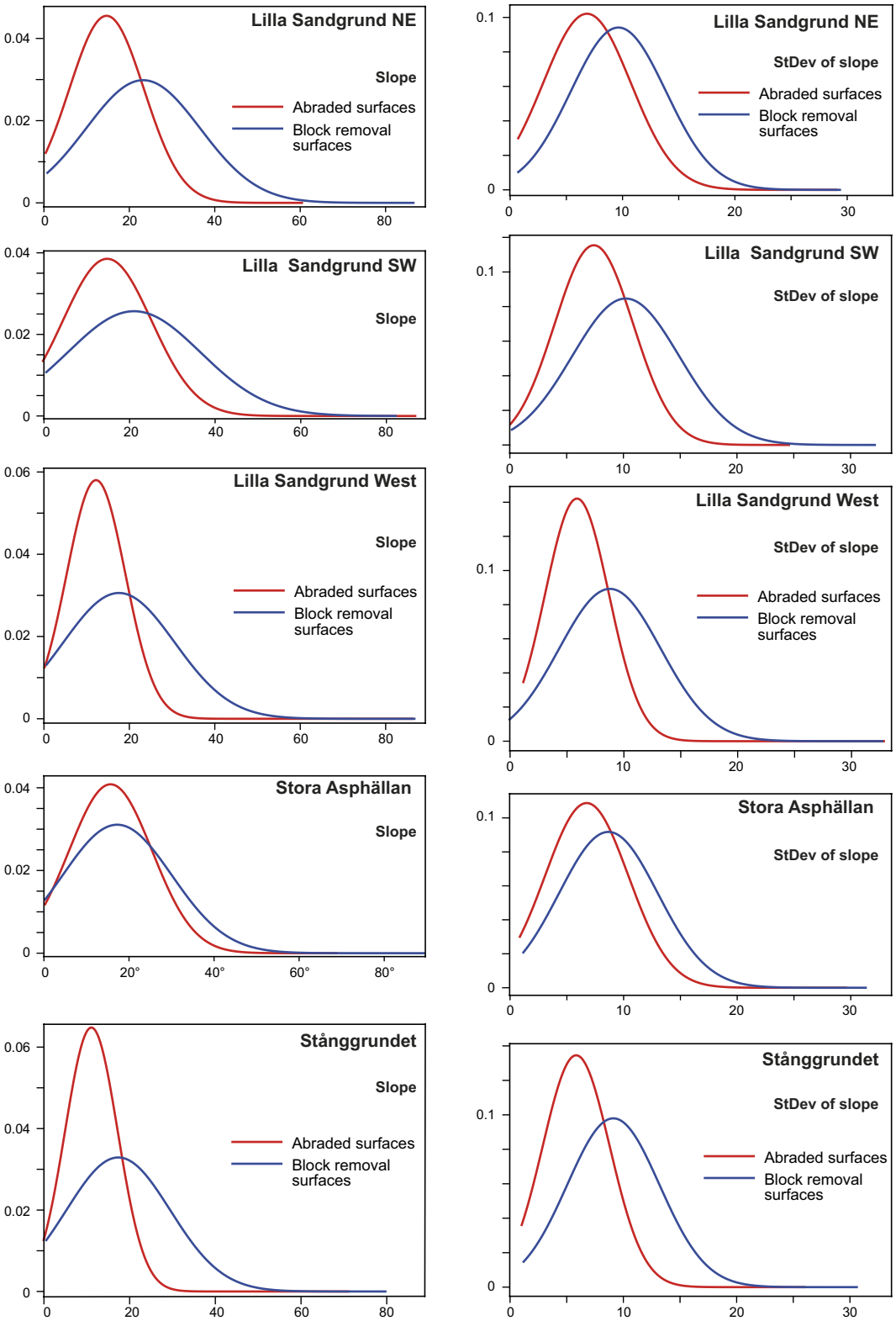

Figure 6-3. *Histograms showing slope values (on left) and standard deviation of slope ('roughness') (on right) of mapped abraded surface (red) and block removal surfaces, including re-abraded surfaces (blue). All five study areas.*

6.2 Surface area proportion of abrasion vs block removal

The GIS-based geomorphological mapping of the five study sites (Figures 5-8B, 5-10B; 5-12B; 5-14B; 5-17B) shows the different mapped surfaces (abraded surfaces, 'fresh' block removal surfaces, re-abraded surfaces) in map view. Both the total areas of the different surfaces and their relative proportion can be quantified (Table 6-1). All Lilla Sandgrund study sites show a broadly equal proportion of abraded surfaces (43–52 %) and combined block removal surfaces (plucked surfaces, sockets and re-abraded surfaces) (48–56 %). Lilla Sandgrund NE shows a much higher proportion of freshly plucked surfaces (36 %), whilst re-abraded surfaces are more prevalent in Lilla Sandgrund West and Lilla Sandgrund SW (34 and 40 % respectively). Stånggrundet is dominated by block removal surfaces (93 %) with only 7 % abraded surfaces; many of the block removal surfaces are freshly plucked but it proved impractical to separate these out from the re-abraded surfaces. Stora Asphällan shows a low proportion of abraded surfaces (20 %) and freshly plucked surfaces (10 %), but a high proportion of re-abraded surfaces (69 %), in particular on the outcrop of the amphibolite.

Table 6-1. Proportion of surface area classified as different erosional surfaces.

	Lilla Sandgrund NE		**Lilla Sandgrund West**		**Lilla Sandgrund SW**		**Stora Asphällan**		**Stånggrundet**	
	m^2	%	m^2	%	m^2	%	m^2	%	m^2	%
Abraded surfaces	423.6	43	686.4	46	1744.9	52	456.3	20	200	7
Block removal surfaces ('fresh')	351.9	36	310.5	21	215.7	6	226.9	10	(*)	
Re-abraded surfaces	190.8	20	507.3	34	1358.2	40	1592.3	69	(*)	
Sockets	(*)		(*)		58.7	2	13.1	1	(*)	
S-forms	9.7	1	1.9	0	10	0	26.1	1	(*)	
Block removal (combined)	542.7	56	817.8	54	1632.6	49	1832.3	79	2817	93
	(*) counted in Plucked surfaces		(*) counted in Plucked surfaces						(*) not separated	

6.3 Depth of erosion by block removal volume: modelling

The results of the erosion modelling are shown in Figure 6-4 and summarised in Table 6-2. These represent the depths of the present-day surface beneath the modelled extrapolated abrasion surface. Selected cross-sections are shown in Figure 6-5, with both the present-day surface and the modelled extrapolated abrasion surface.

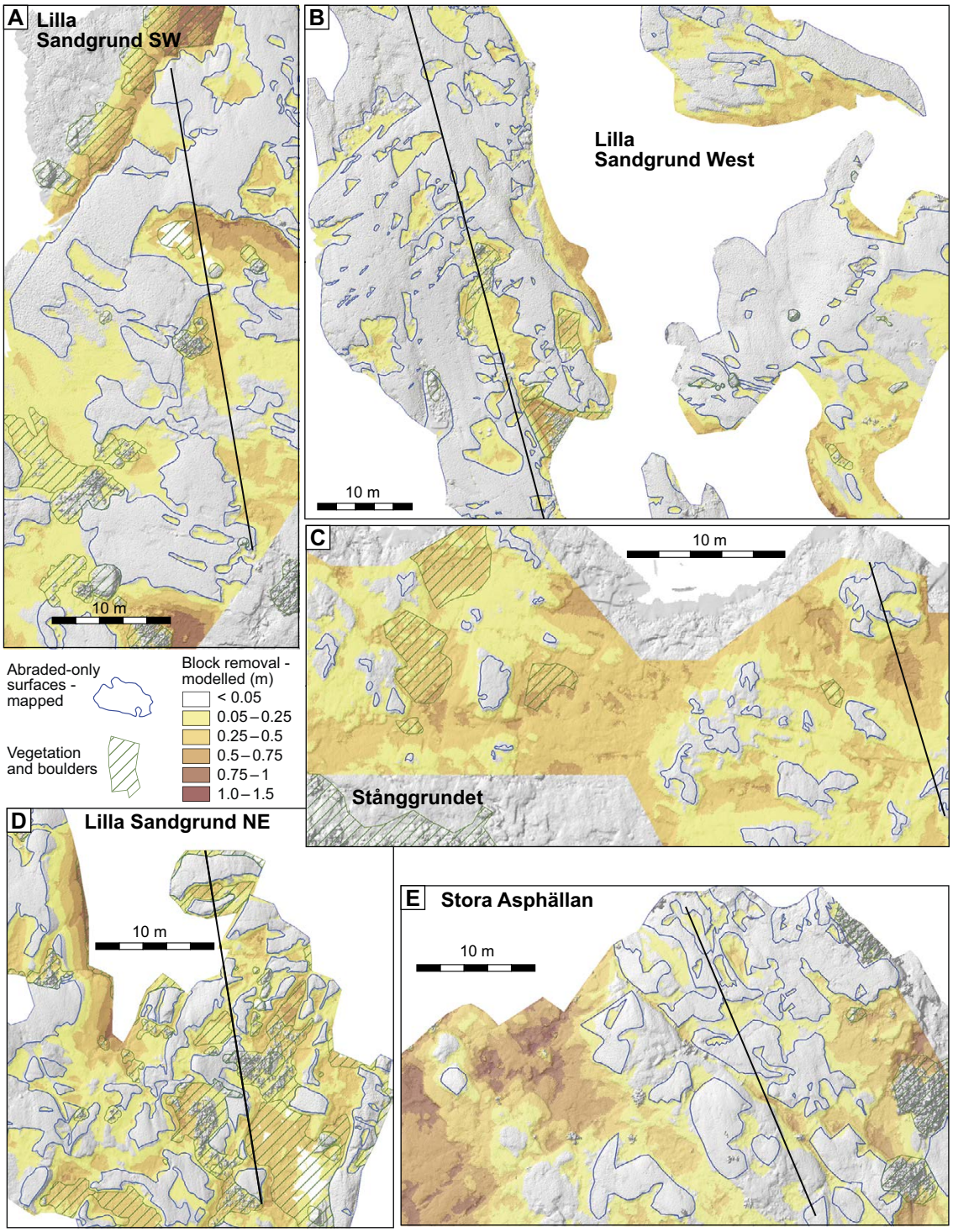

Figure 6-4. *Erosion depth by block removal, modelled, in metres below projected abraded surface. Erosion depth < 0.05 cm not shown. Mapped abraded surfaces shown in blue outline. Areas of vegetation and boulders shown with green hatching. Lines of section in Figure 6-5 as black lines.*

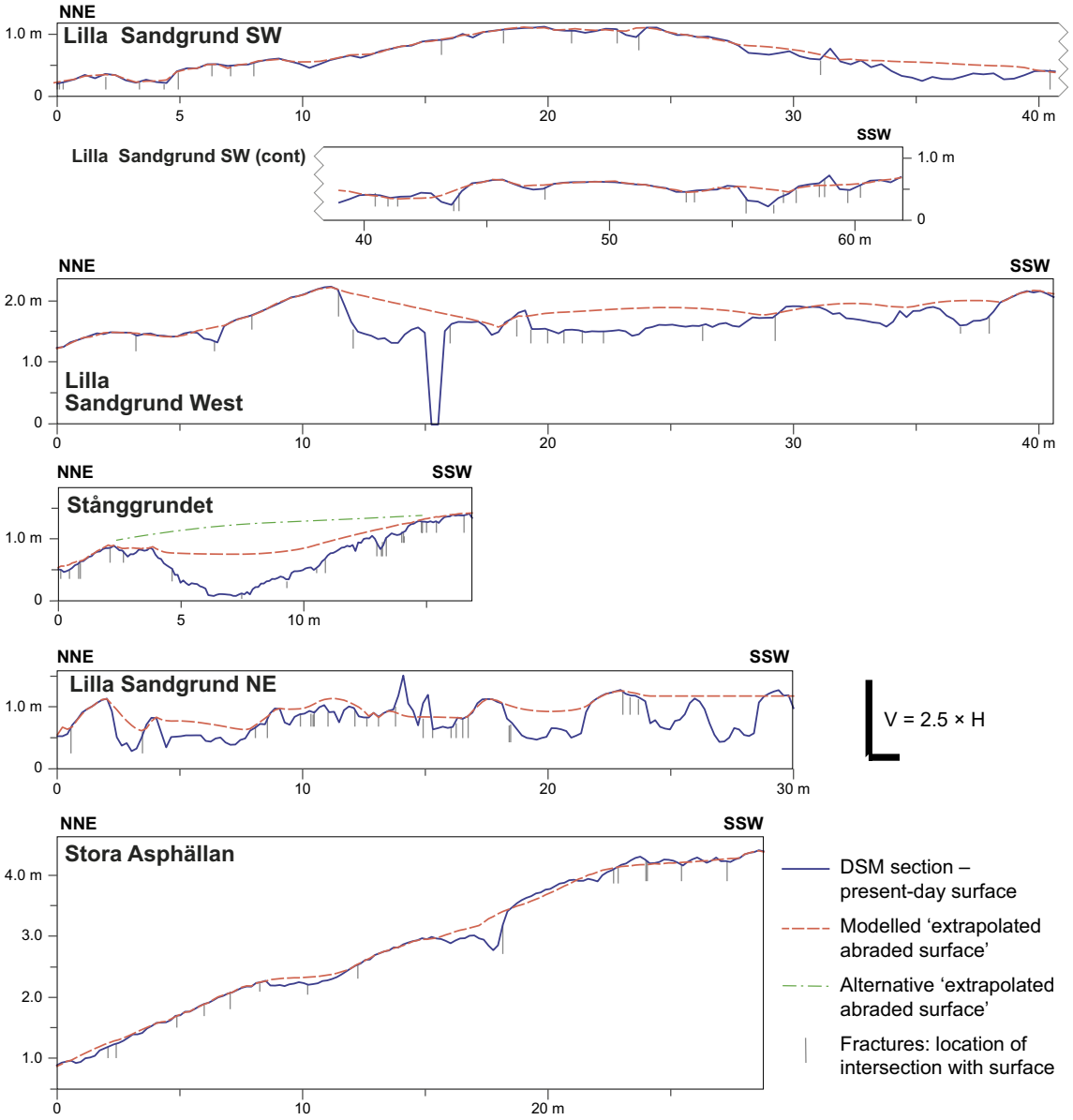

Figure 6-5. *Cross-sections 5 sites, comparison of the present-day DSM surface (solid blue line) with the modelled extrapolated abraded surface (dashed red line). Alternative extrapolated abraded surface (green dashed line) for Stånggrundet is discussed in Section 7.2. Fractures are shown as short vertical lines but may have much lower dip; only shown to give impression of fracture density. Vertical exaggeration 2.5 x. Location of section lines: see Figure 6-4.*

The depth of block removal varies from 0 (abrasion only) to c 1.3 m, with the highest block removal depths ranging from 0.93–1.33 m. The highest block removal depths occurred at Stora Asphällan, adjacent to the amphibolite. Average depth of block removal, where it did occur (i.e. excluding the abraded surfaces), ranges from 0.19–0.34 m. The depth of block removal averaged over the entirety of the study sites (e.g. including the block removal surfaces and the abraded surfaces) ranges from 0.10–0.27 m. The Lilla Sandgrund sites give then the lowest average block removal depths (0.10–0.12 m), whilst both Stora Asphällan and Stånggrundet give higher values (0.27–0.21 m respectively).

Table 6-2. Depth of erosion by block removal. Block removal surface: surface lowering is the lowering of surfaces where block removal did occur. The surface lowering for all surfaces is the average lowering by block removal, averaged over the entirety of a study site. SD = standard deviation; Notes: (1) no direct data from site: average of TCN summit lowering data in other areas; (2) average TCN summit lowering plus average block removal surface lowering; errors not propagated. (3) minimum TCN summit lowering with zero block removal vs. maximum TCN summit lowering and maximum block removal; (4) TCN summit sample not from same site as block removal estimate – may not be valid; (5) only the TCN sample from surface mapped as abraded surface has been considered.

	Lilla Sandgrund NE	Lilla Sandgrund West	Lilla Sandgrund SW	Stora Asphällan	Stånggrundet
Abraded surfaces					
area (m^2)	424	686	1650	459	199
area of total (%)	*44*	*46*	*52*	*20*	*7*
Block removal surfaces					
area (m^2)	542	818	1528	1820	2818
area of total (%)	*56*	*54*	*48 %*	*80*	*93*
surface lowering – average (m)	**0.21**	**0.19**	**0.21**	**0.34**	**0.23**
surface lowering – max (m)	0.93	1.03	1.33	1.13	1.16
surface lowering – SD (m)	0.1541	0.15	0.19	0.28	0.17
All surfaces, combined					
area (m^2)	965	1505	3178	2279	3017
Block removal surface lowering – average (m)	**0.12**	**0.10**	**0.10**	**0.27**	**0.21**
Comparison with TCN erosion depths					
TCN summit lowering (m) – from abraded summits only	c 1.4 ± 0.5 (1)	c 1.4 ± 0.5 (1)	1.32 ± 0.44; 1.57 ± 0.53	1.17 ± 0.40	1.40 ± 0.47 (5);
Total erosion depth (m) (2)	**c 1.55**	**c 1.5**	**c 1.6**	**c 1.45** (4)	**c 1.6**
Total erosion depth – range (m) (3)	**1.5–2.5**	**1.5–2.5**	**1.5–2.6**	**1.1–2.3** (4)	**1.4–2.55**
block removal contribution (%)	**8**	**7**	**6**	**23**	**11**
Abrasion:plucking ratio	**11 : 1**	**13 : 1**	**16 : 1**	**3.3 : 1**	**8 : 1**

6.4 Comparison of block removal and TCN erosion depths

The estimated erosion depths from TCN inventories over the Late Weichselian glaciation are also shown in Table 6-2 and can be compared with the estimated block removal depth.

Per site:

Lilla Sandgrund SW. Two TCN sample sites (FORS-19-03A and FORS-19-04) occur within the mapped area and yield a surface lowering of 1.3 –1.6 m (Hall et al. 2023). The samples were taken from surfaces mapped as abraded-only surfaces in this study, and the erosion depths are hence interpreted herein as erosion by abrasion only. The surface lowering by block removal, where it did occur, was only 20 cm; averaged over the whole area, this amounts to c 10 cm. Thus the contribution of block removal to the total erosion is c 6 %, i.e. an abrasion:plucking ratio of 16:1 This means that erosion is dominated by abrasion, with only a very small proportion of block removal, consistent with the very wide occurrence of smooth, long wavelength abraded surfaces. The total erosion depth, taking into account the range of both the TCN results and the range of block removal depths, then ranges from 1.5–2.6 m over the Late Weichselian glaciation. Note that Hall et al. (2023) interpreted the results from the two TCN samples as caused by abrasion combined with block removal.

Lilla Sandgrund West and Lilla Sandgrund NE. No TCN samples were taken from these areas. Instead, the average of the estimated TCN erosion depth is applied (Table 6-2.). The results of block removal erosion depth, and hence the total erosion depth (1.5–2.5 m) and contribution of block removal to the total erosion (6 –7 %) are all quite similar to those of Lilla Sandgrund SW.

Stora Asphällan. The estimated erosion depth from TCN sample FORS-17-12 is the lowest of all coastal outcrops (1.17 m). However, this site lies c 500 m to east of the mapped study site and has different lithology (felsic rocks) and geomorphology than the bulk of the mapped Stora Asphällan site, dominated by amphibolite. The depth by block removal from the mapped area are quite high: 34 cm where block removal occurred and 23 cm over the entire area. This would suggest a total erosion depth of 1.45 cm, and a relatively high contortion of block removal: 23 % (abrasion:plucking ration of c 4:1). However, this comparison is of limited value as the TCN site was not in the mapped area.

Stånggrundet. TCN sample FORS-17-19 yielded an estimated erosion depth of 1.4 m (Hall et al. 2023). This sample was taken from a surface mapped as an abraded surface in this study. The estimated depth by block removal over the mapped area is quite low: 23 cm where block removal occurred and 21 cm over the entire area; the resultant the abrasion:plucking ration is c 8:1. It is possible that the geomorphological modelling underestimates block removal, since the extrapolated abraded surface (cross-section on Figure 6-5) predicts a dip, which may not have existed as a previous abraded surface: an alternative 'precursor surface' as shown in green on Figure 6-5 would have resulted in a higher estimate of block removal. This would be more consistent with the maximum erosion depth of block removal (1.16 m). TCN sample FORS-17-14 returned an estimated erosion depth of 2.08 m (Hall et al. 2023): this sample site lies outside the mapped area, but within the area covered by the DSM survey. The local surface is similar to those mapped as re-abraded surface, so that this estimated erosion depth was likely caused by a combination of block removal and abrasion.

Overall, the depth of abrasion, taken as the estimated erosion depth from TCN sample sites occurring on abraded surfaces varies between 1.17 to 1.57 m, a fairly narrow range. Erosion depth estimated from block removal varies from 0 (abrasion only) to 1.33 m; the erosion depths averaged over the mapped areas varies from 0.21–0.34 m; the abrasion:plucking ration varies from 3:1 to 16:1. We note that Hall et al. (2023) interpreted the erosion depth of all samples at the study sites as a combination of block removal and abrasion – discussed in Section 7.1.

The total erosion depth (abrasion from TCN sample sites plus site-averaged block removal depth) at the coastal outcrops varies from c 1.1–2.5 m.

7 Discussion

7.1 Uncertainties

7.1.1 Assumption of abraded surfaces

The interpretation of the distinguishing between abrasion and block removal surfaces, and the geomorphological modelling of estimated depth of block removal, rests on the assumption that the abraded surfaces as mapped herein have indeed only experienced abrasion during the Late Weichselian glaciation, and do not represent surfaces that first experienced block removal followed by a phase of abrasion (e.g. re-abraded surfaces). In contrast, Hall et al. (2023) suggested that all TCN sample sites at the coastal outcrops, including the mapped sites in this report, were eroded by a combination of abrasion and block removal, with a phase of block removal early during the last glaciation, followed by a phase of abrasion, and then, locally, by a phase of block removal later during the last glaciation. Hall et al. (2023) justified this order of erosional phases to explain the higher erosion depths (1–1.8 m) from the summit sample sites at the coastal outcrops, compared to the low erosion depths (0.2–0.4 m) at the summit of Wave Rock. Hall et al. (2023) argued that therefore abrasion at the Forsmark site was limited to about 0.4 m (the depth of erosion of the summit of Wave Rock), and that any deeper erosion much have occurred by block removal, before and/or after a phase of abrasion. Hall et al. (2023) further argued that, on the basis of deeper erosion adjacent to the Wave rock summit area (0.8–1.8 m) that the overall abrasion:plucking ratio is in the order of 1:4 to 1:5.

Support for the assumption that the mapped abraded surfaces were formed by abrasion only, as interpreted in this report, includes the following:

a) The mapped abraded surfaces have systematically lower slope, curvatures and roughness than the mapped block removal surfaces and mapped re-abraded surfaces (Section 6.1);

b) The mapped abraded surfaces typically show long wavelengths of their relief (horizontal distance between high points) of 5–30 m or more. This wavelength is similar as seen on the abraded-only surfaces at Närke (Section 5.9), but much greater than the wavelengths seen in the mapped re-abraded surfaces, which are typically < 1 m;

c) The averaged fracture spacing of subhorizontal to gently dipping fractures in four sites (excluding Stånggrundet) is 1–5 m (Table 5-2); equal or greater than the depth of erosion from TCN inventories. This suggests that (i) block removal is unfavourable in these sites, and (ii) is not plausible that large sheets of rocks were previously removed along pre-existing fractures from above the abraded surface by some form of block removal;

d) Where quantified, the edge rounding amounts to an abrasion depth of a maximum of c 20 cm (Section 5.10); much less than the amount of abrasion needed to smooth out the 20–50 cm topography created by block removal;

e) The micro-textures such as millimetre-scale roughness, presence of deep striae and the presence of chipped surfaces, suggest that the abraded surfaces experienced a long period of abrasion only, in contrast to the re-abraded surfaces which are generally smoother (‘polished’) on the millimetre-scale. It is thus not likely that the abraded surfaces represent re-abraded surfaces;

f) Block removal results in surfaces that are rough on the decimetre-scale, with short-wavelength highs and lows (< 1 m), with an average depth of erosion of 0.2–0.3 m, and with maximum depth of erosion by block removal of 0.9–1.3 m in all areas (Table 6-2). If an earlier phase of block removal had occurred, creating a similar rough surface, then a phase of subsequent abrasion-only erosion is required that is greater than the maximum depth of the previous roughness. Since that the depth of erosion as determined by the TCN inventories from summit surfaces is limited to 1–1.5 m, it is implausible that abrasion would be sufficient to transform a previously a rough, low-wavelength surface into the smooth, long wavelength surfaces that are documented here, in particular at the Lilla Sandgrund sites;

g) Hall et al. (2023) invoked a phase of block removal early during the Late Weichselian glaciation. Most or all evidence for such a phase would be erased by the subsequent phase of abrasion, so the veracity of such an early block removal phase affecting the shallow rock mass is difficult to ascer-

tain. Modelling (SKB 2020) suggest long periods of permafrost at Forsmark. Initial ice advance, occurring under conditions of average air temperature below 0° C, likely occurred over frozen ground: any present H_2O in fractures would be ice. Such permafrost greatly increases the rock-mass strength of the shallow rock mass, suppressing block removal. Meltwater activity was similarly low, and any present would not be able to penetrate the rock mass, further suppressing block removal. There is widespread evidence of very low erosion rates in areas farther north in Fennoscandia, normally attributed to cold conditions lasting throughout the last glaciation (Kleman and Stroeven 1997, Hättestrand and Stroeven 2002, Stroeven et al. 2002b, Hall et al. 2013). Overall, this suggest that cold-phase conditions early during a glaciation are not conducive to block removal, so that a significant early phase of block removal for the Forsmark area is not a plausible prospect.

Overall, we are confident in the assumption that the mapped abraded surfaces at our study sites indeed only (or at least predominantly) experienced abrasion during the Late Weichselian glaciation. Given the low overall depth of erosion (10s of m maximum) since exhumation of the sub-Cambrian peneplain (Hall et al. 2019a), it is even possible that these surfaces have only ever experienced abrasion during *all* previous glaciations.

7.1.2 Re-abrasion and block removal during Late Weichselian glaciation?

Where there is evidence of block removal including plucking, it may have occurred during the last glaciation, but equally during a previous one. Erosion depths based on stepped TCN inventories show that both may occur (Hall et al. 2023, Graham et al. 2023). For most of the Forsmark study sites, there is good evidence that much block removal occurred during the last glaciation:

- A very large number of plucked edges are sharp and angular, suggesting a pulse of block removal late during the last glaciation, without opportunity for edge rounding.
- Where edge rounding has occurred, it is limited to a few centimetres (< 10 cm), much less than the interpreted depth of erosion by abrasion.
- In some cases, the fracture coating (e.g. epidote) of a fracture utilised by block removal did show abrasion, but was still present, showing that abrasion was less than 1 cm (epidote fracture fill is typically < 1 cm thick).
- Most step-samples TCN results from the Forsmark area suggest block removal during the last glaciation; only one (FORS-19-06 at Mohägnaden) suggest block removal during a previous glaciation (Hall et al. 2023).

Overall, these observations suggest that most (but not all) block removal at Forsmark occurred during the Late Weichselian glaciation, with a likely intense pulse of block removal just prior to deglaciation. This may be related to thinner ice; more intense meltwater activity (fluctuating water pressures and water volume) and/or the greater availability of large (> 1 m) clasts due to glacial ripping up-ice.

However, on the amphibolite at Stora Asphällan there are distinct plucked faces and steps (on the east of the low hill; Figure 5-14) as well as many very rounded surfaces (Figure 5-16C). It is possible that some block removal did occur during a previous glaciation. Total abrasion on the amphibolite is very low, and arguably less than the edge rounding. TCN site FORS-17-12 suggests c 1.17 m of erosion (given the smoothness of the surface, likely mostly by abrasion), but this site is close to the shore on felsic rock and c 2 m lower than the top of the amphibolite roche moutonnée. Hence the erosion of the top of the amphibolite roche moutonnées was likely lower, possibly as low as 50 cm. This suggest the likelihood that a number of the re-abraded surfaces and their sockets on the amphibolite were inherited from a previous glaciation, suggesting low erosion depth (< 1 m) during the last glaciation. Further discussion in Section 7.2.3.

At Stånggrundet, the large spatial extend of block removal surface (90 %) means it is possible that block removal occurred during a previous glaciation. At this locality, fresher and angular plucked edges may simply follow from headward progression of previous plucked faces, akin to the conceptual model of Rea and Whalley (1996). In the area west of the mapped area, and also at Klubbudden, there are very few if any remnants of abraded surfaces, and it is feasible that the overall plucked nature of the terrain is inherited from plucking and block removal during a previous glaciation. It is likely that these areas experienced slightly higher erosion rates than elsewhere.

7.1.3 Other uncertainties

The depth of erosion by block removal will be underestimated if the local topographic lows are partially filled with boulders, vegetation or water, in which case the present-day surface as portrayed in the DSM is higher than the true block removal surface (indicated on Figures 6-1, 6-2 and 6-4). In the selection of the study sites we avoided such areas as far as possible, but this inevitably introduces a bias against 'deeper holes'.

Conversely, the depth of erosion by block removal can be over-estimated if the extrapolated abraded surface is too high: it is possible that a plucked step (formed during a prior glaciation) occurred in the precursor surface, or that the overall plucked form was inherited from a previous glaciation (See Section 7.1.2). This would mean that the surface prior to the Late Weichselian was (already) *lower* than the extrapolated abraded surfaces, and would imply that the total depth of erosion during the last glaciation was lower than suggested from the DSM analysis (See Figure 1-1).

The TCN sample FORS-17-12 at Stora Asphällan is well to the east of the area of geomorphological mapping. The sample site has a different lithology (fine-grained felsic gneiss) and forms a very flat outcrop (Figure 5-16D), similar to that on the same rock type on the shore further west (Figure 5-15). In contrast, the study site for geomorphological mapping comprises a large body of coarse amphibolite, and forms relatively blunt and high (4 m) roche moutonnee, suggesting low erosion rates. It is thus possible that the erosion rate from the TCN sample FORS-17-12 is not representative for the abrasion rate of the amphibolite at Stora Asphällan. This implies that overall erosion depth of the amphibolite might be lower than shown in Table 6-2.

At Stånggrundet, only 7 % of the interpreted abraded surfaces remain. This means that the modelled extrapolated abraded surface is less well constrained than at the other sites. For instance, an alternative extrapolated abraded surface, shown in green in Figure 6-5 would result in greater depth of block removal than the presented estimates during the last glaciation. Conversely, given the large surface area of block removal, it is feasible that the precursor pre-Late Weichselian surface was not a smooth abraded surface, but was already partially rough and plucked. In that case, the depth of block removal, and with it the total erosion depth for the Late Weichselian glaciation would be lower.

7.2 Variations in erosion depth by block removal and abrasion at the Forsmark site

When including the Wave Rock TCN results (Section 3, see also Hall et al. 2019a, 2023) there are considerable local variations in the depth of block removal, the depth of abrasion as interpreted from summit TCN inventories, and the total estimated erosion depths.

7.2.1 Variations in abrasion rate

The erosion depths from summit TCN samples at Wave Rock are low (c 0.2–0.5 m); Hall et al. (2023) attributed this erosion depth to abrasion-only. In this report, we argue on geomorphological grounds that the erosion depths of summit TCN sample at the coastal outcrops (e.g. FORS-17-12; 19-3A; 19-4; 17-19; Figure 3-1) also record abrasion-only erosion. These return a depth of erosion between 1.1–1.5 m. This would suggest a lower abrasion rate over the last glaciation at Wave Rock compared to the coastal outcrops. Three possible explanations for the lower abrasion rates of the top surface of Wave Rock include:

1. Wave Rock is a coarse-grained rock, whilst all rocks at the TCN sample sites on the coast are fine-grained (< 1–2 mm) rocks. It is feasible that this constitutes a fundamental difference in abrasion resistance under subglacial conditions. The relationship between grain size and abrasion resistance in the engineering literature is somewhat contradictory. For some rock materials, abrasion rate is lower of fine-grained materials (Zhou et al. 2023); whilst other materials it is the opposite (Kazi and Al-Mansour 1980). We note here that most engineering abrasion tests involve steel (with high fracture toughness) abrading rock, whilst under subglacial conditions abrasion constitutes a rock-rock interaction. It is plausible that only coarse debris (gravel-fraction and higher) is able to abrade the coarse-grained rock at Wave Rock effectively, whilst sand-grade fraction may be able to abrade

the finer-grained rocks at the coastal outcrops effectively. In that case, it can be argued that there are, cumulatively over a glaciation, an order of magnitude more effective clast-bed interactions affecting fine-grained rock than coarse-grained rock.

2. Wave Rock is a distinct roche moutonnée, with higher local topography (1–4 m) and steeper slopes along its margins than the coastal outcrops, which are low-relief whalebacks, with very low slopes. It is possible that subglacial debris, which is denser than ice or water, would tend to concentrate in the lower ground, with lower concentrations of subglacial debris sliding over the summit areas (Sugden and John 1976), leading to lower erosion of summit areas, and hence enhancing relief. This effect (see also Krabbendam et al. 2016 and Hall et al. 2019a) would be stronger if local relief is stronger.
3. The coastal outcrops and sample sites further inland at higher elevation experienced different times of post-glacial subaerial exposure. This is because the low ground in east Sweden emerged from the Baltic due to postglacial relative sea level drop. The correction applied (Hall et al. 2019a, 2023) to the raw TCN results to take account of this difference in elevation may not model the true difference in shielding by seawater during emergence.

7.2.2 Variations in block removal depths: importance of fracture network type

Block removal by area varies strongly between the sites (c 50 % at the Lilla Sandgrund sites vs 93 % at Stånggrundet; Table 6-1). Depth of block removal varies less, but is still almost twice as high at Stånggrundet as at the Lilla Sandgrund sites – and maybe underestimated at Stånggrundet (Section 7.1.2). It is likely that higher rates of plucking and block removal are related to the higher fracture density, in line with previous studies (Dühnforth et al. 2010, Krabbendam and Glasser 2011, Hooyer et al. 2012, Skyttä et al. 2023). The detailed fracture analysis of this study can add some further understanding to this. The P21 density of steeply dipping fractures (from the mapview drone image mapping – Table 5-2) at Stånggrundet (1.73 m^{-1}) is higher than at the Lilla Sandgrund sites (0.7–1.15 m^{-1}), but not by much. However, the difference in P21 density of *connected* (C-C) steeply dipping fractures is more pronounced (0.56 m^{-1} at Stånggrundet versus 0.1–0.26 m^{-1} at Lilla Sandgrund). The difference in density of gently inclined and subhorizontal fractures is even higher: 1.65 m^{-1} at Stånggrundet versus 0–0.2 m^{-1} at Lilla Sandgrund – an order of magnitude difference. The statistics at Lilla Sandgrund are potentially not reliable, as so few gently inclined fractures occur: over large areas of the outcrop, gently inclined fractures are in essence absent (e.g. Figure 5-4). Overall, it appears that the largest effect on susceptibility for classic lee-side plucking is the presence of a dense, well-connected orthogonal fracture network, as at Stånggrundet, that includes abundant gently dipping fractures and results in rectangular fracture-bounded blocks (see also Skyttä et al. 2023). The relative abundance of steeply dipping fractures, combined with a lack of gently dipping fractures, may make the Lilla Sandgrund sites more susceptible to crescentic scar development – further discussed in Section 7.6.

7.2.3 The odd one out – amphibolite at Stora Asphällan

There are a number of results and features on the amphibolite outcrop at Stora Asphällan that are different from all other sites. Firstly the particular roche moutonnée is higher (c 4 m) and more ‘blunt’ than the whalebacks at Lilla Sandgrund or the roche moutonnées at Stånggrundet (Figure 6-5; see also Figure 4-25A in Hall et al. 2019a). The site has a high degree of re-abraded surfaces. However, these surfaces show a much higher degree of edge rounding and re-abrasion, and re-abraded areas on the amphibolite at Asphällan show lower slope and roughness (standard deviation of slope) than re-abraded surfaces at the other sites (Figure 6-1 and 6-2).

It should be noted that the top of the amphibolite roche moutonnée lies 2–4 m *above* the TCN sample site FORS-17-12, which is situated just above sea level and comprises felsic gneiss (amphibolite is less suitable for ^{10}Be TCN analysis, due to low quartz content). This suggests that the overall depth of erosion by abrasion was less than the depth of erosion from TCN sample FORS-17-12 (1.17 ± 0.40 m), possibly only a few 10s of cm.

The high degree of re-abrasion and low overall erosion rate may be explained if some of block removal occurred prior to the Late Weichselian glaciation, and experienced abrasion only during this last glaciation, now represented by the strongly re-abraded surfaces. In other words, whilst the block removal

at the other sites is very likely all achieved during the Late Weichselian glaciation, at Asphällan there is circumstantial evidence that block removal occurred during a *previous* glaciation, and that block removal features survived abrasion during the last glaciation. (Block removal during a previous glaciations is also envisaged for the stepped TCN sample FORS-19-06 at Mohägnaden, see Hall et al. 2023). This would suggest that amphibolite has a higher resistance to subglacial abrasion than the more felsic lithologies.

This poses a potential paradox, since S-forms at other sites (e.g. Lilla Sandgrund NE) commonly exploited amphibolite layers, and S-forms at Asphällan are more numerous and deeper than elsewhere. This suggest that amphibolite is *more* susceptible to abrasion by meltwater erosion, which appears at odds at being *less* susceptible to abrasion by subglacial erosion as argued above. One explanation may be that susceptibility of a particular lithology to abrasion by meltwater erosion is controlled by mineral hardness (Mohs mineral hardness of quartz = 7; amphiboles = 5–6); whilst the susceptibility to abrasion by subglacial erosion may be controlled by fracture toughness or grainsize, which is considerably higher in amphibolite than in fine-grained felsic rock (e.g. Jahnke et al. 2022).

7.3 Large-scale limitations of the method

Large-scale limitations of the study include the following.

All study sites comprise relative topographic highs. Topographic lows, such as the trenches (or: fracture-controlled valleys) as described by Hall et al. (2022) were not included, as the research methods would not work since such valleys are commonly covered in post-glacial sediments. It is possible that block removal made a higher relative contribution to the formation of such trenches so that the total integrated depth of erosion by plucking integrated over a large area including trenches is higher than indicated in this study.

The study sites show some variation in fracture density, but little variation in rock hardness (e.g. Glamheden et al. 2007), all rocks being hard metamorphic basement rocks. Other areas, perhaps with a mix of metamorphic and sedimentary rocks, are likely to have larger variability in rock hardness as well as fracture density, including bedding-parallel fractures are present in sedimentary rocks). An example is the NW Highlands of Scotland, where Krabbendam and Glasser (2011) showed that abrasion was dominant in sandstone whilst plucking was dominant in thinly bedded quartzite, under comparable glaciological conditions. Therefore the relative proportion of abrasion of plucking as determined herein for eastern Sweden should *not* be taken as a generally applicable proportion, but rather as an *area-specific* proportion, with a strong dependency on lithology and fracture patterns. This has the more general implication that, for realistic modelling of ice-sheet erosion, a realistic bedrock and fracture network model should be included (cf. Iverson 2012).

7.4 Comparison with other glaciated areas

7.4.1 Abrasion:plucking ratios and erosion coefficient estimates

Assuming the mapped abraded surface were only affected by abrasion during the Late Weichselian glaciation, the abrasion:plucking ratio at Forsmark varies between 16:1 and 3:1 (Section 6.4). This is a considerably higher ratio than reported in studies that used proglacial sediment grain size as proxies (e.g. Loso et al. 2004, Riihimaki et al. 2005). These two studies concerned valley glaciers in Alaska and are underlain by metamorphic sedimentary rocks. Graham et al. (2023) reported broadly equal proportions of abrasion and block removal on basement gneisses from West Greenland during a century long readvance-retreat cycle of the front of the Jakobshavn Isbræ.

It is commonly assumed that erosion rate $\dot{\boldsymbol{E}}$ scales with basal sliding rate $\boldsymbol{U}$, or total erosion depth $\boldsymbol{E}$ with total cumulative basal sliding distance $\int \boldsymbol{d}$ over a glaciation, linked with a constant $\boldsymbol{K}$, commonly referred to as the erosion coefficient (e.g. Harbor et al. 1988, Iverson 2012).

$$\dot{\boldsymbol{E}} = \boldsymbol{K}\,\boldsymbol{U}^{\boldsymbol{n}}$$

Or, alternatively

$$\boldsymbol{E} = \boldsymbol{K} \int \boldsymbol{d}$$

Taking the simplifying assumption that the relation is linear ($\boldsymbol{n}$ = 1; but see Herman et al. 2015 and Koppes et al. 2015), erosion coefficients have been established by several studies (Boulton 1974, Humphrey and Raymond 1994, Koppes et al. 2015, Riihimaki et al. 2005), altogether falling in the range of 10^{-3} to 10^{-4}.

For the Forsmark area, Krabbendam et al. (2022a) estimated a value of $0.3–1.1 \times 10^{-6}$, based on the total erosion depth estimated by Hall et al. (2019a) and the cumulative sliding distance from Näslund et al. (2003). This value is considerably (2–3 orders of magnitude) lower than all other studies in Table 7-1, but are consistent with the generally low erosion rates resulting from the TCN inventories (Hall et al. 2019a, 2023), and with those estimated by Briner et al. (1998) for the Cordilleran ice sheet (0.09–0.35 mm yr^{-1}).

Table 7-1. Comparison of erosion coefficients from different studies.

Locality	Erosion rate (mm yr^{-1})	Sliding velocity (m yr^{-1})	Erosion coefficient K	Reference	Lithology
Glacier d'Argentière, France	< 36	250	1.4×10^{-4}	Boulton (1974)	Granite (assumed)
Breiðamerkurjökull Iceland	c 2.5	15	1.6×10^{-4}	Boulton (1974)	Basalt, volcanic rocks (assumed)
Variegated Glacier, Alaska			1.0×10^{-4}	Humphrey and Raymond (1994)	Not reported
Bench Glacier, Alaska	0.9 – 1.8	1–2	1.0×10^{-3}	Riihimaki et al. (2005)	Cretaceous metasedimentary rocks
'Polar glaciers' (Antarctica)	0.01 – 0.1		10^{-3} to 10^{-4}	Koppes et al. (2015)	Not reported
Temperate glaciers (Patagonia)	0.1–10		c 10^{-3}	Koppes et al. (2015)	Not reported
	Total erosion (m)	**Cumulative sliding distance (m)**			
Fennoscandian Ice Sheet	1.6 – 3.5	$3–5 \times 10^{6}$	$0.3–1.1 \times 10^{-6}$	Näslund et al. (2003) Krabbendam et al. (2022a)	Basement gneiss

Thus, in contrast to many other glaciated areas (but likely similar to other low-relief glaciated terrains), Forsmark shows (i) a low erosion depth over the last glaciation, (ii) a low erosion coefficient and (iii) a high abrasion:plucking ratio (or: a low block removal component). Possible factors that may explain this include:

a) The contribution of block removal in this study is underestimated, because it focusses on topographic highs, whilst those based on proglacial sediment grain size 'sample' the entire footprint of the glacier. However, this would not explain the low erosion coefficient.

b) East Sweden is underlain by high-grade metamorphic igneous basement gneisses, which may have a much higher inherent erosion coefficient and resistance to block removal than lithologies in the other study areas, although it would be expected to be similar to the Mont Blanc granite that underlies the Glacier d'Argentière.

c) Most other studies concern montane valley glaciers, which may experience faster and more efficient erosion than the erosion below an ice sheet such as the Fennoscandian Ice Sheet. For instance, valley glaciers may have a more constant supply of debris, provided by valley-side rock fall, or more vigorous meltwater activity. They may also have a higher component of block removal, although the *a priori* reason for this is not obvious.

d) Eastern Sweden is somewhat unusual, in that the 'starting point' of glacial erosion of basement rocks is the very flat and smooth sub-Cambrian unconformity (Lidmar-Bergström 1993, Lidmar-Bergström et al. 2017, Hall et al. 2019a, 2019b). Such smooth surfaces are not conducive to plucking (no edges, no plucking), as evidenced by the smooth abraded surfaces found near Närke, just beneath the sub-Cambrian unconformity (Section 4.9), and the very smooth planar flats (locally termed 'Slättbergen') surfaces in Västergötland (Hall et al. 2019b). Glacial erosion on such surfaces is by necessity mainly by abrasion, and plucking is strongly suppressed, so that the total erosion rate and hence the erosion coefficient is very low. The same could apply, incidentally, to large parts of the Canadian Shield, close to the Great Unconformity of Laurentia.

e) Assuming that abrasion is favoured by thick ice and block removal by thinner ice (e.g. Evans 1996) and vigorous meltwater activity, then it is feasible to argue that the Forsmark area experienced, over the duration of the last glaciation, a relative long period of 'thick ice' conditions that suppress plucking, compared to a relatively short period of thin ice with vigorous meltwater activity that would favour plucking. This fits with the very fast ice-retreat rates, which swept over East Sweden rapidly (200–300 m yr^{-1}; Strömberg 1994, Hedenström and Risberg 2003).

f) All other studies (Table 7-1) concern modern glaciers that are in a present state of deglaciation, whilst the estimates for the Fennoscandian Ice Sheet herein concern erosion over an entire glaciation. It may be that erosion during deglaciation conditions is more efficient, for instance because more water is available to the base of the ice, or because of more frequent and/or larger basal water pressure variations. This latter point, however, would not apply to the 'Polar glaciers' in the Koppes et al. (2015) study.

Whatever the reason, the wide range (over 3 orders of magnitude) of these values suggests that the concept of a simple erosion rule, or a simple erosion coefficient is of limited value for realistic erosion modelling over a glaciation, unless the reasons of this variability are better understood and can be more reliably predicted.

7.5 Block removal mechanisms

A specific feature of our study sites is the large proportion of block removal features such as crescentic scars and sockets, that differ from features formed by 'classic' lee-side plucking or quarrying (e.g. Rea and Whalley 1996, Iverson 2012, Zoet et al. 2013) or lateral plucking (Krabbendam and Bradwell 2011). Sockets and crescentic scars are particularly abundant at the Lilla Sandgrund sites, which show very limited classic lee-side plucking, in contrast to Stånggrundet where lee-side and lateral plucking are more common. This difference is likely related to the abundance of subhorizontal fractures, generally higher fracture density and their high connectivity and orthogonal ('blocky') nature of the fracture pattern at Stånggrundet (see also Section 7.2.2), suggesting these would favour classic lee-side and lateral plucking. In contrast the relative abundance of subvertical fractures, but relative lack of connected fractures and subhorizontal fractures at Lilla Sandgrund would suppress classic lee-side plucking, but still allow the formation of sockets and crescentic scars.

Hall et al. (2019a) suggested that the sockets were formed as a result of high subglacial water pressure, although no detailed formation model was described.

Crescentic scars are generally thought to form by high, focussed clast-bed contact forces (oblique Hertzian cone stress) exerted by large clast embedded in basal ice (e.g. Gilbert 1906, Ficker et al. 1980, Krabbendam et al. 2017). These forces increase with clast size and the formation of crescentic scars is thus greatly enhanced by the presence of large (> 0.5 m) clasts embedded in basal ice. Models of classic lee-side plucking (e.g. Iverson 2012, Zoet et al. 2013) do not rely on such large, embedded clasts.

As it happens, the widespread occurrence of glacial ripping in the Forsmark area (Hall et al. 2020, Krabbendam et al. 2022a, 2022b) provides a ready supply of large boulders to the ice-bed. This likely enhanced the possibility of erosion by high clast-bed contact forces, down-ice of areas where ripping occurred. Hence, it is possible that the formation of crescentic scars is favoured in areas where there is a higher supply of large boulders, be it by glacial ripping beneath ice sheets or by supraglacial supply in more mountainous settings.

7.6 Evolution and development of roughness of glacial erosion surfaces

Conceptual models of classic lee-side plucking envisage a stepped topography, with fractures dipping down-ice, and a series of plucked rock steps edges facing down-ice (Rea and Whalley 1996, Iverson 2012, Zoet et al. 2013, Ugelvig et al. 2016). Progressive erosion by such lee-side plucking results in a form of headward erosion of individual rock steps, whereby local up-ice directed erosion is faster than the downward erosion of the abraded tops (Figure 7-1A). Crucially, the planform, the surface types, the overall landscape character and the surface roughness do not change as subglacial erosion progresses.

This study suggests the possibility of a very different evolution and development of roughness with progressive glacial erosion (Figure 7-1B). Surfaces are initially smooth, and mainly eroded by abrasion, with the local geomorphology essentially dominated by low-curvature whalebacks. Block removal starts with the development of sockets and crescentic scars, which can occur anywhere on the whaleback (stoss-side, top, lee-side). Sockets and crescentic scars are enlarged by flaking and plucking into larger composite sockets, scars and hollows. These may occur on the lee-side of whaleback, but equally on the top. The result is a progressive increase in roughness (on the decimetre to metre scale) of the glaciated surface.

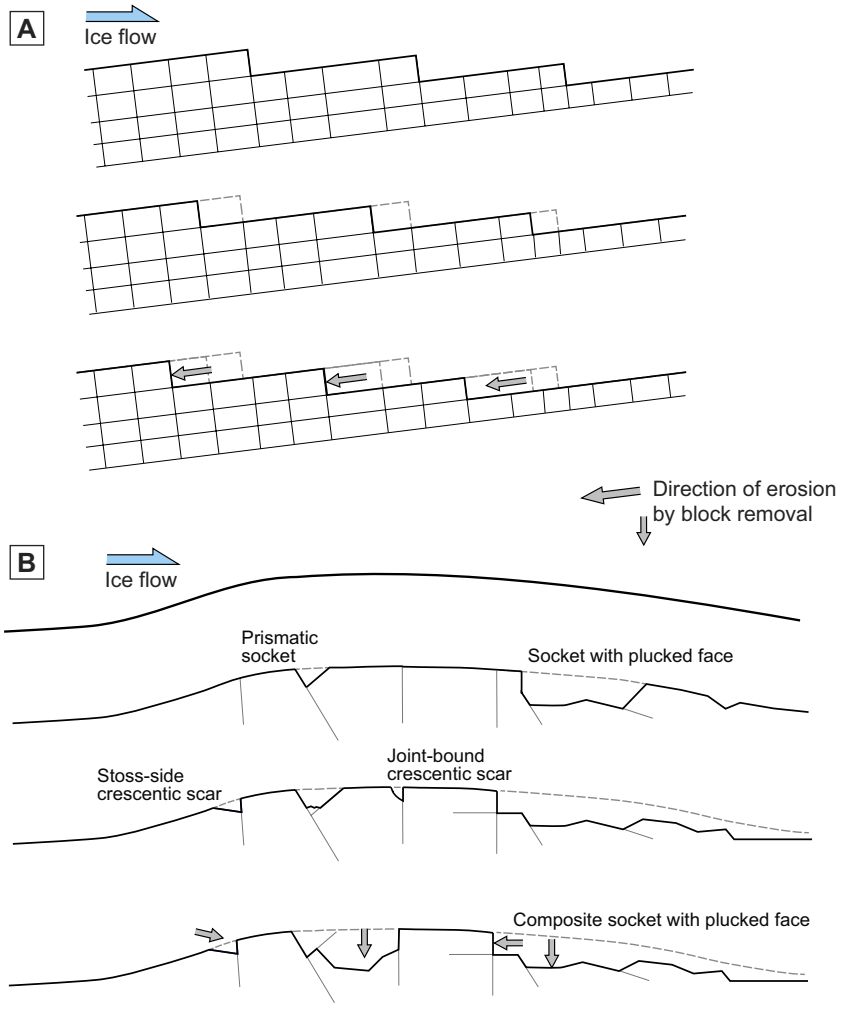

Figure 7-1. *A. Conceptual model of glacial surface evolution, dominated by classic lee-side plucking (e.g. Rea and Whalley 1996, Iverson 2012). B. Conceptual model of subglacial bedrock surface evolution with progressive development of sockets, crescentic scars, plucking. Direction of net erosion by block removal indicated by grey arrows.*

Which mode of geomorphological evolution is dominant is controlled by the prevailing fracture network, but also likely on the nature of the pre-glacial landscape, e.g. whether or not the preglacial landscape is controlled by a very flat smooth surface, such as the sub-Cambrian unconformity in Baltica and in Laurentia, further discussed in Section 7.7.

7.7 Controls on abrasion, block removal and glacial erosion

A number of controls on abrasion, block removal and subglacial erosion rates emerge from this study. These are here discussed in a wider context. Following controls emerge:

- **Glaciological controls.** It is commonly assumed that thick ice suppresses cavity formation and hence plucking and thus (relatively speaking) favours abrasion; conversely thin ice would favour cavity formation and hence plucking (e.g. Evans 1996). Although the mechanism of plucking is uncertain, it is also likely that variable water pressure in cavities, including short-term overpressure events, assist or contribute to plucking (Iverson 1991, 2012, Zoet et al. 2013). Such water pressure variations are particular active in the ablation zone of ice sheets, such as the Greenland Ice Sheet (Doyle et al. 2013, Andrews et al. 2014, Wright et al. 2016, Harper et al. 2019). Glaciological controls integrated over the duration of a glaciation are not likely to vary much in a small area (with respect to the overall glacier or ice sheet) since such a small area will have experienced broadly the same sequence of glaciological conditions during that glaciation. Therefore different glacial conditions cannot explain spatial differences in landform development at the small scale. However, at Forsmark, there is qualitative evidence for an intense late phase of block removal: socket formation and crescentic scars at Lilla Sandgrund and lee-side and lateral plucking at Stånggrundet al. having a higher number of sharp edges than would be expected if block removal (and re-abrasion) rates where constant throughout Late Weichselian ice cover. This is consistent with the notion that block removal is suppressed by thick ice but enhanced by thin ice (and, likely, meltwater activity) and thus suggest a temporal (rather than spatial) glaciological control on erosion mechanisms in east Sweden. In east Sweden it can then be argued that the period of thin ice with high meltwater activity was very short compared to the much longer period of thick ice cover. Ice-margin retreat after the cold Younger Dryas period was very rapid in east Sweden (200–300 m yr^{-1}; Strömberg 1994, Hedenström and Risberg 2003), likely resulting in a relatively short period of time during which thin ice with meltwater activity conditions were prevalent in any particular location. The time period of such ablation-zone conditions may have lasted as little as 1–2 ka, compared to the overall c 25 ka duration of ice cover (SKB 2020) during the Late Weichselian glaciation at Forsmark. The relative short period during which block removal was favourable can then provide a plausible explanation for (i) the relative high abrasion:plucking ratio; (ii) the relative low erosion rates; (iii) the relative low erosion coefficients, compared to other studies, especially those on mountain glaciers and hence most compared in Section 7.4.2 and Table 7-2. In particular Holocene mountain glaciers are mostly thought to be temperate throughout and have long-lived (> 10 ka) ablation zones in their lower reaches. In summary, over a glaciation, the proportion of time at a particular site being under ‘thick-ice’ conditions vs. under ‘ablation-zone’ conditions may have a strong effect on the total erosion depth and the dominant erosion mechanisms.
- **Fracture control:** Although rather ignored in the 20th century, it is now widely accepted that densely fractured rock is more susceptible to plucking than more sparsely fractured rock (Dühnforth et al. 2010, Krabbendam and Glasser 2011, Hooyer et al. 2012, Lane et al. 2015, Iverson 2012, Skyttä et al. 2023). This is confirmed in this study, where the higher fracture density at Stånggrundet suggests at least a higher proportion of the surface area affected by plucking. However, this study also suggest that the *type* of fracture network has a more subtle effect, namely:
  A. Classic-lee side plucking is favoured by an orthogonal fracture pattern that includes gently dipping fractures, which delineates approximate rectangular blocks, as at Stånggrundet;
  B. Formation of crescentic scars and sockets is favoured by a fracture network dominated by steeply dipping fractures, as at the Lilla Sandgrund sites; however the relative lack of gently dipping fractures implies that classic-lee side plucking is suppressed by such a fracture network.

- **Abrasion resistance.** It is generally accepted that 'softer' rocks have lower abrasion resistance than 'harder' rocks (e.g. Boulton 1979, Hallet 1979). However, the issue is what constitutes 'softer' and 'harder'.
  A. Mineralogical differences: carbonate rocks would be expected to be softer that silicate rocks (basement rocks and siliciclastic sedimentary rocks), simply because carbonate minerals have a lower Mohs hardness than quartz and feldspar.
  B. Within the (wide) group of silicate rocks, Schmidt Hammer hardness, a reasonable proxy for uniaxial compressive strength (UCS), has been shown to be related to abrasion resistance (Krabbendam and Glasser 2011). At the grain scale, this likely relates to how densely packed, indurated or recrystallized the grains are within the intact rock mass.
  C. A further potential effect proposed here (Section 7.2.1) is that, other things being equal, fine-grained rocks may have lower abrasion resistance than coarse-grained rocks. The rationale is that, within a given time period and with a given grain size distribution within subglacial debris, there will be more particles in the debris that are coarser than the fine-grained rocks and less that are coarser than the coarse-grained rocks. Thus, in fine-grained rocks more damaging debris-rock interactions will occur that result in effective abrasion. This hypothesised control deserves further study.
- **Precursor surface.** Lastly, the precursor surface prior to glaciation may control the susceptibility to block removal – an effect to our knowledge not previously discussed. The rationale behind this is as follows: block removal from a smooth surface, without steps, is more difficult than from a stepped surface. In essence, some sort of stepped edge is necessary for plucking to occur. No steps: no plucking. Conversely, a precursor surface with considerable roughness likely comprises abundant down-ice steps, which would be susceptible to plucking. For example, preglacial weathering can result in an uneven weathering front; if then subjected to glacial erosion, whalebacks and roche moutonnées can form that have a strong morphological component of inheritance (e.g. Lindström 1988, Lidmar-Bergström 1995, Olvmo et al. 2005, Lidmar-Bergström et al. 2017). This has been documented widely in west and south Sweden, presumably due to the highly uneven Mesozoic weathering fronts in those areas (in contrast to the much flatter sub-Cambrian unconformity in central and east Sweden).

The suppression of plucking by very flat precursor surfaces in east Sweden is supported by:

a) The occurrence of very smooth surfaces mapped as abraded surfaces at Lilla Sandgrund sites, and the different landforms that suggest progressive roughening of such smooth surfaces as proposed in Section 7.6;
b) The occurrence of smooth whalebacks, without evidence of block removal, at Närke (Section 5.9);
c) The occurrence of very smooth planar flats (locally termed *Slättbergen*), just beneath the sub-Cambrian unconformity in Västergötland (Hall et al. 2019b, Goodfellow et al. 2019): these surfaces show striations but are so flat and smooth that plucking is not possible and has not occurred on the tops of the planar flats themselves, only at their edges. Hall et al. (2019b) interpreted these surfaces as reflecting the original flatness of the sub-Cambrian unconformity; whereas Goodfellow et al. (2019) suggested they were formed by removal of basement bedrock along very long, horizontal fractures (sheet joints). Regardless of their exact origin, neither of these very detailed studies mentions evidence of block removal from these surfaces.

It does appear that very smooth surfaces suppress block removal, forming a kind of carapace or armour, and only allowing abrasion to proceed. Once this armour has been breached and roughened by sockets or crescentic scars (or in other settings by subglacial meltwater erosion, for instance along fracture zones), these can be expanded rapidly by subsequent plucking (Section 7.6). Once the surface has been roughened (at the decimetre – metre scale) block removal can occur more widely and, given the right glacial conditions, more rapidly.

Whilst the occurrence of such flat precursor surface, likely with strong geological control, may appear rather rare and coincidental, they may occur more widely than previously thought. The sub-Cambrian unconformity in Baltica (Scandinavia) has its counterpart as the Great Unconformity in Laurentia (North America), and glaciated surfaces at the southern edge of the Canadian Shield have a similar overall flatness and smoothness, for instance along the shores of Georgian Bay, Ontario. At a scale

smaller than Unconformities, very flat surfaces also occur at the tops of the inselbergs of Halleberg, Hunneberg and Billingen in Västergötland (e.g. Figure 3-43 in Hall et al. 2019b), perhaps related to the top of the quartz-dolerite sill that forms these hills.

7.8 Depth of erosion at Forsmark during the Late Weichselian glaciation

The depth of glacial erosion by the Fennoscandian Ice Sheet during the Late Weichselian glaciation was low. The contribution of abrasion varies from c 0.2–0.5 m (at Wave Rock) to c 1.1–1.5 m at the coastal outcrops. These values are consistent with similarly low abrasion depths estimated by Briner and Swanson (1998) for the Cordilleran ice sheet over the last glaciation (0.25–1 m). Late stage block removal, by a combination of sockets, crescentic scars and lee-side and lateral plucking, contributed 0–1.6 m of erosion. Thus, the range of total erosion is between c 0.2–2.6 m over the Late Weichselian glaciation. The different interpretation as to the relative contribution of abrasion and block removal by Hall et al. (2023) does as such not change these overall erosion depth estimates.

Elsewhere, glacial ripping contributed *locally* a further 2–4 m of erosion but, near Forsmark, this affected only c 10–20 % of the bed (Krabbendam et al. 2022a). These low erosion depths, totalling a few metres at most, are consistent with the overall results of the TCN analysis, which yielded inheritance in all samples (Hall et al. 2019a, 2023). It is also consistent with the depth of erosion of basement rocks (over multiple glaciations) below the flat sub-Cambrian unconformity which Hall et al. (2019a) estimated at Forsmark to be 12 m maximum. Somewhat deeper erosion occurred in trenches and valleys, as discussed in Hall et al. (2022).

8 Conclusions

Detailed geomorphological analysis of high-resolution DSM data can provide quantitative estimates of the depth of erosion by block removal over a glaciation. Combined with erosion depth estimates from TCN inventories on summit surfaces, the relative and absolute contribution of abrasion and block removal over a glaciation can be estimated. This study focusses on erosion depths over the last, Late Weichselian, glaciation at Forsmark, east Sweden.

DSM analysis, geomorphological, fracture and bedrock mapping were performed at five selected sites at the Forsmark site: at Stora Asphällan, Stånggrundet and three sites on Lilla Sandgrund. The geomorphological mapping separated out three surface types:

A. abraded surfaces, with low roughness, long-wavelength (> 10 m), low slope, showing only evidence of abrasion;
B. block-removal surfaces, with higher roughness, locally steep slopes, fresh fracture surfaces and a small (< 2 m) wavelength of topographic highs. These surfaces include surfaces subjected to typical lee-side and lateral plucking (quarrying) but also crescentic scars and sockets;
C. re-abraded block-removal surfaces, with similar shape as the block-removal surfaces, except showing signs of abrasion, polishing and edge rounding.

Morphometric analysis of the DSM supports the systematic distinction between abraded and block-removal surfaces. Field mapping showed both sharp and rounded edges in block removal domains. The abundance of sharp edges suggest that block removal was particularly active just prior to deglaciation. However, block removal also must have occurred somewhat earlier during the Late Weichselian to allow significant edge rounding to occur, typical edge rounding involved erosion of 1–15 cm.

The spatial extent of block removal surfaces (fresh and re-abraded) varies from c 50 % at sites on Lilla Sandgrund to c 90 % at Stånggrundet; fresh block removal surfaces vary from 6 – 37 % of surfaces (not separated for Stånggrundet).

By modelling an extrapolated abraded surface over the present-day surface, the depth of erosion by block removal can be spatially estimated. The estimated depth of block removal ranges from 0–1.3 m, and averaged 0.2–0.35 m where it did occur, i.e. excluding the abraded surfaces. Averaged over the entire area, including the abraded surfaces, the average depth of block removal amounted to 0.1–0.3 m. These estimates can be combined or compared with estimates of erosion depths over the Late Weichselian glaciation at Forsmark based on TCN inventories from previous work (Hall et al. 2019a, 2023). TCN erosion depth estimates from summit surfaces mapped as abraded surfaces range between 1.17–1.40 m; results from other surfaces, including re-abraded surfaces reach 2.18 m. Comparing the interpreted abrasion and block removal depth results in abrasion:plucking ratios from 16:1 to 3:1.

These estimates are applicable to relative topographic highs: the excavation of topographic lows (such as trenches, joint-valleys) would need to be added to a regionally averaged erosion depth.

Depth of erosion by abrasion and block removal, and their relative importance, are spatially variable. Estimates of abrasion depth from Wave Rock summit areas, further inland, c 0.2–0.4 m (Hall et al. 2023), considerably less than the 1.17–1.40 m interpreted at the costal outcrops. Differences in interpreted abrasion depths between Wave Rock and coastal outcrops at Forsmark may be related to differences in grain size and/or higher local relief at Wave Rock.

Variability of block removal is strongly linked to bedrock fracture density and fracture connectivity. Rock surfaces with a dense, well-connected fracture pattern that delineates small blocks (e.g. Stånggrundet) are significantly more susceptible to block removal than rock surfaces with lower fracture density, and/or lower connected, fracture patterns. Rock surfaces with predominant steeply inclined fractures are less susceptible to lee-side and lateral plucking, but appear more susceptible to other block removal mechanisms, such as formation of sockets and various crescentic scars. The Forsmark rock surfaces, in particular the Lilla Sandgrund sites, show a rich variety and abundance of such crescentic scars, which may be related to the abundance of large (> 1 m) boulders, likely formed up-ice by glacial ripping. Such boulders, embedded in basal ice, would potentially exert very high clast-bed forces.

The development of block removal surfaces at some sites does not follow up-ice migration of lee-side steps. Rather, progressive glacial erosion in the Forsmark area is characterised by a progressive destruction of smooth abraded-only surfaces. This process starts with the development of sockets and crescentic scars, which progressively amalgamate into composite block removal surfaces, allowing classic-lee side plucking to proceed. Overall this leads to a progressive roughening of the surface.

Compared to other glacial erosion studies, the overall erosion depth in east Sweden during the Late Weichselian glaciation is low, with a low erosion coefficient and a high abrasion:plucking ratio. This may be explained by a combination of:

- hard basement rocks, with locally fracture patterns unfavourable for plucking (quarrying);
- a very flat starting surface controlled by the sub-Cambrian unconformity, suppressing plucking;
- thick-ice conditions (suppressing block-removal including plucking) lasting the majority of the Late Weichselian glaciation, followed by a very short period of thin-ice, ablation-zone conditions during deglaciation that favoured subglacial erosion by block-removal including plucking, and locally glacial ripping.

Overall, the depth of erosion at Forsmark during the Late Weichselian glaciation was low. Abrasion contributed between 0.2 to 1.5 m of erosion, in line with results from other ice-sheet settings. Block removal by plucking and formation of sockets and crescentic scars contributed another 0–1.6 m of erosion, so that in most areas abrasion depth exceeded block removal depth. These low erosion depths of a maximum of 0.2 to 3 m are consistent with the overall results of the TCN analysis, which showed inheritance in all samples (Hall et al. 2019a, 2023). Locally, affecting perhaps 10–20 % of the area, glacial ripping added a further 2–4 m of erosion. Somewhat deeper erosion occurred in trenches and valleys.

References

SKB's (Svensk Kärnbränslehantering AB) publications can be found at www.skb.com/publications.

Alley R, Cuffey K, Zoet L, 2019. Glacial erosion: status and outlook. Annals of Glaciology 60, 1–13.

Andrén T, Björck S, Andrén E, Conley D, Zillén L, Anjar J, 2011. The development of the Baltic Sea Basin during the last 130 ka. In Harff J, Björck S, Hoth P (eds). The Baltic Sea Basin. Berlin: Springer, 75–97.

Andrews L C, Catania G A, Hoffman M J, Gulley J D, Lüthi M P, Ryser C, Hawley R L, Neumann T A, 2014. Direct observations of evolving subglacial drainage beneath the Greenland Ice Sheet. Nature 514, 80–83.

Asch K, 2005. IGME 5000: 1:5 Million International Geological Map of Europe and Adjacent Areas. Hannover: Federal Institute for Geosciences and Natural Resources.

Benn D I, Evans D J A, 2010. Glaciers and glaciation. 2nd edition ed. London: Hodder Education.

Boulton G S, 1974. Processes and patterns of glacial erosion. Glacial Geomorphology Springer, 41–87.

Boulton G S, 1979. Processes of glacier erosion on different substrata. Journal of glaciology 23, 15–38.

Briner J P, Swanson T W, 1998. Using inherited cosmogenic ^{36}Cl to constrain glacial erosion rates of the Cordilleran ice sheet. Geology 26, 3–6.

Carlsson A, 1979. Characteristic Features of a Superficial Rock Mass in Southern Sweden. Uppsala Societas Upsaliensis pro Geologia Quaternaria. (Striae 11), 1–79.

Cox R, Lopes W A, Jahn K L, 2018. Quantitative roundness analysis of coastal boulder deposits. Marine Geology 396, 114–141.

Doyle S H, Hubbard A L, Dow C F, Jones G A, Fitzpatrick A, Gusmeroli A, Kulessa B, Lindback K, Pettersson R, Box J E, 2013. Ice tectonic deformation during the rapid in situ drainage of a supraglacial lake on the Greenland Ice Sheet. The Cryosphere 7, 129–140.

Drewry D, 1986. Glacial geologic processes. London: Edward Arnold.

Dühnforth M, Anderson R S, Ward D, Stock G M, 2010. Bedrock fracture control of glacial erosion processes and rates. Geology 38, 423–426.

Embleton C, King C A M, 1975. Glacial geomorphology. 2nd edition ed. London: Edward Arnold.

Evans I S, 1996. Abraded rock landforms (whalebacks) developed under ice streams in mountain areas. Annals of Glaciology 22, 9–16.

Eyles N, 2006. The role of meltwater in glacial processes. Sedimentary Geology 190, 257–268.

Ficker E, Sonntag G, Weber E, 1980. Ansätze fur mechanischen Deutung des Rissentstehung bei Parabelrissen und Sichelbrüchen auf glazial geformten Felsoberflächen. Zeitschrift für Gletscherkunde und Glazialgeologie 16, 25–43.

Gabrielsen R H, Nystuen J P, Jarsve E M, Lundmark A M, 2015. The Sub-Cambrian Peneplain in southern Norway: its geological significance and its implications for post-Caledonian faulting, uplift and denudation. Journal of the Geological Society 172, 777–791.

Gilbert G K, 1906. Crescentic gouges on glaciated surfaces. Bulletin of the Geological Society of America 17, 303–316.

Glamheden R, Fredriksson A, Roeshoff K, Karlsson J, Hakami H, Christiansson R, 2007. Rock mechanics Forsmark. Site descriptive modelling Forsmark stage 2.2. SKB R-07-31, Svensk Kärnbränslehantering AB.

Glasser N F, Bennett M R, 2004. Glacial erosional landforms: origins and significance for palaeoglaciology. Progress in Physical Geography 28, 43–75.

Goodfellow B W, Stroeven A P, Martel S J, Heyman J, Rossi M, Caffee M W, 2019. Exploring alternative models for the formation of conspicuously flat basement surfaces in southern Sweden. SKB TR-19-22, Svensk Kärnbränslehantering AB.

Graham B L, Briner J P, Young N E, Balter-Kennedy A, Koppes M, Schaefer J M, Poinar K, Thomas E K, 2023. In situ 10 Be modeling and terrain analysis constrain subglacial quarrying and abrasion at Jakobshavn Isbræ, Greenland. The Cryosphere 17, 4535–4547.

Greenwood S L, Clason C C, Nyberg J, Jakobsson M, Holmlund P, 2017. The Bothnian Sea ice stream: early Holocene retreat dynamics of the south-central Fennoscandian Ice Sheet. Boreas 46, 346–362.

Hall A M, Ebert K, Hättestrand C, 2013. Pre-glacial landform inheritance in a glaciated shield landscape. Geografiska Annaler: Series A, Physical Geography 95, 33–49.

Hall A M, Ebert K, Goodfellow B W, Hättestrand C, Heyman J, Krabbendam M, Moon S, Stroeven A P, 2019a. Past and future impact of glacial erosion in Forsmark and Uppland. SKB TR-19-07, Svensk Kärnbränslehantering AB.

Hall A M, Krabbendam M, van Boeckel M, Ebert K, Hättestrand C, Heyman J, 2019b. The sub-Cambrian unconformity in Västergötland, Sweden: Reference surface for Pleistocene glacial erosion of basement. SKB TR-19-21, Svensk Kärnbränslehantering AB.

Hall A M, Krabbendam M, van Boeckel M, Goodfellow B W, Hättestrand C, Heyman J, Palamakumbura R, Stroeven A P, Näslund J-O, 2020. Glacial ripping: geomorphological evidence from Sweden for a new process of glacial erosion. Geografiska Annaler: Series A, Physical Geography 102, 333–353.

Hall A M, Krabbendam M, van Boeckel M, 2022. Glacial erosion in the Öregrund archipelago. Potential for headward erosion towards Forsmark in future glaciations? SKB TR-22-08, Svensk Kärnbränslehantering AB.

Hall A M, Heyman J, Hein A S, 2023. Glacial erosion rates at Forsmark derived from Terrestrial Cosmogenic Nuclides: additional results. SKB TR-23-21, Svensk Kärnbränslehantering AB.

Hallet B, 1979. A theoretical model of glacial abrasion. Journal of Glaciology 23, 39–50.

Hangl M, Danzer R, Paar R, 1997. Edge toughness of brittle materials. Engineering Ceramics' 96: Higher Reliability Through Processing, 327–335.

Harbor J M, Hallet B, Raymond C F, 1988. A numerical model of landform development by glacial erosion. Nature 333, 347–349.

Harper J T, Meierbachtol T, Humphrey N F, 2019. Greenland ICE Project, Final Report. SKB R-18-06, Svensk Kärnbränslehantering AB.

Harris Jr S E, 1943. Friction cracks and the direction of glacial movement. The Journal of Geology 51, 244–258.

Hedenström A, Risberg J, 2003. Shore displacement in northern Uppland during the last 6 500 calendar years. SKB TR-03-17, Svensk Kärnbränslehantering AB.

Hermansson T, Stephens M B, Page L M, 2008. 40Ar/39Ar hornblende geochronology from the Forsmark area in central Sweden: constraints on late Svecofennian cooling, ductile deformation and exhumation. Precambrian Research 167, 303–315.

Herman F, Beyssac O, Brughelli M, Lane S N, Leprince S, Adatte T, Lin J Y, Avouac J-P, Cox S C, 2015. Erosion by an Alpine glacier. Science 350, 193–195.

Heyman J, Goodfellow B W, Stroeven A P, Hall A M, Caffee M, Hättestrand C, Ebert K, Näslund J-O, Hippe K, Martel S, Moon S, Perron J T, Stuart F M, 2019. Erosion of low-relief basement by the Fennoscandian ice sheet based on bedrock ^{10}Be and ^{26}Al. In 20th International Union for Quaternary Research, Dublin, 25–31 July 2019. Utrecht: INQUA Foundation.

Hildes D H, Clarke G K, Flowers G E, Marshall S J, 2004. Subglacial erosion and englacial sediment transport modelled for North American ice sheets. Quaternary Science Reviews 23, 409–430.

Hooyer T S, Cohen D, Iverson N R, 2012. Control of glacial quarrying by bedrock joints. Geomorphology 153–154, 91–101.

Humphrey N F, Raymond C, 1994. Hydrology, erosion and sediment production in a surging glacier: Variegated Glacier, Alaska, 1982–83. Journal of Glaciology 40, 539–552.

Hättestrand C, Stroeven A P, 2002. A relict landscape in the centre of Fennoscandian glaciation: Geomorphological evidence of minimal Quaternary glacial erosion. Geomorphology 44, 127–143.

Iverson N R, 1991. Potential effects of subglacial water-pressure fluctuations on quarrying. Journal of Glaciology 37, 27–36.

Iverson N R, 2012. A theory of glacial quarrying for landscape evolution models. Geology 40, 679–682.

Jahnke B, Ruplinger C, Bate C E, Trzeciak M, Sone H, Wang H F, 2022. Fracture toughness of schist, amphibolite, and rhyolite from the Sanford Underground Research Facility (SURF), Lead, South Dakota. Scientific Reports 12, 1594.

Jahns R H, 1943. Sheet structure in granites: its origin and use as a measure of glacial erosion in New England. The Journal of Geology 51, 71–98.

Kazi A, Al-Mansour Z R, 1980. Influence of geological factors on abrasion and soundness characteristics of aggregates. Engineering Geology 15, 195–203.

Kirkbride M P, Bell C M, 2010. Edge-roundness of boulders of Torridonian Sandstone (northwest Scotland): applications for relative dating and implications for warm and cold climate weathering rates. Boreas 39, 187–198.

Kleman J, Stroeven A P, 1997. Preglacial surface remnants and Quaternary glacial regimes in northwestern Sweden. Geomorphology 19, 35–54.

Kleman J, Hättestrand C, Clarhäll A, 1999. Zooming in on frozen-bed patches: scale-dependent controls on Fennoscandian ice sheet basal thermal zonation. Annals of Glaciology 28, 189–194.

Kleman J, Stroeven A P, Lundqvist J, 2008. Patterns of Quaternary ice sheet erosion and deposition in Fennoscandia and a theoretical framework for explanation. Geomorphology 97, 73–90.

Koppes M, Hallet B, Rignot E, Mouginot J, Wellner J S, Boldt K, 2015. Observed latitudinal variations in erosion as a function of glacier dynamics. Nature 526, 100–103.

Kor P, Shaw J, Sharpe D, 1991. Erosion of bedrock by subglacial meltwater, Georgian Bay, Ontario: a regional view. Canadian Journal of Earth Sciences 28, 623–642.

Korja A, Heikkinen P, Aaro S, 2001. Crustal structure of the northern Baltic Sea palaeorift. Tectonophysics 331, 341–358.

Krabbendam M, Bradwell T, 2011. Lateral plucking as a mechanism for elongate erosional glacial bedforms: explaining megagrooves in Britain and Canada. Earth Surface Processes and Landforms 36, 1335–1349.

Krabbendam M, Glasser N, 2011. Glacial erosion and bedrock properties in NW Scotland: Abrasion and plucking, hardness and joint spacing. Geomorphology 130, 374–383.

Krabbendam M, Eyles N, Putkinen N, Bradwell T, Arbelaez-Moreno L, 2016. Streamlined hard beds formed by palaeo-ice streams: A review. Sedimentary Geology 338, 24–50.

Krabbendam M, Bradwell T, Everest J D, Eyles N, 2017. Joint-bounded crescentic scars formed by subglacial clast-bed contact forces: Implications for bedrock failure beneath glaciers. Geomorphology 290, 114–127.

Krabbendam M, Palamakumbura R, Arnhardt C, Hall A, 2021. Rock fracturing by subglacial hydraulic jacking in basement rocks, eastern Sweden: the role of beam failure. GFF 143, 1–16.

Krabbendam M, Hall A M, Palamakumbura R, Finlayson A, Diogardi F, Arnhardt C, 2022a. Glacial ripping as a significant erosion mechanism in eastern Sweden – Field evidence and modelling, SKB TR-22-09, Svensk Kärnbränslehantering AB.

Krabbendam M, Hall A M, Palamakumbura R N, Finlayson A, 2022b. Glaciotectonic disintegration of roches moutonnées in east Sweden: a transient phase during glacial ripping. Geografiska Annaler: Series A, Physical Geography 104, 35–56.

Lane T P, Roberts D H, Rea B R, Cofaigh C Ó, Vieli A, 2015. Controls on bedrock bedform development beneath the Uummannaq Ice Stream onset zone, West Greenland. Geomorphology 231, 301–313.

Leijon B, 2005. Forsmark site investigation: Investigations of superficial fracturing and block displacements at drill site 5. SKB P-05-199, Svensk Kärnbränslehantering AB.

Lidmar-Bergström K, 1993. Denudation surfaces and tectonics in the southernmost part of the Baltic Shield. Precambrian Research 64, 337–345.

Lidmar-Bergström K, 1995. Relief and saprolites through time on the Baltic Shield. Geomorphology 12, 45–61.

Lidmar-Bergström K, Olvmo M, Bonow J M, 2017. The South Swedish Dome: a key structure for identification of peneplains and conclusions on Phanerozoic tectonics of an ancient shield. GFF 139, 244–259.

Lindström E, 1988. Are roches moutonnées mainly preglacial forms? Geografiska Annaler: Series A, Physical Geography 70, 323–331.

Loso M G, Anderson R S, Anderson S P, 2004. Post–Little Ice Age record of coarse and fine clastic sedimentation in an Alaskan proglacial lake. Geology 32, 1065–1068.

Lundmark A M, Lamminen J, 2016. The provenance and setting of the Mesoproterozoic Dala Sandstone, western Sweden, and paleogeographic implications for southwestern Fennoscandia. Precambrian Research 275, 197–208.

Näslund J-O, Rodhe L, Fastook J L, Holmlund P, 2003. New ways of studying ice sheet flow directions and glacial erosion by computer modelling—examples from Fennoscandia. Quaternary Science Reviews 22, 245–258.

Nielsen A T, Schovsbo N H, 2011. The Lower Cambrian of Scandinavia: depositional environment, sequence stratigraphy and palaeogeography. Earth-Science Reviews 107, 207–310.

Olvmo M, Lidmar-Bergström K, Ericson K, Bonow J M, 2005. Saprolite remnants as indicators of pre-glacial landform genesis in southeast Sweden. Geografiska Annaler: Series A, Physical Geography 87, 447–460.

Okko V, 1950. Friction cracks in Finland. Helsinki: Geological Survey of Finland (Bulletin de Commission Geologique Finlande 23), 45–50.

Palamakumbura R, Krabbendam M, Whitbread K, Arnhardt C, 2020. Data acquisition by digitizing 2-D fracture networks and topographic lineaments in geographic information systems: further development and applications. Solid Earth 11, 1731–1746. https://doi.org/10.5194/se-11-1731-2020

Patton H, Hubbard A, Andreassen K, Auriac A, Whitehouse P L, Stroeven A P, Shackleton C, Winsborrow M, Heyman J, Hall A M, 2017. Deglaciation of the Eurasian ice sheet complex. Quaternary Science Reviews 169, 148–172.

Prest V K, 1983. Canada's heritage of glacial features. Ottawa: Geological Survey of Canada. (Geological Survey of Canada Miscellaneous Report 28)

Quinn J, Su L, Flanders L, Lloyd I, 2000. "Edge toughness" and material properties related to the machining of dental ceramics. Machining Science and Technology 4, 291–304.

Rand C, Goehring B M, 2019. The distribution and magnitude of subglacial erosion on millennial timescales at Engabreen, Norway. Annals of Glaciology 60, 73–81.

Rastas J, Seppälä M, 1981. Rock jointing and abrasion forms on roches moutonnées, SW Finland. Annals of Glaciology 2, 159–163.

Rea B R, Whalley W B, 1996. The role of bedrock topography, structure, ice dynamics and preglacial weathering in controlling subglacial erosion beneath a high-latitude, maritime ice field. Annals of Glaciology 22, 121–125.

Riihimaki C A, MacGregor K R, Anderson R S, Anderson S P, Loso M G, 2005. Sediment evacuation and glacial erosion rates at a small alpine glacier. Journal of Geophysical Research: Earth Surface 110.

Sanderson D J, Nixon C W, 2015. The use of topology in fracture network characterization. Journal of Structural Geology 72, 55–66.

Sandström B, Tullborg E, Smellie J, MacKenzie A, Suksi J, 2008. Fracture mineralogy of the Forsmark site. SKB R-08-102, Svensk Kärnbränslehantering AB.

Sandström B, Tullborg E-L, Larson S Å, Page L, 2009. Brittle tectonothermal evolution in the Forsmark area, central Fennoscandian Shield, recorded by paragenesis, orientation and $^{40}Ar/^{39}Ar$ geochronology of fracture minerals. Tectonophysics 478, 158–174.

Shackleton C, Patton H, Hubbard A, Winsborrow M, Kingslake J, Esteves M, Andreassen K, Greenwood S L, 2018. Subglacial water storage and drainage beneath the Fennoscandian and Barents Sea ice sheets. Quaternary Science Reviews 201, 13–28.

Sharp M, Gomez B, 1986. Processes of debris comminution in the glacial environment and implications for quarts sand-grain micromorphology. Sedimentary Geology 46, 33-47.

Singhal B B S, Gupta R P, 2010. Applied hydrogeology of fractured rocks. Dordrecht: Springer Dordrecht.

SKB, 2020. Post-closure safety for the final repository for spent nuclear fuel at Forsmark. Climate and climate-related issues, PSAR version. SKB TR-20-12, Svensk Kärnbränslehantering AB.

Skyttä P, Nordbäck N, Ojala A, Putkinen N, Aaltonen I, Engström J, Mattila J, Ovaskainen N, 2023. The interplay of bedrock fractures and glacial erosion in defining the present-day land surface topography in mesoscopically isotropic crystalline rocks. Earth Surface Processes and Landforms 48, 1956–1968.

Slocum R D, 1978. Friction cracks as directional indicators of glacial flow on Mt. Desert Island, Maine. The Ohio Journal of Science 78, 11–17.

Smith M W, 2014. Roughness in the earth sciences. Earth-Science Reviews 136, 202–225.

Sohlenius G, Hedenström A, Rudmark L, 2004. Forsmark Site Investigation: Mapping of Unconsolidated Quaternary Deposits 2002–2003: Map Description. SKB R-04-39, Svensk Kärnbränslehantering AB.

Speth J D, 1972. Mechanical basis of percussion flaking. American Antiquity 37, 34–60.

Stephens M B, 2010. Forsmark site investigation. Bedrock geology – overview and excursion guide. SKB R-10-04, Svensk Kärnbränslehantering AB.

Stephens M B, Bergman T, Isaksson H, Petersson J, 2008. Bedrock geology Forsmark. Modelling stage 2.3. Description of the bedrock geological map at the ground surface. SKB R-08-128, Svensk Kärnbränslehantering AB.

Strömberg B, 1994. Younger Dryas deglaciation at Mt. Billingen, and clay varve dating of the Younger Dryas/Preboreal transition. Boreas 23, 177–193.

Stroeven A P, Fabel D, Hättestrand C, Harbor J, 2002a. A relict landscape in the centre of Fennoscandian glaciation: cosmogenic radionuclide evidence of tors preserved through multiple glacial cycles. Geomorphology 44, 145–154.

Stroeven A P, Fabel D, Harbor J, Hättestrand C, Kleman J, 2002b. Quantifying the erosional impact of the Fennoscandian ice sheet in the Torneträsk–Narvik corridor, northern Sweden, based on cosmogenic radionuclide data. Geografiska Annaler: Series A, Physical Geography 84, 275–287.

Stroeven A P, Hättestrand C, Kleman J, Heyman J, Fabel D, Fredin O, Goodfellow B W, Harbor J M, Jansen J D, Olsen L, Caffe M W, Fink D, Lundqvist J, Rosqvist G C, Strömberg B, Jansson K N, 2016. Deglaciation of Fennoscandia. Quaternary Science Reviews 147, 91–121.

Sugden D E, John B S, 1976. Glaciers and landscape: a geomorphological approach. London: Edward Arnold.

Sugden D E, Glasser N, Clapperton C M, 1992. Evolution of large roches moutonnées. Geografiska Annaler: Series A, Physical Geography 74, 253–264.

Söderlund P, Hermansson T, Page L M, Stephens M B, 2009. Biotite and muscovite 40 Ar–39 Ar geochronological constraints on the post-Svecofennian tectonothermal evolution, Forsmark site, central Sweden. International Journal of Earth Sciences 98, 1835–1851.

Ugelvig S V, Egholm D L, 2018. The influence of basal-ice debris on patterns and rates of glacial erosion. Earth and Planetary Science Letters 490, 110–121.

Ugelvig S V, Egholm D L, Iverson N R, 2016. Glacial landscape evolution by subglacial quarrying: A multiscale computational approach. Journal of Geophysical Research: Earth Surface 121, 2042–2068.

Whalley W B, Krinsley D H, 1974. A scanning electron microscope study of surface textures of quartz grains from glacial environments. Sedimentology 21, 87–105.

Wintges T, 1985. Studies on crescentic fractures and crescentic gouges with the help of close-range photogrammetry. Journal of Glaciology 31, 340–349.

Wirsig C, Ivy-Ochs S, Reitner J M, Christl M, Vockenhuber C, Bichler M, Reindl M, 2017. Subglacial abrasion rates at Goldbergkees, Hohe Tauern, Austria, determined from cosmogenic ^{10}Be and ^{36}Cl concentrations. Earth Surface Processes and Landforms 42, 1119–1131.

Wright P J, Harper J T, Humphrey N F, Meierbachtol T W, 2016. Measured basal water pressure variability of the western Greenland Ice Sheet: Implications for hydraulic potential. Journal of Geophysical Research: Earth Surface 121, 1134–1147.

Zhou L, Zhang J, Li S, Tian Y, Wang J, Huang M, Yuan Q, Li X, Kou Z, Zhan G, 2023. Effects of hardness and grain size on wear resistance of polycrystalline cubic boron nitride. International Journal of Refractory Metals and Hard Materials 111, 105766.

Zoet L, Alley R B, Anandakrishnan S, Christianson K, 2013. Accelerated subglacial erosion in response to stick-slip motion. Geology 41, 159–162.

Appendix 1

Outcrop photo fracture analysis – Stånggrundet and Klubbudden

Fracture analyse was undertaken by taken accurately scaled photos in the field, georeferencing these against a grid (which is subvertical in three dimensions) and digitising fractures within a window. The method is described in more detail in Palamakumbura et al. (2020) and was also used for outcrop fracture analysis in Krabbendam et al. (2022a). For results see Appendix 2, Table A2-5.

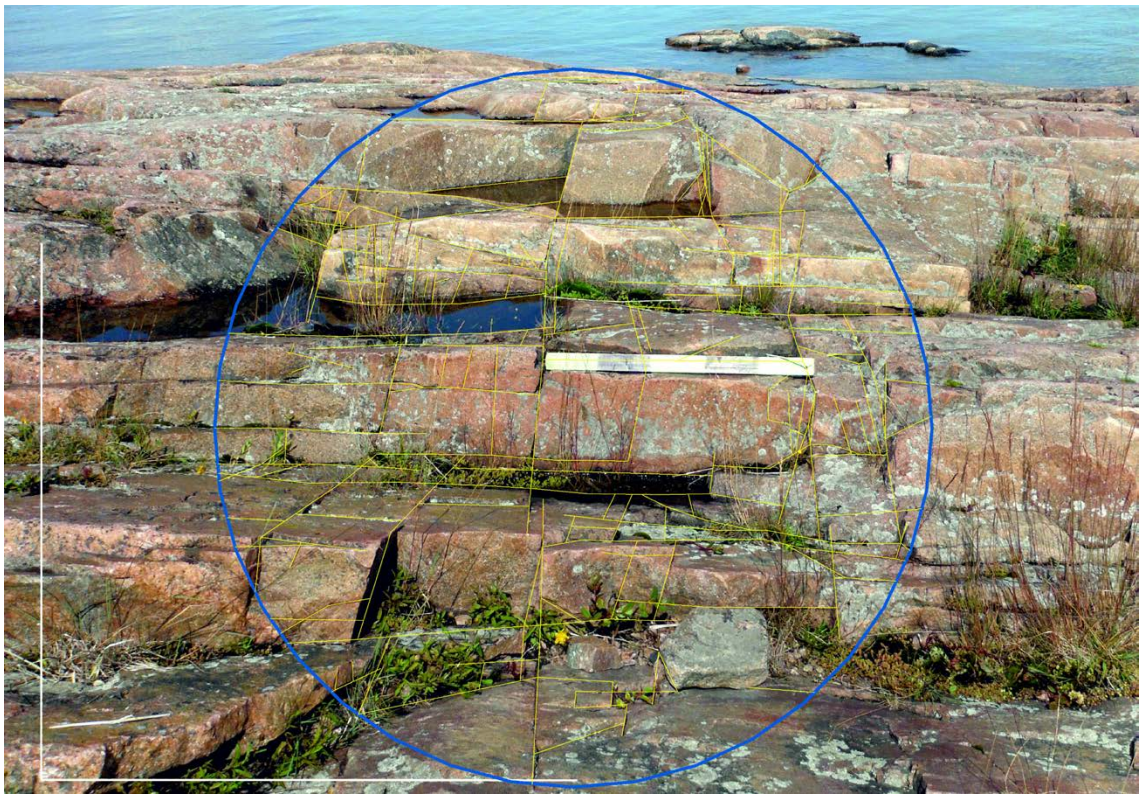

Figure A1-1. *Outcrop photo at Klubbudden, with digitised fractures in yellow, within a circular window, in blue (subvertical in 3D). View to the NW.*

Figure A1-2. *Outcrop photo at Stånggrundet, with digitised fractures in yellow, within an irregular window, in blue (subvertical in 3D). View to the west.*

Appendix 2

Fracture results – full

For explanation of the Pxy system, see Sanderson and Nixon (2015) with x = sample window dimension and y = dimension of measured features.

- P10 (1D frequency) is the number of fractures observed along a 1D scanline and has dimension m^{-1}.
- P11 (Intensity) is the total length of fractures along a 1D scanline and is dimensionless.
- P20 (Frequency) is the number of fractures within a window, with dimension m^{-2}.
- P21 (Density) the total length of fractures within a window and has dimension m^{-1}.

Table A2-1. Drone mapping fracture analysis (Lidar and orthophoto interpretation – mapview).

Region	Window Area (m^2)	Σ Fracture Length (m)	n	Density (P21) (m^{-1})	Spacing (m)	Frequency (P20) (m^{-2})
Lilla Sandgrund NE	994.84	1 141.65	785	1.15	0.87	0.79
Lilla Sandgrund SW	2 889.16	2 372.89	1 229	0.82	1.22	0.43
Lilla Sandgrund W	1 950.9	1 362.98	869	0.7	1.43	0.45
Asphällan	1 894.26	2 088.32	1 611	1.1	0.91	0.85
Stånggrundet	2 120.32	3 668.67	2 098	1.73	0.58	0.99

Table A2-2. Linear scanlines – field observations.

Region	Line	Scanline length (m)	Σ Fracture Length (m)	n	Intensity (P11)	1D Frequency (P10) (m^{-1})
Lilla Sandgrund NE	1	16.28	76.90	25	4.72	1.54
Lilla Sandgrund NE	2	13.37	39.51	19	2.95	1.42
Lilla Sandgrund NE	3	5.78	13.33	4	2.31	0.69
Lilla Sandgrund SW	4	14.44	32.52	15	2.25	1.04
Lilla Sandgrund SW	5	18.21	71.04	21	3.9	1.15
Lilla Sandgrund SW	6	9.29	39.97	19	4.3	2.05
Stånggrundet	7	6.68	44.81	35	6.71	5.24
Stånggrundet	7	6.68	44.81	35	6.71	5.24
Stånggrundet	8	4.29	25.84	9	6.03	2.1
Asphällan	9	4.60	21.34	17	4.64	3.7
Asphällan	10	5.08	12.19	3	2.4	0.59
Asphällan	11	19.66	74.90	12	3.81	0.61
Asphällan	12	9.15	34.64	24	3.79	2.62

Table A2-3. Subhorizontal fractures field observations – oblique window.

Site	Line	Window Length (m)	Window Width (m)	Length corrected (m)	Window Area (m^2)	Fracture length (m)	n	Density (P21) (m^{-1})	Frequency (P20) (m^{-2})	Spacing (m)
Asphällan	13	12.10	9.91	10.5	103.80	18.29	40	0.18	0.39	5.68
Asphällan	14	6.20	2.75	5.4	14.77	22.65	43	1.53	2.91	0.65
Stånggrundet	15	7.57	3.44	6.6	22.55	22.71	39	1.01	1.73	0.99
Stånggrundet	16	5.57	3.37	4.8	16.26	8.39	7	0.52	0.43	1.94
Stånggrundet	17	6.51	2.98	5.6	16.80	5.24	10	0.31	0.60	3.21
Lilla Sandgrund NE	18	3.52	4.67	3	14.24	2.85	2	0.20	0.14	4.99
Lilla Sandgrund W	19	9.68	9.52	8.4	79.77	11.58	14	0.15	0.18	6.89
Lilla Sandgrund SW	20	9.06	7.22	7.8	56.63	0.28	1	0.00	0.02	202.2

Table A2-4. Outcrop photo fracture mapping (Stånggrundet and Klubbudden; see Appendix 1).

Site	Photo	Σ Fracture length (m)	Window Area (m^2)	Density (P21) (m^{-1})	Spacing (m)
Klubbudden	Figure A1-1	31.47	1.40	22.42	0.04
Stånggrundet	Figure A1-2	71.97	5.02	14.35	0.07

Table A2-5. Orientations of main fracture sets.

Site	Drone sets – map view	Field steep sets	Field shallow sets
Lilla Sandgrund NE	**Main:** NW–SE **Minor:** NNE–SSW, NE–SW, E–W	**Main:** WNW–ESE **Minor:** NE–SW	**Main:** N–S, NW–SE **Minor:**
Lilla Sandgrund W	**Main:** E–W **Minor:** NW–SE, NE–SW	**Main:** NE–SW, NW–SE **Minor:** E–W	**Main:** NW–SE **Minor:** ENE = WSW
Stånggrundet	**Main:** NE–SE, WNW–ESE **Minor:** N–S	**Main:** NNE–SSW **Minor:** NNW–SSE, NW–SE, E–W	**Main:** NNW–SSE **Minor:** NE–SW
Asphällan	**Main:** NW–SE **Minor:** NE–SW, N–S	**Main:** NE–SW, NW–SE **Minor:** N–S	**Main:** NE–SW **Minor:** WNW–ESE

Table A2-6. Connectivity data.

Sites	I-I	I-C	C-C	Total n	Window Area (m^2)	Sum L I-I	Sum L I-C	Sum L C-C	Connected (%)	Partial connected (%)	Connected density	Partial connected density
Lilla Sandgrund W	413	609	226	1248	1950.9	526.2	537.48	199.96	18.1	66.9	0.1	0.38
Lilla Sandgrund SW	474	1112	513	2099	2889.16	723.88	1036.96	493.49	24.4	77.4	0.17	0.53
Lilla Sandgrund NE	291	641	321	1253	994.84	273.0	508.3	263.47	25.6	76.8	0.26	0.78
Stånggrundet	450	2155	1798	4403	2120.32	538.36	1590.82	1197.87	40.8	89.8	0.56	1.32
Asphällan	638	1245	673	2556	1894.26	472.83	879.92	540.74	26.3	75	0.29	0.75

Arkitektkopia AB, Bromma, 2024

SKB is responsible for managing spent nuclear fuel and radioactive waste produced by the Swedish nuclear power plants such that man and the environment are protected in the near and distant future.

skb.se